PERSOONLIJK EN VERTROUWELIJK

B.A.T NEDERLAND B.V.

BROWN & WILLIAMSON TOBACCO CORPORATION

SCIENTIFIC SUBMISSION

At The Hague

December 7, 1982

CONTENTS

I. INTRODUCTION

Brown & Williamson is pleased to submit the following document containing papers presented to Dutch scientists and officials on December 7, 1982.

The file contains a commentary on the draft papers written by Drs. Baker, Cain, Kamm, Fine, van Rossum, Gori, Darby and McNamee. These papers are drafts which are in the process of being submitted for publication in scientific journals.

These papers are for your use and should be treated as confidential. Brown & Williamson will be pleased to direct any questions you may have to the appropriate scientists.

II. COMMENTARY

The Aerodynamics of Actron

Dr. Baker's aerodynamic modelling of the Actron filter used on Barclay cigarettes describes how the smoke turbulence is developed. The model also shows how smoke turbulence is reduced if sleeves are added to the filter.

Sensory Aspects of the Barclay Cigarette

Dr. Gain explains how Barclay cigarettes provide increased flavor. By taking advantage of certain known principles of sensory functioning (spatial summation), the stimulus is used more effectively. He also describes an experiment in which the blend flavor and filter contributions of Barclay can be separately assessed.

Finally, he shows how his findings with consumer panels are in accord with Dr. Baker's theoretical predictions.

Measurements of Lip Pressure Exerted on a Cigarette During Normal Smoking

The measurements made by Dr. Kamm provide reliable evidence on the pressures applied when smokers hold the cigarette filter between the lips.

To obtain these measurements, special methods had to be developed so that the pressure device was both appropriate to the situation and sensitive enough to measure the very low pressures applied in these circumstances.

Pressure measurements are also given for three different cigarette holders. The results obtained for two of these holders are such that their use in assessing smoke deliveries would appear to be wholly inappropriate [see Table 2 Kamm].

Filter Interactions with Lip Mucosa

Dr. Fine provides a detailed description of the interactions of cigarette filters with lip mucosa. Fiberoptics are used to view inside the mouth during cigarette puffing with subjects covering the range of anatomical variation.

The constraints imposed by certain laboratory cigarette holding devices are critically examined. Decreases in available surface area, limit insertion depths and alter the lip to filter end relationships.

Dr. Fine concludes that under normal conditions, smokers do not obstruct the groove openings on Barclay's Actron filter.

Pharmacokinetics of Nicotine and Cotinine

The work of Prof. Dr. J. van Rossum provides the basic information on the pharmacokinetics of nicotine and cotinine. Van Rossum's analysis delineates the underlying requirements when using cotinine plasma concentration data as a marker for nicotine absorption in human smoking experiments. For a reliable measure of nicotine absorption, a steady state cotinine condition must be achieved, and for the purpose of comparative absorption assessment, use of a self matching design.

In addition, van Rossum's paper includes an extensive bibliography which is arranged by relevant categories for analysis of nicotine and cotinine.

Smoker Intake From Cigarettes in the 1 mg Tar Class

The work of Dr. G. Gori presents the experimental design, data base, and details of the experimental methodology. An extremely important aspect of Dr. Gori's work (based on a very large data base) provides a calibration of the existing in vitro FTC procedure for the class of cigarettes tested. The observed linear correlation between average baseline cotinine plasma concentration and FTC nicotine content, for the first time, shows that this (FTC) in vitro test indeed is a good measure of nicotine (tar) uptake in humans over the range tested [see Figure 3 of Gori]. In essence, this result indicates that the in vitro test should predict the likely findings of the population mean for the class of cigarette tested.

Comparison of Human Uptake Among Cigarette Brands Rated As One Milligram Tar Yield

The paper of Darby, McNamee and van Rossum is an independent analysis of the data generated by Gori. The analysis focuses on the nicotine (tar) uptake, as measured by cotinine plasma levels in individuals.

This analysis, based on approximately 60,000 cigarettes smoked by individuals in their natural environment, indicates the following [see Figure 1-5 of Darby, et al]:

1. Individuals differ greatly in their plasma cotinine concentration despite comparable consumption of numbers of cigarettes. Reasons are presented for this difference in the discussion section of the report.
2. Individuals with high plasma cotinine concentrations, while smoking one brand, tend to have high plasma cotinine concentrations on all brands investigated. The same statement is true for individuals with low plasma cotinine concentrations.
3. On the average, a smoker's plasma cotinine concentration is proportional to the brand yield values obtained by measurement utilizing the standard smoking machine procedures.
4. If the individuals who obtain greater than average yield are considered to be a problem, then these data support the conclusions that all ventilated filter cigarette brands share in the problem.
5. The large number of smokers who obtain lower than average plasma cotinine concentrations, while smoking ultra low tar cigarette brands, benefit from the reduced nicotine and thus tar intake.

III. CLOSING COMMENTS:

It is believed that the results presented in this file, based on a number of different human studies, place into perspective the role of various aspects of smoking behavior and current in vitro test methodology in the use and assessment of highly ventilated low tar cigarettes available in the United States.

APPENDIX I

Guests and Program

The Hague, December 7, 1982

AGENDA FOR CONFERENCE

Tuesday, 07.12.1982

"BABYLON" Hotel, The Hague, Conference Room "SIRIUS"

GUESTS:

Drs. P.H. Berben, Chief Inspector, Hoofd-Inspectie Levensmiddelen, Ministerie van Volksgezondheid, Leidschendam.

Ir. W.J. de Koe, Inspector, Hoofd-Inspectie Levensmiddelen, Ministerie van Volksgezondheid, Leidschendam.

Drs. H.A. de Kok, Director Keuringsdienst van Waren, Alkmaar.

Ing. M. Hissink, MT TNO, Hoofdgroep Maatschappelijke Technologie TNO, Apeldoorn.

Drs. R. Bosman, MT TNO, Hoofdgroep Maatschappelijke Technologie TNO, Delft.

Drs. P.J. Groenen, CIVO-TNO, Zeist.

09.00 - 09.15 Greetings and introduction by
Mr. F. van Vliet, B.A.T NEDERLAND B.V. Amsterdam

09.15 - 09.30 Introduction
Prof. Dr. T.D. Darby, University of South Carolina, School of Medicine

FILTERDESIGN AND ITS INFLUENCE ON SENSORY PERCEPTION OF CIGARETTE SMOKE

09.30 - 10.00 Aerodynamics of Actron
Prof. Dr. A.J. Baker, University of Tennessee, Inst. Engineering and Sciences

10.00 - 10.30 Sensory Aspects of Actron Testing in US
Prof. Dr. Wm. Cain, J.B. Pierce Foundation, Yale University

10.30 - 10.45 Discussion

10.45 - 11.00 Coffee Break

FILTER PERFORMANCE OF CIGARETTES IN THE HUMAN MOUTH AND IN SMOKING MACHINES

11.00 - 11.30 Measurements of Lip Pressure Exerted on a Cigarette during Normal Smoking
Prof. Dr. R.D. Kamm, Massachusetts Institute of Technology, Dept. Mechanical Engineering

11.30 - 12.00 Influence of Mouth Structure on Smoking Behaviour
Prof. Dr. L. Fine, University of Chicago, School of Medicine

12.00 – 13.00 Lunch

NICOTINE UPTAKE IN THE HUMAN BODY IN RELATION TO NICOTINE AND TAR DELIVERY BY CIGARETTES

13.00 – 13.30 Pharmacokinetics of Nicotine and Cotinine
Prof. Dr. J.M. van Rossum, University of Nijmegen
Dept. Pharmacology

13.30 – 14.00 Smoker Intake from Cigarettes in the One Milligram Tar Class
Prof. Dr. G.B. Gori, Director of Human Studies, Franklin Institute

14.00 – 14.30 Comparison of Human Uptake Among Cigarette Brands rated as One Milligram Tar Yield
Prof. Dr. J.E. McNamee, University of South Carolina, School of Medicine

14.30 – 15.00 Discussion and Closing Comments.

PRESENTATION SUMMARY

- Dr. Baker will explain the aerodynamics of ACTRON. The four grooves introduce outside air at high velocity that mixes with smoke in the mouth causing a rapid swirling effect.

- Dr. Cain will demonstrate the taste characteristics of ACTRON. He will show how the swirling dispersion of smoke results in more taste and flavour.

- Dr. Kamm will explain his measurements of pressure exerted on a cigarette filter by human lips and by various filter holders. He concludes that the grooves of ACTRON will not be collapsed in normal smoking.

- Dr. Fine will explain the interaction of human lips and cigarette filters to show (1) that lips will not normally occlude the ACTRON grooves and (2) that a dilution device fabricated by one competitor virtually forces occlusion.

- Dr. Van Rossum will discuss aspects of his research on the pharmacokinetics of nicotine - cotinine in humans.

- Dr. Gori will speak about the research study conducted using cotinine as a marker for nicotine to measure tar uptake by humans smoking 1 mg tar products produced in the U.S.A.

- Dr. McNamee will present an independent analysis of the cotinine data utilizing a variety of statistical techniques.

BRIEF ABOUT SPEAKERS

Dr. A. J. Baker...is Professor of Engineering Science and Mechanics at the University of Tennessee. Prior to that, he was a scientist at Bell-Aerospace Group conducting advanced research in aerodynamics and computational fluid mechanics. He is a consultant to NASA and the U.S. Air Force in the areas of aerodynamics and computational fluid dynamics.

Dr. W. S. Cain...is Professor of Epidemiology and Psychology at Yale University. He has done extensive research in the area of sensory measurement with particular emphasis on the chemical senses. He is active in several areas of sensory research at the international level.

Dr. R. D. Kamm...is Professor of Mechanical Engineering at Massachusetts Institute of Technology. He has conducted research studies in the areas of biomechanics and biomedical fluid mechanics for several U.S. governmental agencies. In addition, he has developed various electro-mechanical systems/devices in conjunction with some of the leading medical institutions in the U.S.

Dr. L. Fine...is Professor of Dental Surgery and Maxillofacial Prosthodontics at Zoller Clinic, University of Chicago Medical School. In addition, he is Director of Maxillofacial Prosthodontic Research. He has conducted numerous research projects under the auspicies of various U.S. government agencies in the area of lip tissue and intra-oral diseases.

Dr. J. van Rossum...is Professor at University of Nijmegen School of Medicine, Nijmagen, The Netherlands. Prof. van Rossum (along with Prof. Dr. Oettli) is, as you probably well know, regarded as the founding father of pharmacokinetics on the European Continent. Prof. van Rossum has published extensively in pharmacology/ pharmacokinetics and has been principle author of several texts in the field. His research work in recent years has been dedicated to the disposition and fate of drugs in the human body and affect on the human nervous system.

Dr. G. Gori...is Director of Human Studies at the Franklin Institute Policy Center. Prior to joining the Franklin Institute, he was Director of Smoking and Health Research program at the National Cancer Institute. He has conducted numerous studies over the past 18 years in human smoking and related biochemical reactions.

Dr. T. D. Darby...is Professor of Pharmacology and Associate Dean at the University of South Carolina School of Medicine. Prior to joining the Medical School, he was Director of Cardiovascular Pharmacology at Baxter-Travenol. He has published extensively in the areas of Pharmacology, Pharmacokinetics and Toxicology.

Dr. J. E. McNamee...is a Professor in the Department of Physiology at the University of South Carolina School of Medicine. His primary research interests are in the area of pulmonary physiology. Prior to joining the Medical School he was at the Cardio Vascular Research Institute at University of California, San Francisco. His background also includes training in Engineering. He has published extensively in the areas of Physiology and Pharmacology, with particular emphasis on the analysis of data emanating from human studies.

100506846

APPENDIX II

THE AERODYNAMICS OF ACTRON

by

A. J. Baker, Ph.D.
University of Tennessee
Knoxville, Tennessee

and

PREDICTION OF SECONDARY VORTEX FLOWFIELDS INDUCED BY MULTIPLE FREE-JETS ISSUING IN CLOSE PROXIMITY

by

A. J. Baker, Ph.D.
University of Tennessee
Knoxville, Tennessee

J. A. Orzechowski, Ph.D.
Computational Mechanics Consultants, Inc.
Knoxville, Tennessee

G. E. Stungis, Ph.D.
Brown & Williamson Tobacco Corporation
Louisville, Kentucky

DRAFT
COMMERCIAL IN CONFIDENCE

THE AERODYNAMICS OF ACTRON

THEORETICAL ANALYSIS

1005062849

VISUALIZATION OF ACTRON FLOWFIELD

THEORETICAL ANALYSIS

BASIC IDENTIFICATIONS

- Differential Equation System
- Turbulence Closure
- Numerical Solution Algorithm
- Verification Tests

ANALYSIS SPECIFICATIONS

- Solution Domain
- Boundary Conditions
- Initial Conditions
- Closure Model Constants

DIFFERENTIAL EQUATIONS

CONTINUITY, MOMENTUM AND ENERGY

- First Order Effects
  - Downstream Diffusion Negligible
  - Transverse Momenta Governs Pressure
  - Continuity Governs Transverse Velocities
- Reynolds Stress Components of Equal Order
- Well - Posed Problem Statement Required

TURBULENCE CLOSURE

- TKE - Epsilon Two-Equation System
- Reynolds Stress Constitutive Model

TURBULENT THREE-DIMENSIONAL AERODYNAMIC FLOW

3D Thin Layer Navier-Stokes Equations $(1 \leq i \leq 3)$ $(2 \leq \ell \leq 3)$

$$L(Q) = \text{CONVECTION} + \text{SOURCE} + \text{DIFFUSION} + \text{SINK} = 0$$

$$L(\bar{\rho}) = \frac{\partial}{\partial x_i}(\bar{\rho}\tilde{u}_i) = 0$$

$$L(\tilde{u}_1) = \frac{\partial}{\partial x_i}(\bar{\rho}\tilde{u}_i\tilde{u}_1) + \frac{\partial \bar{p}}{\partial x_1} - \frac{\partial}{\partial x_\ell}\left[\frac{\mu}{Re}\frac{\partial \tilde{u}_1}{\partial x_\ell} - \overline{\rho u_1' u_\ell'}\right] = 0$$

$$L(\tilde{u}_2) = \frac{\partial}{\partial x_i}(\bar{\rho}\tilde{u}_i\tilde{u}_2) + \frac{\partial \bar{p}}{\partial x_2} - \frac{\partial}{\partial x_\ell}\left[\frac{\mu}{Re}\left(\frac{\partial \tilde{u}_2}{\partial x_\ell} + \frac{\partial \tilde{u}_\ell}{\partial x_2}\right) - \overline{\rho u_2' u_\ell'}\right] = 0$$

$$L(\tilde{u}_3) = \frac{\partial}{\partial x_i}(\bar{\rho}\tilde{u}_i\tilde{u}_3) + \frac{\partial \bar{p}}{\partial x_3} - \frac{\partial}{\partial x_\ell}\left[\frac{\mu}{Re}\left(\frac{\partial \tilde{u}_3}{\partial x_\ell} + \frac{\partial \tilde{u}_\ell}{\partial x_3}\right) - \overline{\rho u_3' u_\ell'}\right] = 0$$

$$L(k) = \frac{\partial}{\partial x_i}(\bar{\rho}\tilde{u}_i k) + \overline{\rho u_i' u_\ell'}\frac{\partial \tilde{u}_i}{\partial x_\ell} - \frac{\partial}{\partial x_i}\left[\frac{\mu}{Re} + \bar{\rho}C_k\frac{k}{\epsilon}\overline{u_i' u_\ell'}\frac{\partial k}{\partial x_\ell}\right] + \bar{\rho}\epsilon = 0$$

$$L(\epsilon) = \frac{\partial}{\partial x_i}(\bar{\rho}\tilde{u}_i\epsilon) + C_1\overline{\rho u_i' u_\ell'}\frac{\epsilon}{k}\frac{\partial \tilde{u}_i}{\partial x_\ell} - \frac{\partial}{\partial x_i}\left[\bar{\rho}C_\epsilon\frac{k}{\epsilon}\overline{u_i' u_\ell'}\frac{\partial \epsilon}{\partial x_\ell}\right] + C_2\frac{\epsilon^2}{k} = 0$$

REYNOLDS STRESS CLOSURE MODEL

FROM CONTINUUM MECHANICS:

$$\overline{u_i' u_j'} = \alpha_1 \delta_{ij} + \alpha_2 E_{ij} + \alpha_3 E_{ik} E_{kj} + \cdots, \qquad E_{ij} \equiv \left[\frac{\partial \tilde{u}_i}{\partial x_j} + \frac{\partial \tilde{u}_j}{\partial x_i}\right]$$

PARABOLIZED PLUS 2ND ORDER:

$$\overline{u_1' u_1'} = C_1 k - 2C_1 \frac{k^2}{\epsilon} \frac{\partial \tilde{u}_1}{\partial x_1} - C_2 \frac{k}{\epsilon} C_4 \frac{k^2}{\epsilon} \left[\frac{\partial \tilde{u}_1}{\partial x_\ell} \frac{\partial \tilde{u}_1}{\partial x_\ell}\right]$$

$$\overline{u_2' u_2'} = C_3 k - 2C_1 \frac{k^2}{\epsilon} \frac{\partial \tilde{u}_2}{\partial x_2} - C_2 \frac{k}{\epsilon} C_4 \frac{k^2}{\epsilon} \left[\frac{\partial \tilde{u}_1}{\partial x_\ell} \frac{\partial \tilde{u}_1}{\partial x_\ell}\right]$$

$$\overline{u_3' u_3'} = C_3 k - 2C_1 \frac{k^2}{\epsilon} \frac{\partial \tilde{u}_3}{\partial x_3} - C_2 \frac{k}{\epsilon} C_4 \frac{k^2}{\epsilon} \left[\frac{\partial \tilde{u}_1}{\partial x_\ell} \frac{\partial \tilde{u}_1}{\partial x_\ell}\right]$$

$$\overline{u_1' u_2'} = - C_4 \frac{k^2}{\epsilon} \frac{\partial \tilde{u}_1}{\partial x_2}$$

$$\overline{u_1' u_3'} = - C_4 \frac{k^2}{\epsilon} \frac{\partial \tilde{u}_1}{\partial x_3}$$

$$\overline{u_2' u_3'} = - C_4 \frac{k^2}{\epsilon} \left[\frac{\partial \tilde{u}_2}{\partial x_3} + \frac{\partial \tilde{u}_3}{\partial x_2}\right] - C_2 \frac{k}{\epsilon} C_4 \frac{k^2}{\epsilon} \left[\frac{\partial \tilde{u}_1}{\partial x_2} \frac{\partial \tilde{u}_1}{\partial x_3}\right]$$

THREE-DIMENSIONAL DIRECTED FLOWFIELDS

PARABOLIC ALGORITHM STRUCTURES

CONTINUITY:

- PSEUDO - PRESSURE CORRECTION
  SPALDING ET. AL. (1970 - 78)
- POTENTIAL FUNCTION / AXIAL VORTICITY
  BRILEY ET. AL. (1974 - 80),
  GHIA (1974 - 76), DODGE (1976 - 80)
- PENALTY DIFFERENTIAL CONSTRAINT
  BAKER ET. AL. (1979 - 81)

PRESSURE:

- AXIAL MASS - CONSERVING GRADIENT
  "PARTIALLY - PARABOLIC"
- INVISCID POISSON EQUATION
  WALL MODIFICATIONS
- ORDERED POISSON EQUATION
  COMPLEMENTARY SOLUTION (3D POTENTIAL FLOW)
  PARTICULAR SOLUTION (TURBULENCE + CONVECTION)

TWO - DIMENSIONAL PARABOLIC NAVIER - STOKES

STEADY, UNIDIRECTIONAL TURBULENT FLOWS

FINITE ELEMENT PENALTY ALGORITHM

FORMULATIONAL STRUCTURE FROM CLASSICAL VARIATIONAL CONCEPTS :

$$I\left(\bar{u}_p^h, \bar{v}_p^h, \lambda_p\right) = \int_\Omega \mathfrak{f}\left(\vec{u}_p^h\right) + \frac{1}{2}\lambda_p \int_\Omega \left(\nabla \cdot \vec{u}_p^h\right)^2$$

$$= \frac{1}{2Re}\left(\nabla \vec{u}_p^h\right)^2 + \ldots$$

WEIGHTED RESIDUALS GALERKIN ALGORITHM :

$$\bar{u}_p^h \equiv \bigcup_e \vec{u}^e(x,y) = \bigcup_e \left[\left\{N_k(y)\right\}^T \left\{QI(x)\right\}_e\right]$$

$$\int_{R^1} \left\{N_k\right\} L^\delta\left(\bar{v}^h\right) - \frac{\lambda}{2}\int_{R^1} \nabla\left\{N_k\right\} L^1\left(\bar{\rho}_o^h\right) \equiv \{0\}$$

$$\int_{R^1} \left\{N_k\right\} L^1\left(\bar{u}^h, k^h, \epsilon^h, \bar{v}^h\right) \equiv \{0\}$$

TWO - DIMENSIONAL PARABOLIC NAVIER - STOKES

STEADY, UNIDIRECTIONAL TURBULENT FLOWS

FINITE ELEMENT PENALTY ALGORITHM

PENALTY FUNCTION FORM :

$$L^1(\bar{\rho}_o^h) = \nabla \cdot \vec{u}^h \neq 0$$
$$\equiv \nabla^2 \phi_p^h$$

BOUNDARY CONDITIONS ON ϕ_p^h :

- POROUS - DIRICHLET
- NON - POROUS - NEUMANN

$$\nabla \phi^h \cdot \hat{n} = \vec{u}^h \cdot \hat{n} = 0$$

PENALTY PARAMETER :

$$\lambda_p \Rightarrow C \Delta x \left[U_p(x_1, x_2) \right]$$

3DPNS FINITE ELEMENT PENALTY CONSTRAINT ALGORITHM

FINITE ELEMENT SOLUTION ALGORITHM:

- SEMI - DISCRETE APPROXIMATION ON R^3:

$$q_{0\alpha}^{h}(x_1, x_l) \equiv \sum_e \left\{N_k(x_l)\right\}^T \left\{QI(x_1)\right\}_e$$

- APPROXIMATION ERROR EXTREMIZATION:

$$\int_{R^2}\{N\} L(q_{0\alpha}^{h}) + \oint_{\partial R}\{N\}\, \ell(q_{0\alpha}^{h}) \equiv \{0\}$$

- TRANSVERSE MOMENTUM CONTINUITY CONSTRAINT:

$$\int_{R^2}\{N\} L(u_l^h) + \vec{\lambda}\cdot\int_{R^2}\nabla\{N\} L(\rho^h) \equiv \{0\}$$

- IMPLICIT INTEGRATION ON X_1

$$\{FI\} \equiv \{QI\}_{j+1} - \{QI\}_j - \Delta x_1 \{QI\}'_{j+1/2} \equiv \{0\}$$

3D PARABOLIC NAVIER-STOKES EQUATIONS

SPACE MARCHING :

- $\tilde{U}_1$, k, e, $\tilde{H}$
- $\tilde{U}_2$, $\tilde{U}_3$ (CONSTRAINED S.T. $\nabla \cdot \vec{U} = 0$)

POISSON EQUATIONS :

- PRESSURE ($P_C + P_P$)
- CONTINUITY FUNCTION

ALGEBRAIC :

- EQUATION OF STATE
- REYNOLDS STRESSES

YIELDS 16 VARIABLES / NODE POINT

VERIFICATION TESTS

CONFIGURATIONS:

- Bounded Flows
  - Turbulence Closure
  - Vortex Structures
- Free Jets
  - Entrainment
  - Discreteness
  - Vortex Structures
- Shear Layers
  - Decay Rate
  - Reynolds Stresses

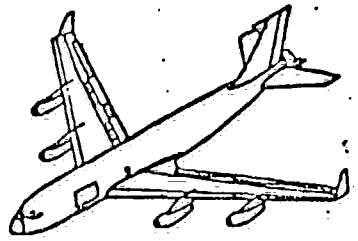

SOLUTIONS:

- C' M C: 3DPNS Computer Program
- CDC Cyber / 203

3-DIMENSIONAL PARABOLIC NAVIER-STOKES

TURBULENT FLOW IN RECTANGULAR DUCT

TRANSVERSE PLANE VELOCITY DISTRIBUTIONS

(BAKER, ET. AL., ASME, 1981)

MASS CONSERVATION ONLY

$U_m = 0.005$

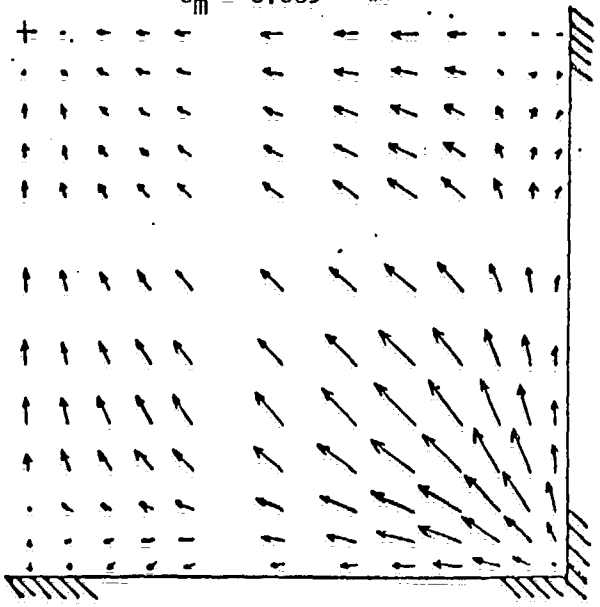

EDDY VISCOSITY MODEL, X1/D = 30.

$U_m = 0.0003$

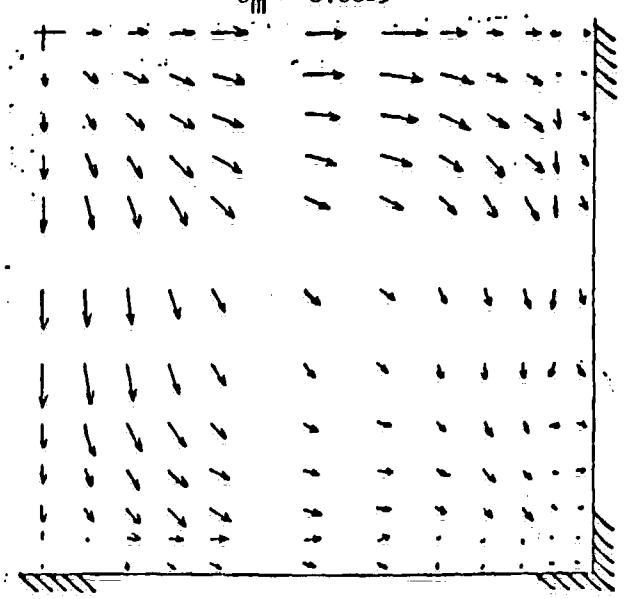

THREE-DIMENSIONAL PARABOLIC NAVIER STOKES

TURBULENT FLOW IN RECTANGULAR DUCT

PROBLEM DEFINITIONS

BASIC CONFIGURATION

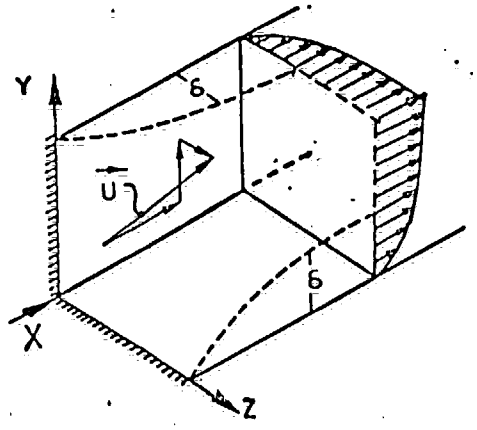

BOUNDARY CONDITIONS

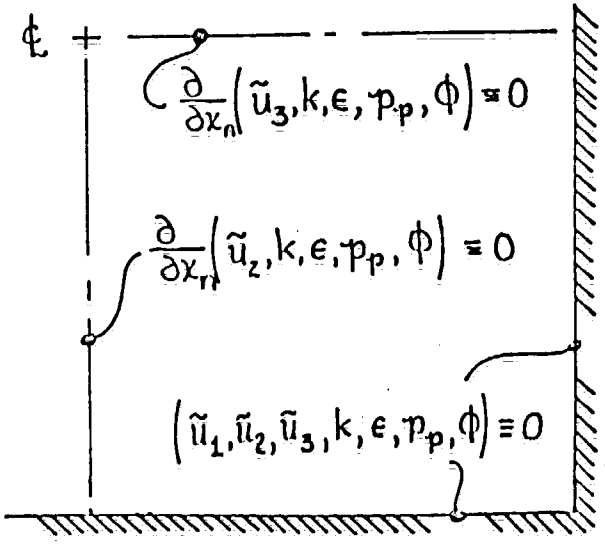

3-DIMENSIONAL PARABOLIC NAVIER-STOKES

TURBULENT FLOW IN RECTANGULAR DUCT

TRANSVERSE PLANE VELOCITY DISTRIBUTIONS

EXPERIMENTAL DATA, X/D = 37

MELLING & WHITELAW (JFM, 1976)

$U^M = .008$

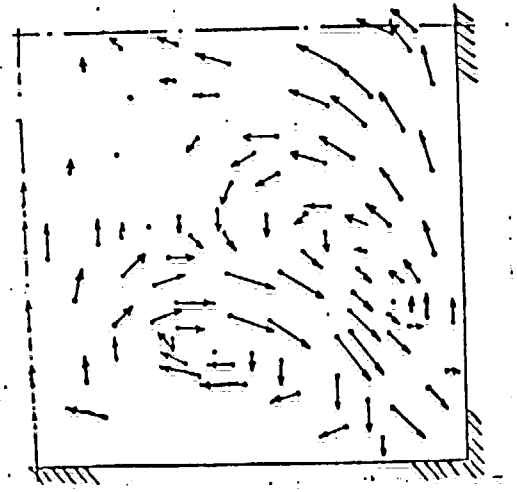

FINER DISCRETIZATION $M = 25^2$

BAKER et al. (AIAA J, 1983) $U^M = .004$

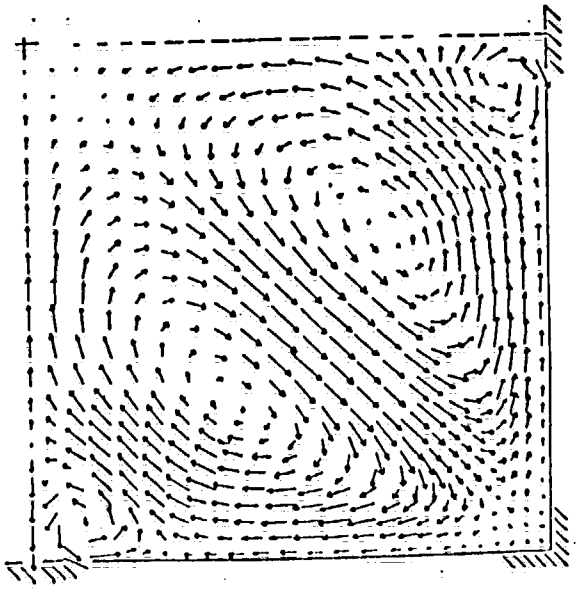

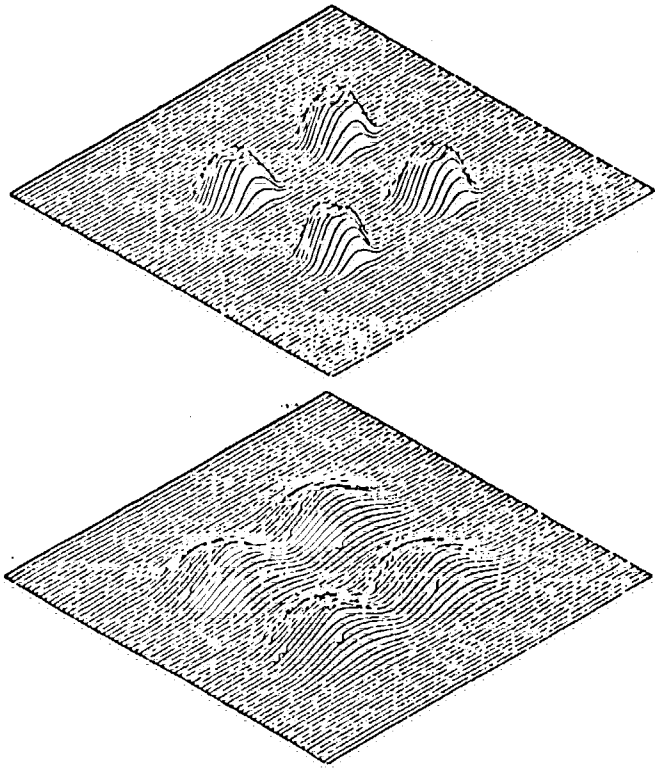

Figure 11. Penalty Algorithm Prediction of Turbulent Kinetic Energy Distributions, Four Multiple Jet Geometry, $\bar{u}_j^o$ = 12 m/s, a) x_1/R = 0.0, k^o = 0.005, b) x_1/R = 0.12, k_m = 0.02, c) x_1/R = 0.25, k_m = 0.035, d) x_1/R = 1.5, k_m = 0.039.

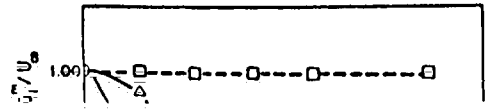

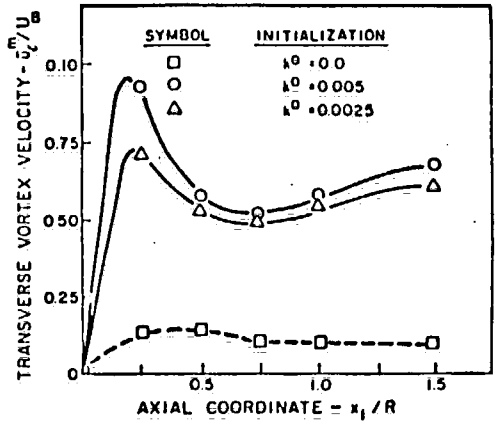

Figure 13. Summary of Penalty Algorithm Prediction of Transverse Plane Mean Velocity $\bar{u}_R$ Extrema as Function of Jet Initial Turbulent Kinetic Energy Level.

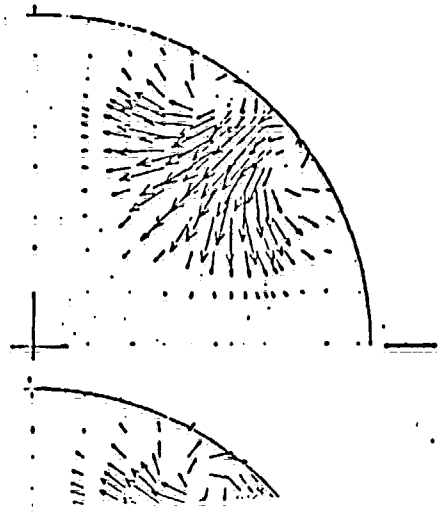

Figure 11. Penalty Algorithm Prediction of Turbulent Kinetic Energy Distributions, Four Multiple Jet Geometry, $\bar{u}_j$ = 12 m/s, a) x_j/R = 0.0, k^o = 0.005, b) x_j/R = 0.12, k_m = 0.02, c) x_j/R = 0.25, k_m = 0.035, d) x_j/R = 1.5, k_m = 0.039.

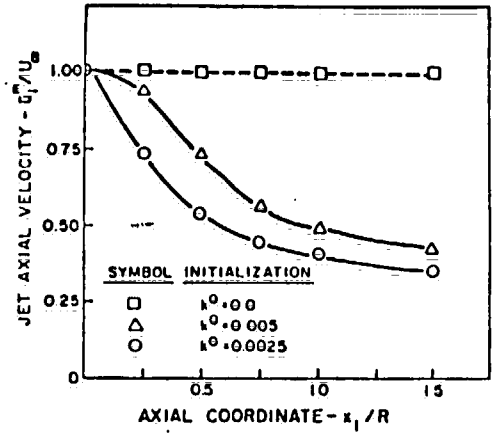

Figure 12. Summary of Penalty Algorithm Prediction of Axial Mean Velocity $\bar{u}_j$ Decay as Function of Jet Initial Turbulent Kinetic Energy Level.

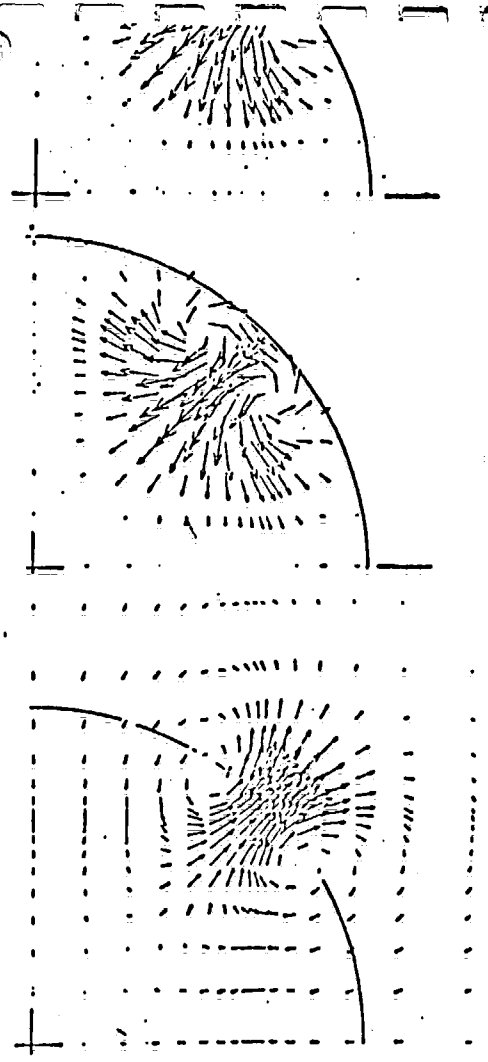

Figure 14. Penalty Algorithm Prediction of Transverse Plane Mean Velocity $\bar{u}_\ell$ Distributions as Function of Locator Radius Extension, Four Multiple Jet Geometry, $\bar{u}_j$ = 12 m/s, a) One Millimeter Extension, x_j/R = 0.25, $\bar{u}_\ell/\bar{u}_j$ = 0.182, b) Three Millimeter Extension, x_j/R = 0.75, $\bar{u}_\ell/\bar{u}_j$ = 0.052, c) One Millimeter Extension, x_j/R = 1.5, $\bar{u}_\ell/\bar{u}_j$ = 0.055.

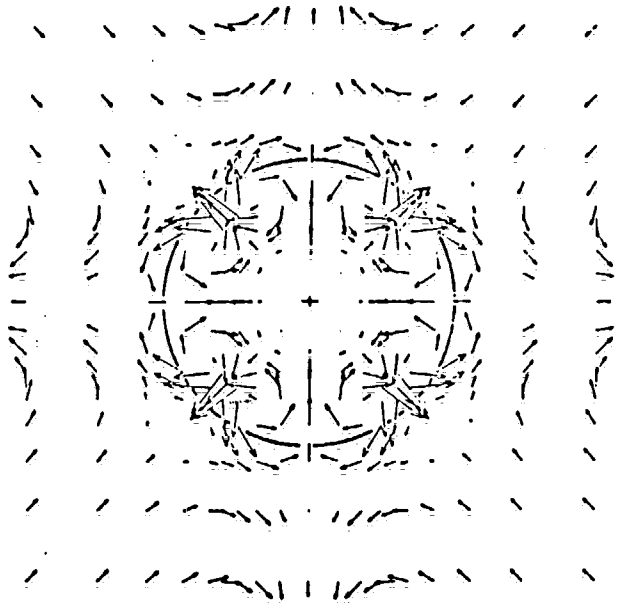

Figure 15. Penalty Algorithm Prediction of Transverse Plane Velocity $\bar{u}_\ell$ Distribution On Half Discretization of Full Solution Domain, $\bar{u}_\infty^0$ = 12 m/s, x_1/R = 1.5, u_ℓ^m = 0.084, M = 19 x 19.

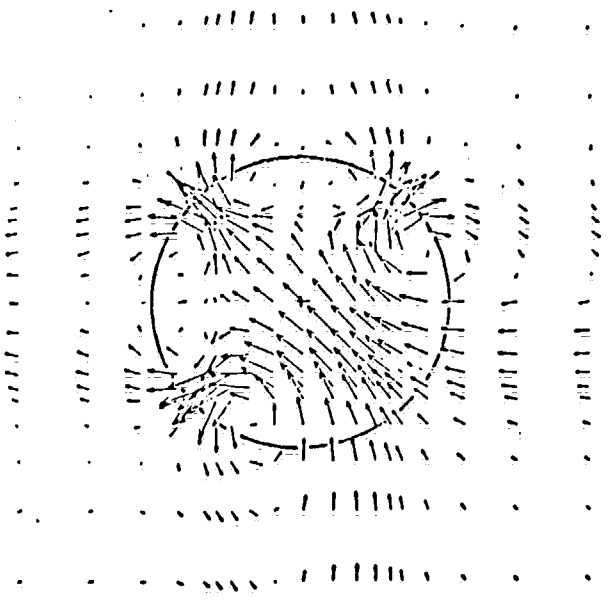

Figure 16. Penalty Algorithm Prediction of Transverse Plane Velocity $\bar{u}_\ell$ Distribution, Four Multiple Jet Geometry with One Jet Off, $\bar{u}_\infty^0$ = 12 m/s, x_1/R = 1.5, u_ℓ^m = 0.126, M = 19x19.

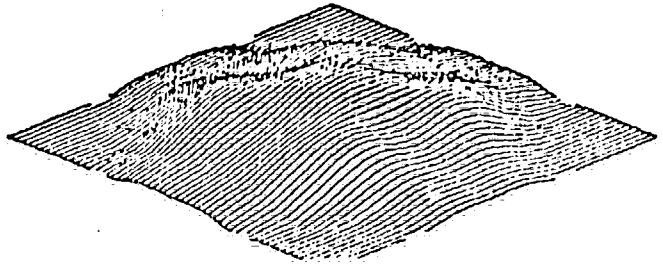

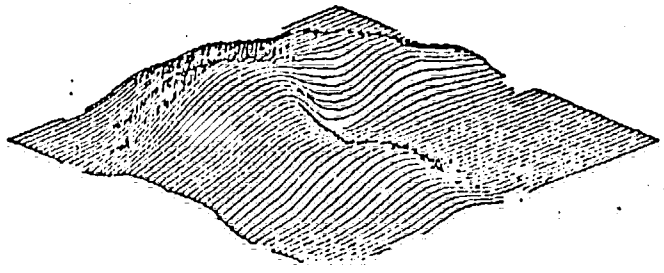

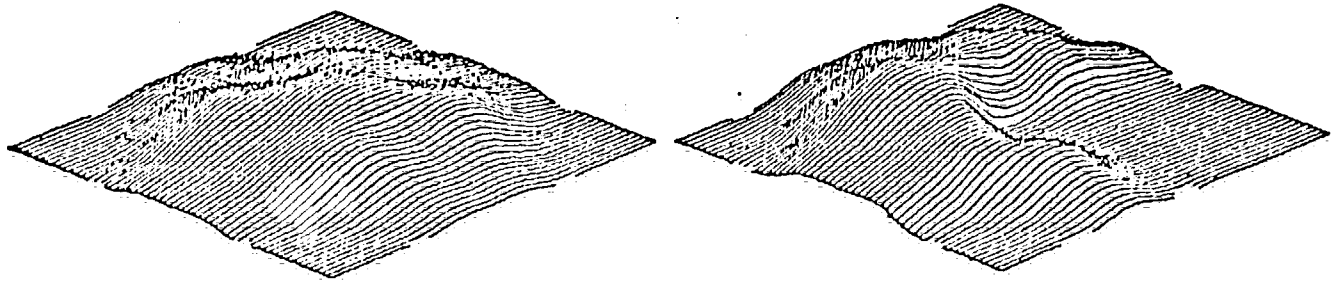

Figure 17. Penalty Algorithm Prediction of Smoke Visualization Distributions On Full Solution Domain, $\bar{u}_1^p$ = 12 m/s, x_1/R = 6.0, a) Four Jets Operating, Y_m = 53%, b) Three Jets Operating, Y_m = 59%.

C M C: 3DPNS ANALYSIS - INITIAL CONDITIONS

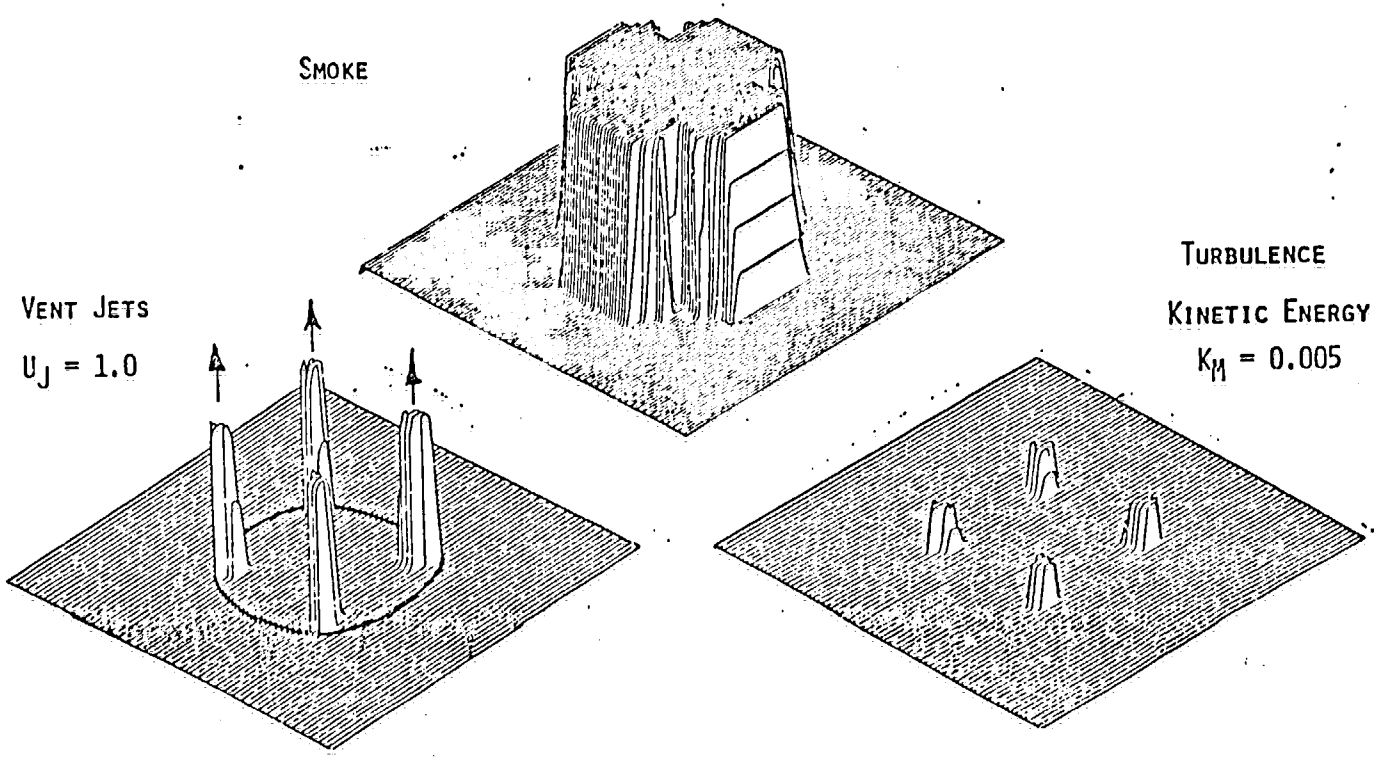

THREE-DIMENSIONAL PARABOLIC NAVIER-STOKES

MULTIPLE FREE-JET SECONDARY VORTEX FIELD

3DPNS ANALYSIS DESCRIPTION

GEOMETRY / DISCRETIZATION

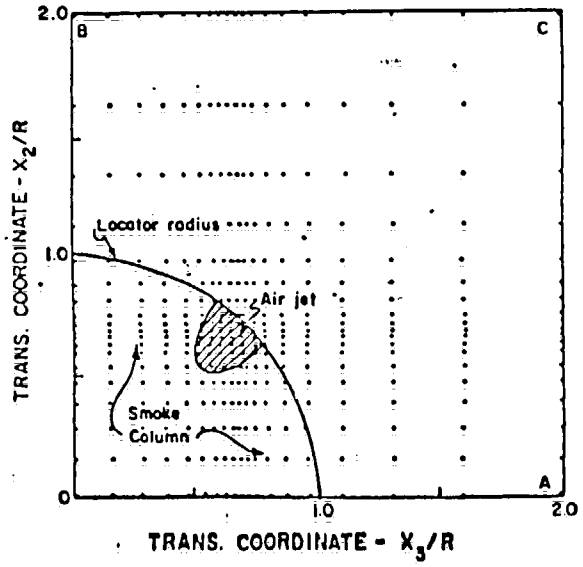

TRANSVERSE PLANE VORTEX FIELD

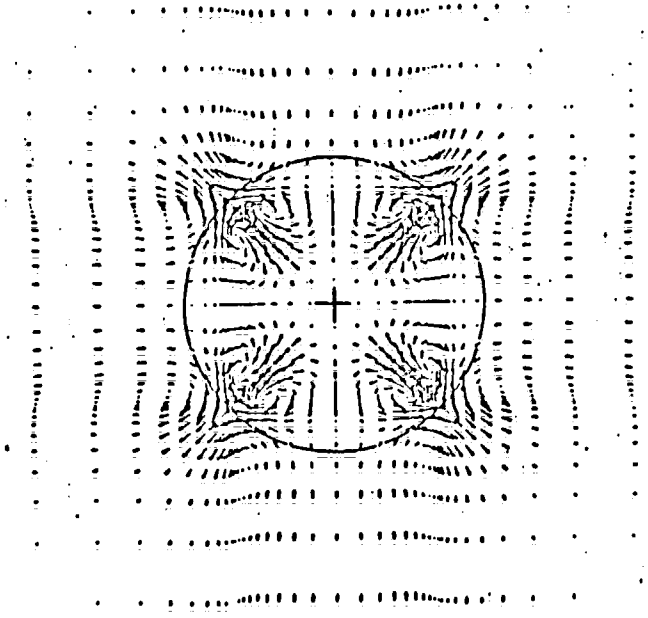

SECONDARY VORTEX FLOW DUE TO FOUR TURBULENT FREE JETS

(Baker, et.al., 1983)

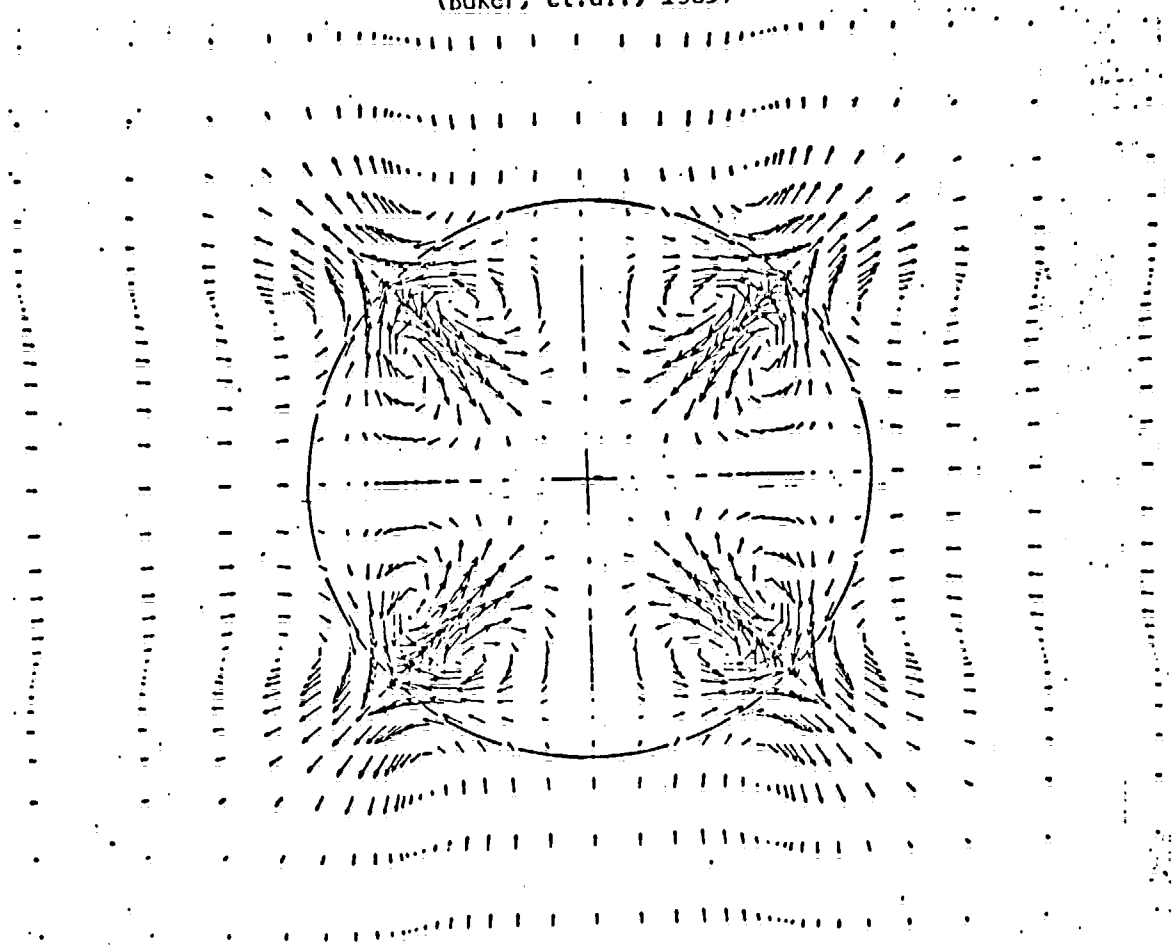

ACTRON FILTER

GENERATION OF VORTEX VELOCITY FIELD

X / R = 0%

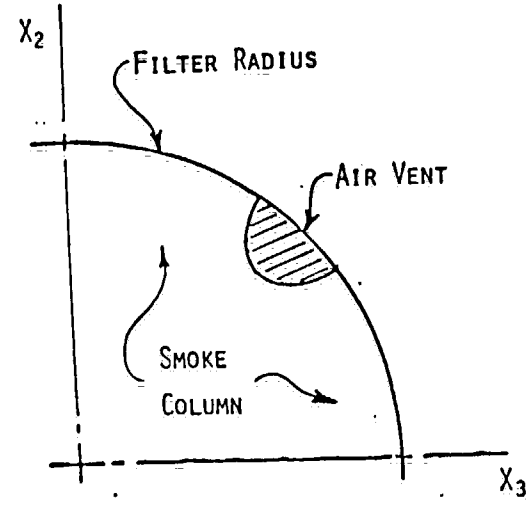

SYMMETRIC QUARTER - PLANE

X / R = 50%

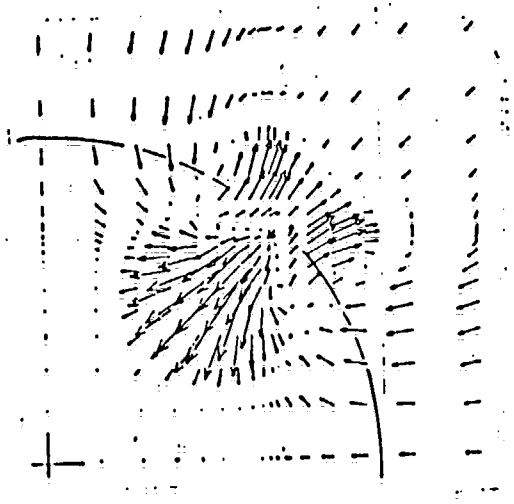

ACTRON FILTER

GENERATION OF VORTEX VELOCITY FIELD

X / R = 100%

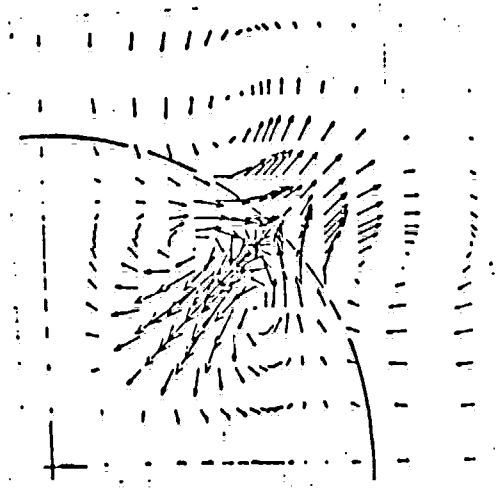

X / R = 150%

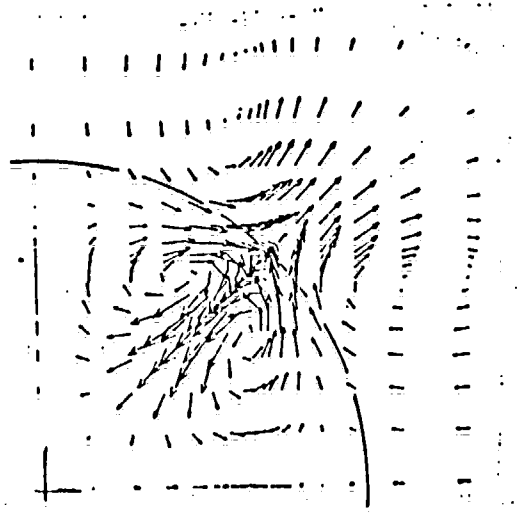

THREE-DIMENSIONAL PARABOLIC NAVIER-STOKES

MULTIPLE FREE-JET SECONDARY VORTEX FIELD

EXTREMUM VORTEX VELOCITY FIELD COMPARISONS

SMOKE FLOW VISUALIZATION

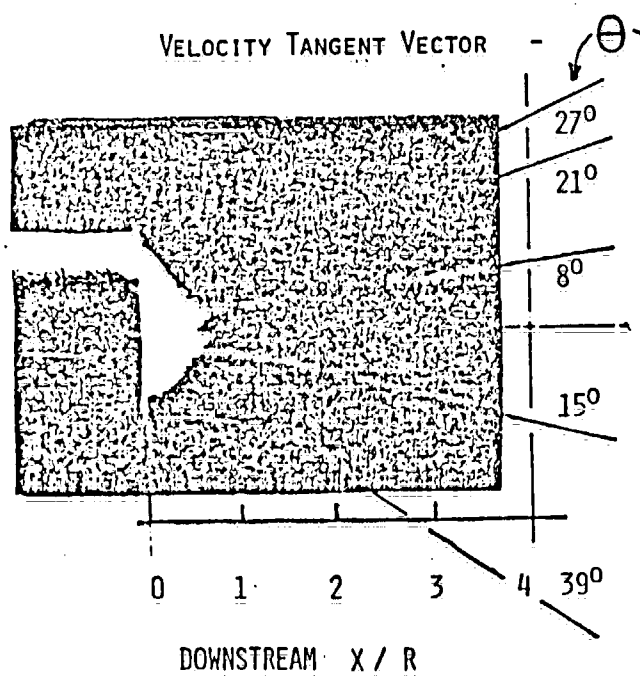

3DPNS PREDICTION

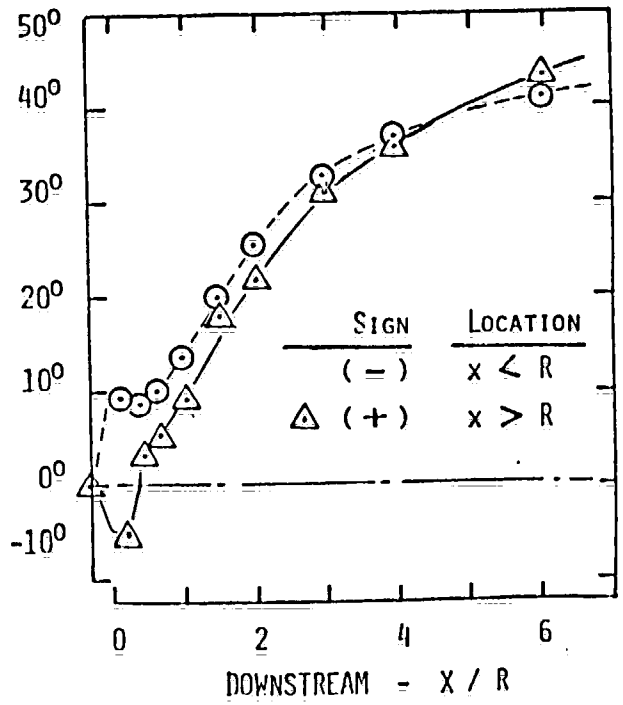

C M C: 3DPNS ANALYSIS - DISPERSION OF SMOKE

STANDARD INITIATION, 7° SWIRL

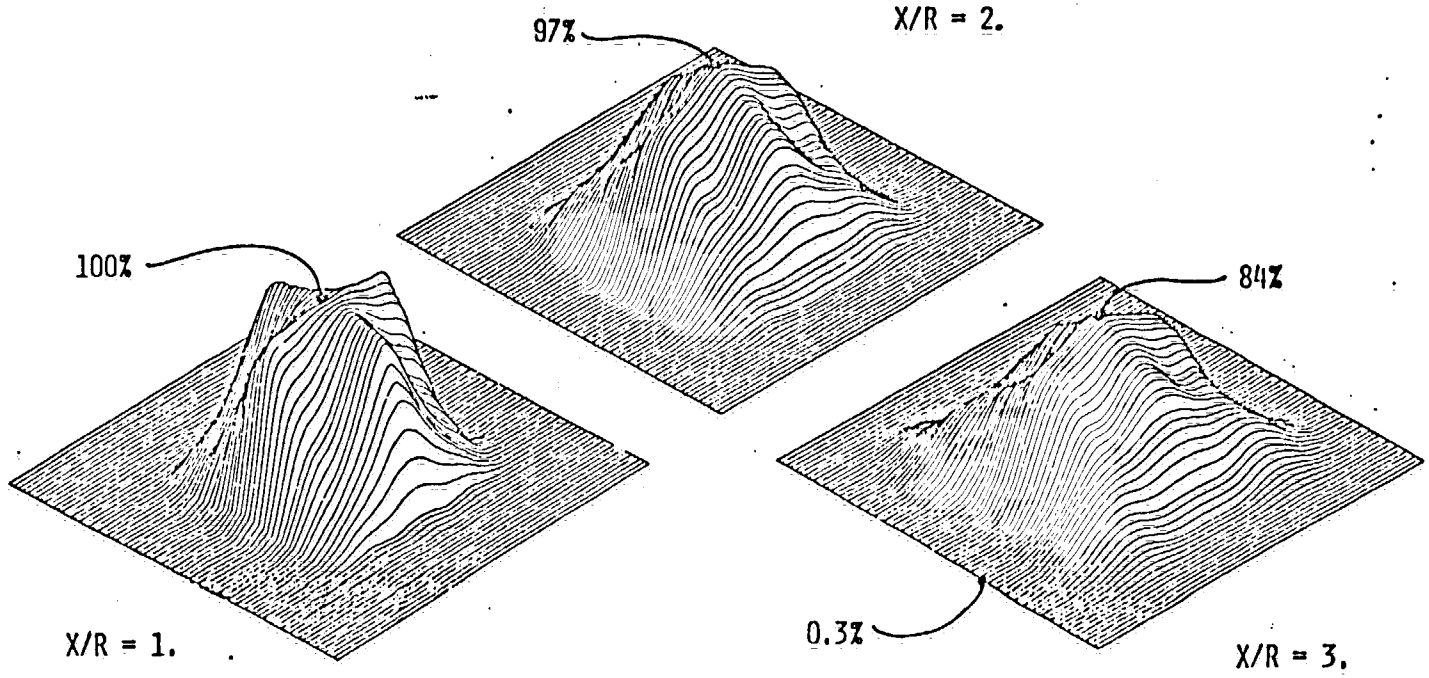

C M C: 3DPNS ANALYSIS - DISPERSION OF SMOKE

STANDARD INITIATION, 7° SWIRL

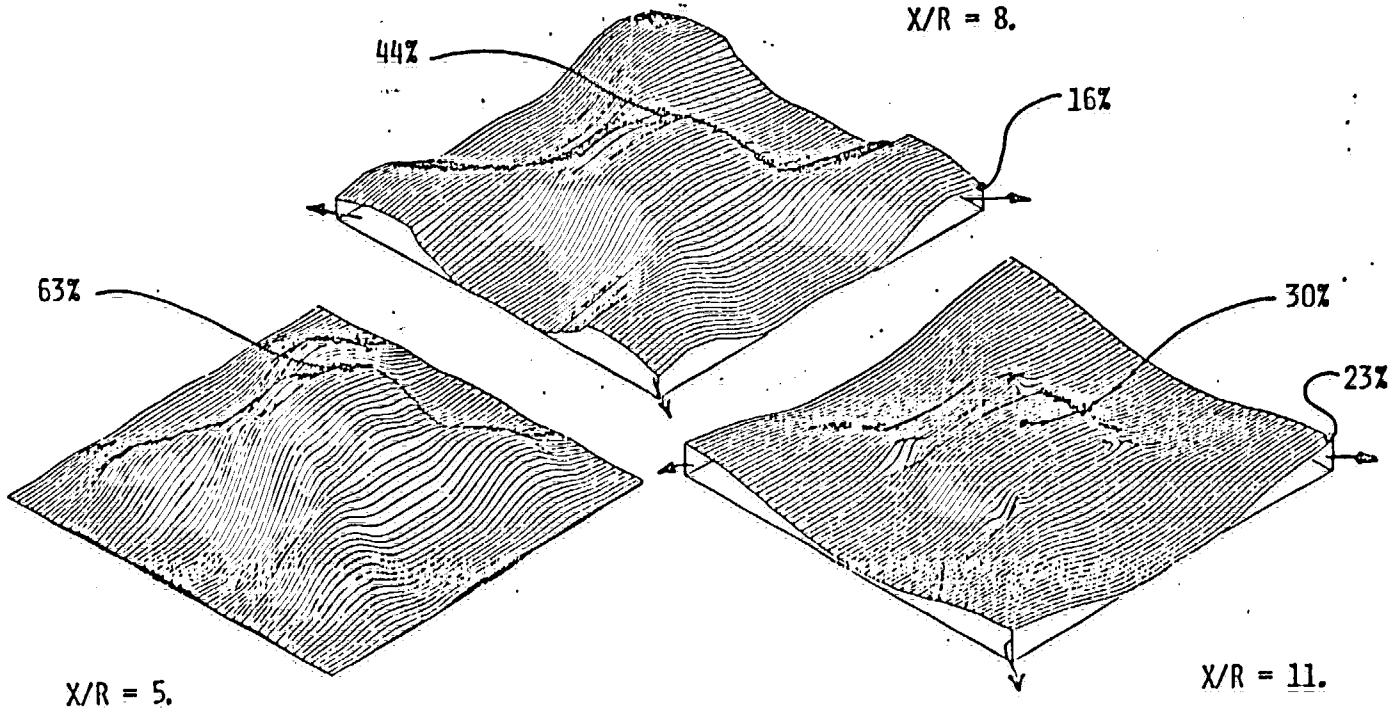

C M C: 3DPNS ANALYSIS - TURB. KINETIC ENERGY

STANDARD INITIATION - NO 7° SWIRL

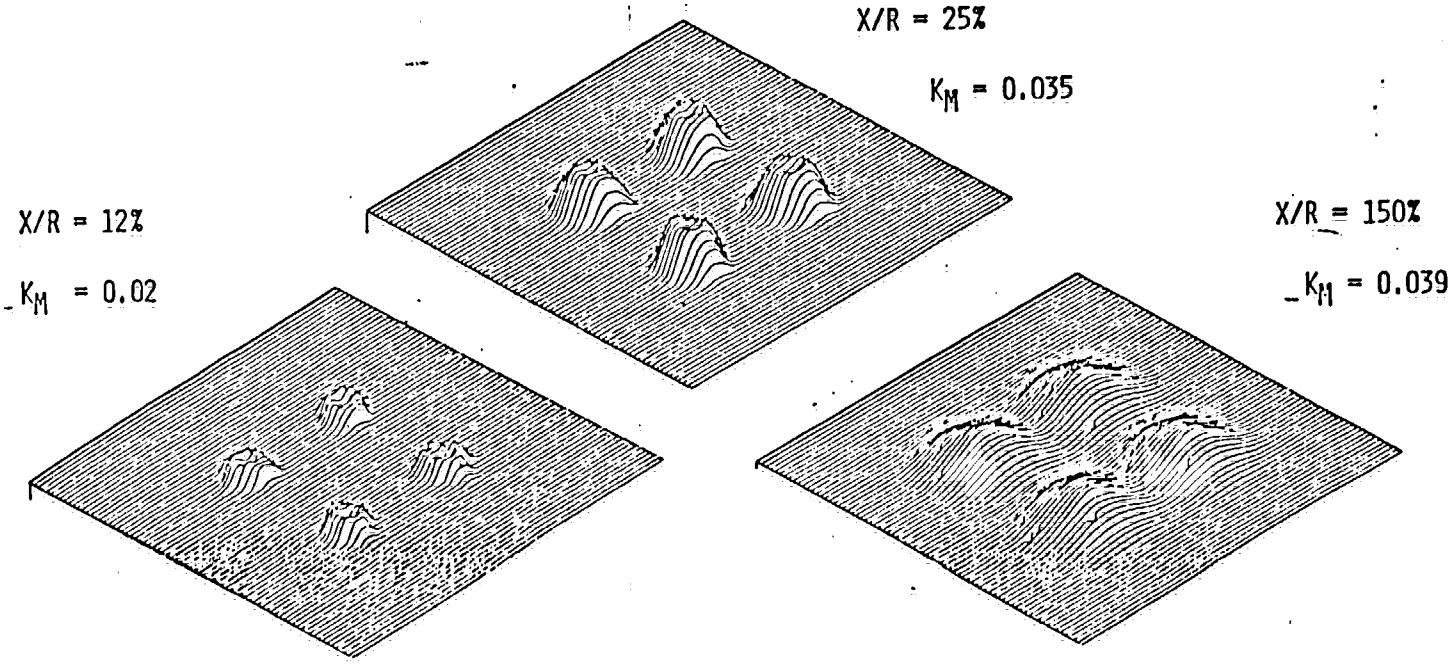

THREE-DIMENSIONAL PARABOLIC NAVIER-STOKES

MULTIPLE FREE-JET SECONDARY VORTEX FIELD

INFLUENCE OF INITIAL TURBULENCE UNCERTAINTY - X / R = 1.5

$k^o = 0.005$, $U_\ell^M = 0.067$ | $k^o = 0$, $U_\ell^M = 0.009$, | $k^o = 0.0025$, $U_\ell^M = 0.059$

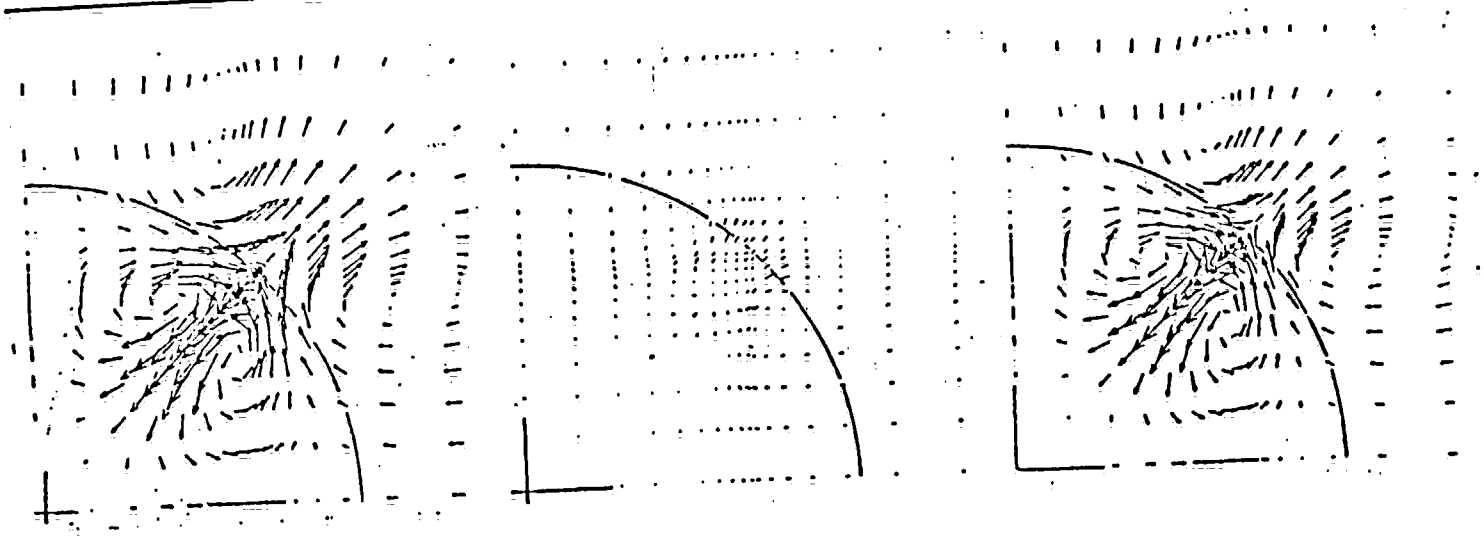

ACTRON FILTER

EFFECT OF TURBULENCE ON AERODYNAMICS

VENT VELOCITY DECAY

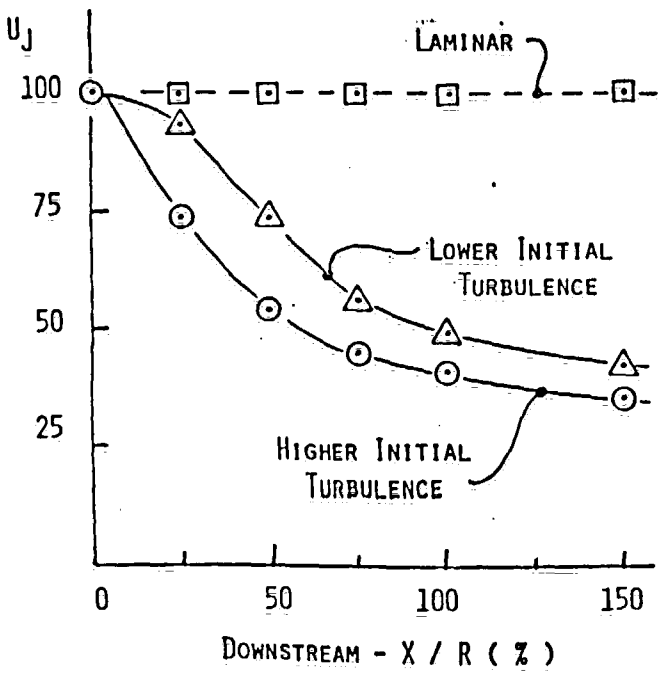

VORTEX VELOCITY MAXIMUM

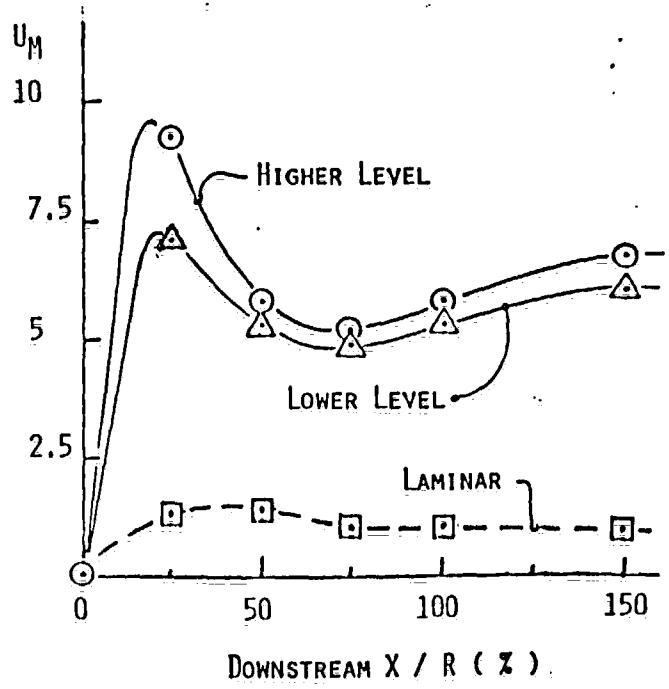

ACTRON FILTER

SLEEVE EFFECT ON VORTEX VELOCITY FIELD

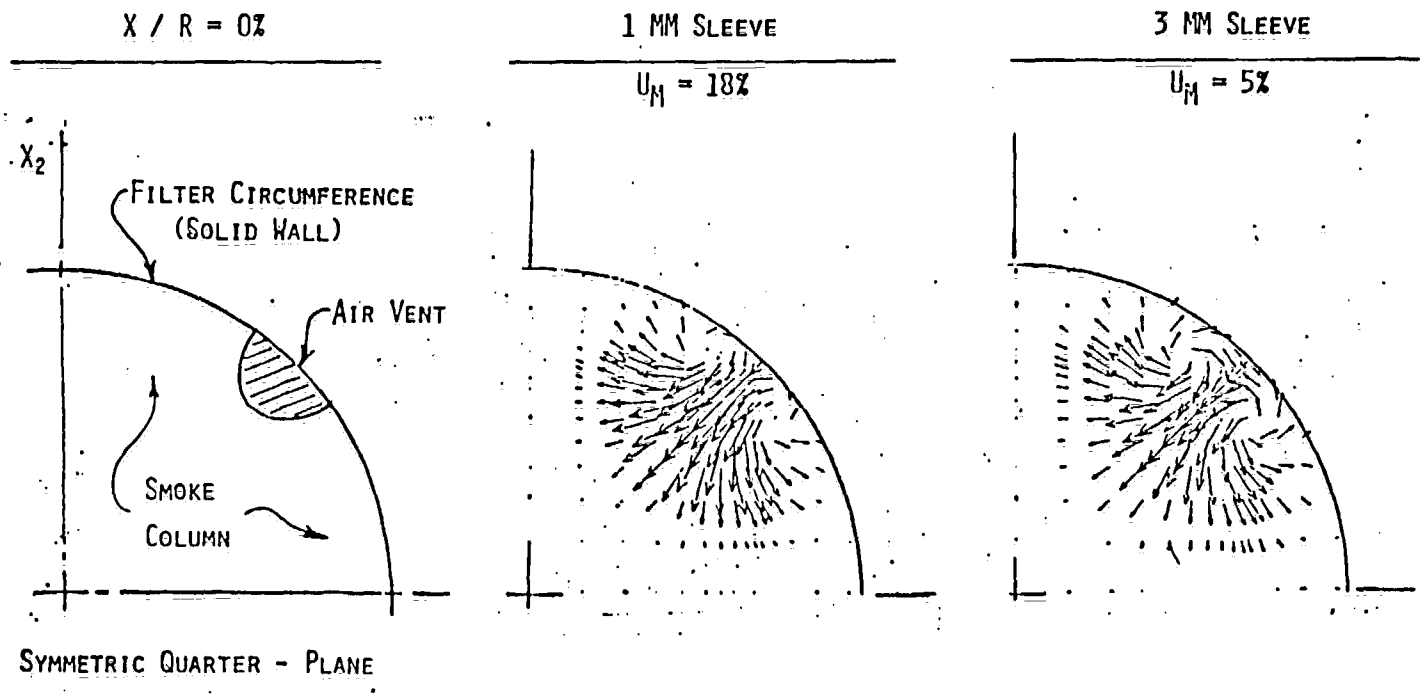

ACTRON FILTER

VORTEX VELOCITY FIELD, X/R = 150%

No Sleeve, U_M = 7%

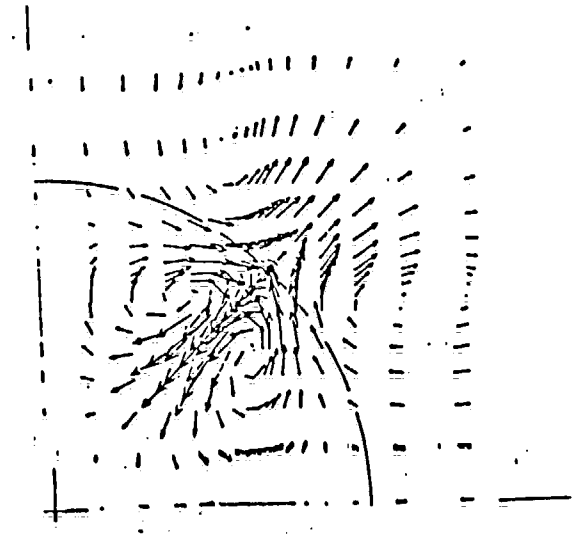

1 MM Sleeve, U_M = 5%

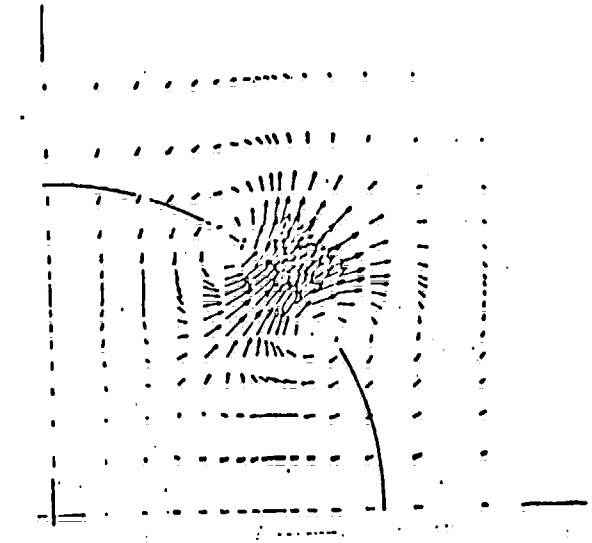

ACTRON FILTER

AERODYNAMICS MODIFICATIONS BY SLEEVED VENT

VORTEX VELOCITY MAXIMUM

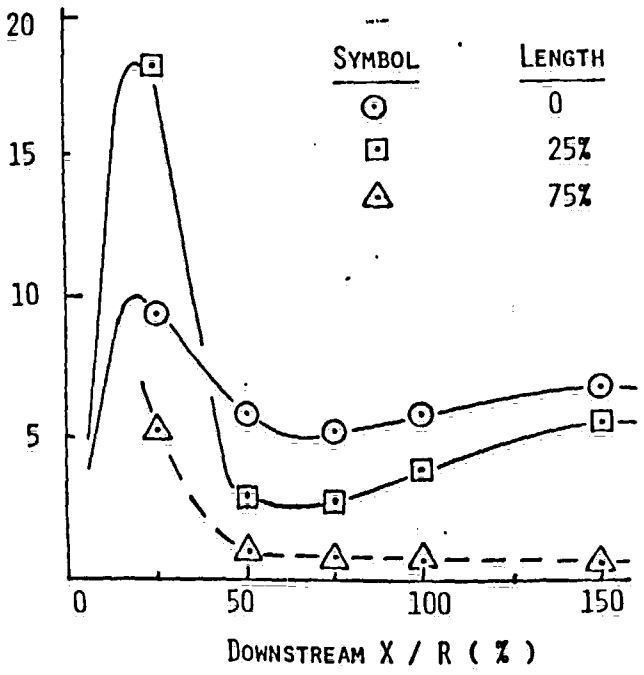

ESSENTIAL ACTION

NEARFIELD

- ENHANCE VENT DECAY
- PREVENT ENTRAINMENT
- STRENGTHEN VORTEX

FARTHER FIELD

- DISSIPATE VENT
- NO ENTRAINMENT
- WEAKEN VORTEX

ACTRON FILTER

AERODYNAMICS MODIFICATIONS BY SLEEVED VENT

VORTEX VELOCITY MAXIMUM

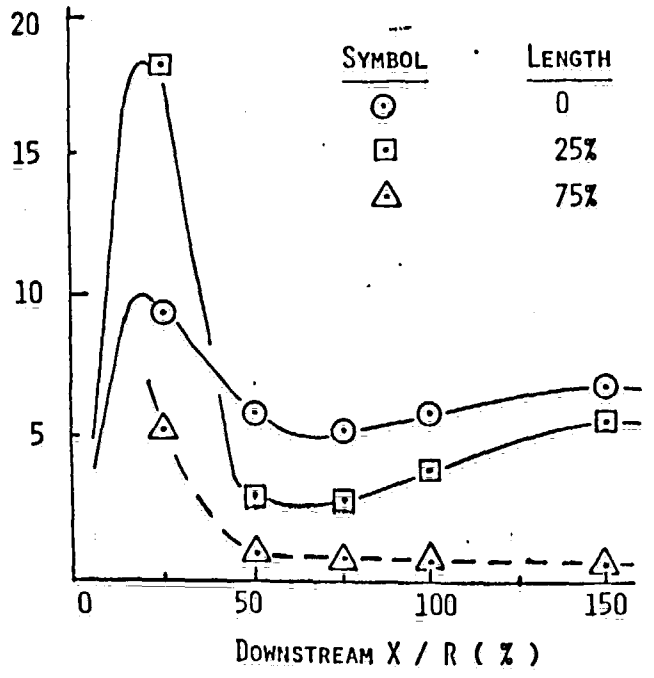

SENSORY RESPONSE EXPERIMENT

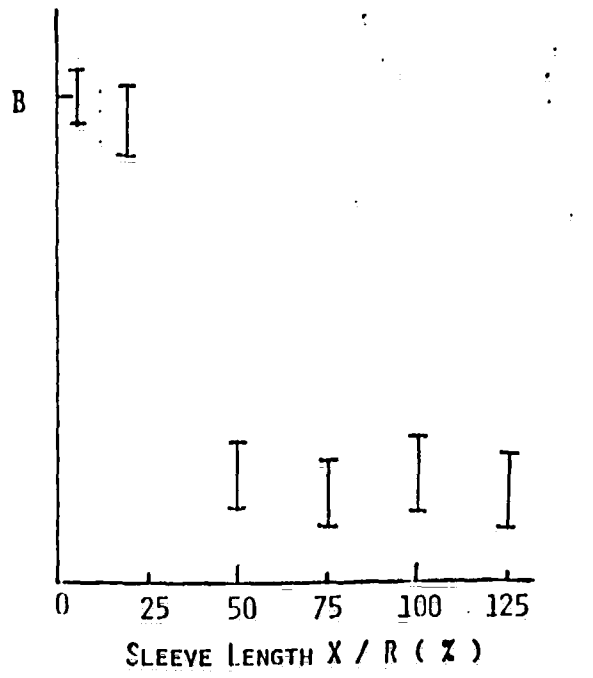

DRAFT ACCEPTED FOR PUBLICATION

AIAA COPY SHEETS

PREDICTION OF SECONDARY VORTEX FLOWFIELDS INDUCED BY MULTIPLE FREE-JETS ISSUING IN CLOSE PROXIMITY

A. J. Baker*, J. A. Orzechowski**, and G. E. Stungis*

Abstract

A continuity-constraint finite element numerical algorithm, for solution of the three-dimensional parabolic Navier-Stokes equations for subsonic turbulent flows, is applied to prediction of secondary vortex flowfields induced by multiple free-jets issuing in close proximity. The combined action of axial decay of the high speed jets, induced entrainment from the farfield, and geometric discreteness of the jets yields prediction of eight counter-rotating vortex pairs for a four-jet configuration. The extremum magnitude of the induced transverse vortex velocity can exceed 10% of that of the jet initial axial velocity. The results of the numerical predictions compare well with available video-graphic data, including the effects of geometric and initial flowfield modifications.

I. Introduction

An important aerodynamics problem class is assessment of the steady-flow interaction of multiple subsonic free-jets issued in close proximity. Dependent upon geometric parameters, and whether the jets are laminar or turbulent, this uniaxial initial configuration can induce detailed three-dimensional velocity fields characterized by large scale vortex structures. A substantial challenge in computational fluid mechanics is to identify and evaluate a numerical solution algorithm for prediction of this type of three-dimensional turbulent flowfield.

Figure 1 illustrates the essential geometry of a representative aerodynamic multi-jet system. Provided there is no reversal of the dominant component of velocity, parallel to the axis of the jets, the three-dimensional parabolic Navier-Stokes (PNS) equation system is a candidate for solution of the problem class. A formal order of magnitude PNS analysis confirms[1] that axial diffusion processes are negligible, and that the transverse momentum equations govern transverse plane pressure distributions. The continuity equation governs first order effects on momentum. For the free-jet problem class, the complementary solution to the resultant pressure Poisson equation is a homogeneous constant, where the Poisson equation is obtained from the divergence of the transverse momentum equations. A turbulence closure model is also required, and the parabolic form of the two-equation turbulence kinetic energy-isotropic dissipation system is representative of the minimum acceptable level of simplicity.

With the basic governing equation system thus defined, construction of a suitable algorithm requires addressing the ordering analysis and the farfield boundary conditions. A primitive variables formulation must rearrange the continuity equation to yield a deterministic system for transverse velocities, cf. Baker et.al.[1], Dodge[2], Patankar[3]. Alternatively, a vector potential function can be defined to identically satisfy the continuity equation, and a vorticity equation derived to replace the transverse momentum equations, cf. Briley et.al.[4], Ghia et.al.[5]. One dominant factor controlling this basic decision is that the multiple free-jet solution domain is unbounded. Hence, flowfield specification in the farfield is a priori unknown, ie., the entrainment action of the jet interaction that induces inflow/efflux across surfaces located arbitrary distances from the jet is a solution output. For this required flexibility, and the inherent mathematical robustness, the finite element penalty function algorithm[1] was selected. This paper presents a statement of the algorithm, boundary condition specifications, and the results of computational experiments compared with experimental data.

II. Problem Statement

The three-dimensional PNS equation system for the steady, subsonic turbulent flow of an isoenergetic fluid, to the principal scale of ordering[1], is

$$L(\bar{p}) = \frac{\partial}{\partial x_j}\left[\bar{\rho}\bar{u}_j\right] = 0 \tag{1}$$

$$L(\bar{u}_1) = \frac{\partial}{\partial x_1}\left[\bar{\rho}\bar{u}_1\bar{u}_1 + \bar{p}\right] + \frac{\partial}{\partial x_\ell}\left[\bar{\rho}\bar{u}_\ell\bar{u}_1 + \overline{\rho u_\ell u_1} - \frac{1}{Re}\frac{\partial \bar{u}_1}{\partial x_\ell}\right] = 0 \tag{2}$$

$$L(\bar{u}_k) = \frac{\partial p}{\partial x_k} + \frac{\partial}{\partial x_\ell}\left[\overline{\rho u_k u_\ell}\right] = 0 \tag{3}$$

$$L(k) = \frac{\partial}{\partial x_1}\left[\bar{\rho}\bar{u}_1 k\right] + \frac{\partial}{\partial x_\ell}\left[\bar{\rho}\bar{u}_\ell k + \bar{\rho}\left(C_k\frac{k}{\varepsilon}\overline{u_j u_\ell} - \bar{\nu}\delta_{j\ell}\right)\frac{\partial k}{\partial x_j}\right] + \bar{\rho}\,\overline{u_1 u_\ell}\frac{\partial \bar{u}_1}{\partial x_\ell} + \bar{\rho}\varepsilon = 0 \tag{4}$$

$$L(\varepsilon) = \frac{\partial}{\partial x_1}\left[\bar{\rho}\bar{u}_1\varepsilon\right] + \frac{\partial}{\partial x_\ell}\left[\bar{\rho}\bar{u}_\ell\varepsilon + \bar{\rho}C_\varepsilon\frac{k}{\varepsilon}\overline{u_j u_\ell}\frac{\partial \varepsilon}{\partial x_j}\right] + C_\varepsilon^1\bar{\rho}\,\overline{u_1 u_\ell}\frac{\varepsilon}{k}\frac{\partial \bar{u}_1}{\partial x_\ell} + C_\varepsilon^2\bar{\rho}\frac{\varepsilon^2}{k} = 0 \tag{5}$$

The variables appearing in equations 1-5 have their usual interpretation in fluid mechanics, where superscript bar denotes conventional time averaging[6], and the cross coupling of fluctuations in density and velocity have been assumed negligible. The tensor index summation convention is implied, with x_1 aligned with the principal flow direction, and $1 \le j \le 3$ and $2 \le (k,\ell) \le 3$. The turbulence kinetic energy k is the trace of the Reynolds stress tensor, ε is the isotropic dissipation function, and Re is the characteristic Reynolds number.

*Professor of Engineering Science, University of Tennessee, Knoxville, TN, Associate Fellow AIAA.

**Principal Programmer, Computational Mechanics Consultants, Inc., Knoxville, TN.

*Research Consultant, Brown & Williamson Tobacco Corp., Louisville, KY.

For the reported results, the Reynolds stress tensor field constitutive model of Baker et.al.[1] is employed. The PNS ordering analysis indicates the extremum significance of components of $\overline{u_i u_j}$ is one order smaller than unity. Simplifying the constitutive equation to this order yields

$$\overline{u_1u_1} = C_1 k - C_2 C_\mu \frac{k^2}{\varepsilon^2}\left[\left(\frac{\partial \bar{u}_1}{\partial x_2}\right)^2 + \left(\frac{\partial \bar{u}_3}{\partial x_3}\right)^2\right]$$

$$\overline{u_2u_2} = C_1 k - C_2 C_\mu \frac{k^2}{\varepsilon^2}\left[\frac{\partial \bar{u}_1}{\partial x_2}\right]^2$$

$$\overline{u_3u_3} = C_1 k - C_2 C_\mu \frac{k^2}{\varepsilon^2}\left[\frac{\partial \bar{u}_1}{\partial x_3}\right]^2$$

$$\overline{u_1u_2} = - C_\mu \frac{k^2}{\varepsilon}\frac{\partial \bar{u}_1}{\partial x_2}$$

$$\overline{u_1u_3} = - C_\mu \frac{k^2}{\varepsilon}\frac{\partial \bar{u}_1}{\partial x_3}$$

$$\overline{u_2u_3} = - C_2 C_\mu \frac{k^2}{\varepsilon^2}\left[\frac{\partial \bar{u}_1}{\partial x_2}\frac{\partial \bar{u}_1}{\partial x_3}\right] \qquad (6)$$

The coefficients C_α, $1 \le \alpha \le 4$, in equation 6 are correlation constants; the standard values $C_\alpha = \{0.94, 0.067, 0.56, 0.068\}$ were used for the present study.

In the primitive form, equations 1-6 do not represent a well-posed initial-boundary value problem discription for the subsonic flow, multiple free-jet problem class. As a consequence of the ordering, the scalar continuity equation governs both components of velocity in the transverse plane perpendicular to x_1. As cited in the Introduction, various algorithm constructions have been formulated to address this issue. The approach taken in the present analysis is to employ a finite element penalty function formulation, and to append the order (δ) transverse plane momentum equations,

$$L^\delta(\bar{u}_k) = \frac{\partial}{\partial x_1}\left[\bar{\rho}\bar{u}_1\bar{u}_k\right] + \frac{\partial}{\partial x_\ell}\left[\bar{\rho}\overline{u_\ell u_k} - \frac{1}{Re}\frac{\partial \bar{u}_k}{\partial x_\ell}\right] = 0 \qquad (7)$$

to equation 3. Further, equation 3 is rearranged to the pressure Poisson equation.

$$L(\bar{p}) \equiv \frac{\partial}{\partial x_k} L(\bar{u}_k) = \frac{\partial}{\partial x_k}\left[\frac{\partial \bar{p}}{\partial x_k} + \frac{\partial}{\partial x_\ell}\left(\bar{\rho}\,\overline{u_k u_\ell}\right)\right] = 0 \qquad (8)$$

Equation 8 represents a quasi-linear elliptic boundary value problem, possessing complementary and particular solutions[1]. For the free-jet problem class, the complementary solution is a homogeneous constant equal to the farfield reference pressure. The particular solution to equation 8 is thus obtained using homogeneous Dirichlet boundary conditions. Upon addition of equations 3 and 7, $L(\bar{u}_k) + L^\delta(\bar{u}_k)$ represents a well-posed initial-boundary value problem for $\bar{u}_k$, upon addition of the order (δ^2) terms to the appropriate scalar components of the Reynolds stress tensor, which are

$$\overline{u_\ell u_k}\Big|_{\delta^2} = - C_\mu \frac{k^2}{\varepsilon}\left[\frac{\partial \bar{u}_\ell}{\partial x_k} + \frac{\partial \bar{u}_k}{\partial x_\ell}\right] \qquad (9)$$

III. Finite Element Penalty Algorithm

Theoretical Statement

For the dependent variable set $\bar{q}(x_j) = \{\bar{u}_i, k, \varepsilon, \bar{p}, \overline{u_i u_j}\}$, equations 2, 3 + 7, 4, 5, 8, 6 + 9 represent a well-posed, initial-boundary value problem description on the three dimensional domain $\Omega = R^2 \times x_1 = \{x_1, x_\ell = x_\ell \in R^2$ and $x_1 \in [x_1, x_1]\}$. There is the additional fundamental requirement that equation 1 be rigorously satisfied, since it governs first order phenomena. The problem statement is completed with a polytropic equation of state for determination of $\bar{\rho}$ for the isoenergetic flow.

As the consequence of the PNS reformulation, each of the first six members of the set $\bar{q}$ are eligible for constraint, on the boundary ∂R of R^2, by a linear combination of Dirichlet and Neumann boundary conditions. The first five of these members are also required specified as an initial-condition on the plane $R^2 \times x_1$. No boundary conditions are appropriate for the algebraic equations governing $\overline{u_i u_j}$.

The finite element penalty algorithm, for determination of the semi-discrete approximation $\bar{q}^h(x_j)$ to $\bar{q}(x_j)$, is based on classical concepts for differential constraints in the statement of variational boundary value problems. These concepts are extended to the very non-linear PNS problem class using a Galerkin weighted-residuals formulation. Deferring details[7], the transverse plane domain R^2 is discretized into the union of non-overlapping subdomains R^2_e, wherein the functional form for the x_ℓ dependence of the semi-discrete approximaiton $\bar{q}^h$ is assumed a priori specifiable. A convenient form is the cardinal basis $\{N_k(x_\ell)\}$, the members of which are polynomials on x_ℓ complete to degree k. Hence, the semi-discrete approximation becomes the union of elemental approximations,

$$\bar{q}(x_j) \doteq \bar{q}^h(x_j) \equiv \bigcup_e \bar{q}^e(x_j) \qquad (10)$$

$$\bar{q}^e(x_j) \equiv (N_k(x_\ell))^T \{Q\}_e \qquad (11)$$

where subscript and/or subscript e denotes pertaining to the (finite element) domain R^2_e. Further, $\{Q\}_e$ represents the values taken by $\bar{q}^e$ at the nodes of the domain R^2_e and $1 \le l \le 12$ is a tensor index denoting the appropriate (nodal) vector dependent variable set of $\bar{q}^h$.

With definition of $\bar{q}^h$, equations 10-11 permit direct evaluation of the semi-discrete approximation error $L(\bar{q}^h)$ in each of the PNS governing differential equations. The basic concept in the calculus of a discretized variational boundary value problem is to render this error extremum in some norm. In the Galerkin weighed-residuals extension of this concept, this is accomplished by requiring this error to be orthogonal to the space of functions $\{N_k\}$ selected to define the semi-discrete approximation, i.e.

$$\int_{R^2} (N_k)\, L(\bar{q}^h)\, d\tau = \sum_e \int_{R^2_e} (N_k) L(\bar{q}^e)\, d\tau \equiv (0) \qquad (12)$$

The middle expression in equation 12 emphasizes that the actual calculus operations are performed on the elemental domains R^2_e. The resultant element (column) matrices are projected to the matrix structure of the global domain using the assembly operator S_e, which is simply matrix addition by rows[7].

Equation 12 defines the numerical solution algorithm for the complete set $\tilde{q}^h$ with the exception of the combined equations 3 and 7 for $\tilde{u}_k$. Here, the definition of the extremum must be augmented (penalized) such that the continuity equation is also satisfied. The functional form for this statement, which is an extension of the classical concept[7], is

$$\int_{R^2}(N_k)\left[L\left(\tilde{u}_k^h\right) + L^\delta\left(\tilde{u}_k^h\right)\right]d\tau - \lambda\int_{R^2}\frac{\partial(N_k)}{\partial x_k}L\left(\tilde{p}^h\right)d\tau \equiv \{0\} \tag{13}$$

The actual calculus operations defined in equation 13 are again performed on an elemental basis and assembled, and λ is an (arbitrary) parameter penalizing the statement of semi-discrete error orthogonalization for $\tilde{u}_k^h$.

Equations 12-13 define the finite element penalty algorithm for the PNS equation system. The theoretical arbitrariness remaining is solely the degree k of the cardinal basis $\{N_k\}$, spanning either three-sided or four-sided-element domains R^2_e, and the penalty parameter λ and functional form for $L(\tilde{p}^h)$. However, equations 12-13 are definitions of non-linear matrices, and resolution of the resultant problem definitions in linear algebra remains. For the semi-discrete approximations $\{\tilde{u}_i, k^h, \tilde{p}^h\}$, equations 12-13 are matrix statements expressing the x_j-ordinary derivative of the appropriate elements of $\{QI\}_e$, equation 11. A Taylor series defines the matrix algebra statement for the assembly of these elements of $\{QI\}$, $1 \le I \le 5$, as

$$\{FI\} \equiv \{QI\}_{j+1} - \{QI\}_j - \Delta x\{QI\}'_{j+\theta} - \ldots \equiv \{0\} \tag{14}$$

In equation 14, $\{QI\}'_{j+\theta}$ represents this ordinary derivative evaluated at some location on the interval $x_{j+1} - x_j = \Delta x$ as defined by the parameter $0 \le \theta \le 1$.

Equation 12, evaluated for $\tilde{p}^h$ and $\widetilde{u_i u_j}^h$, yields directly the appropriate column matrix statement $\{FI\} = \{0\}$, $6 \le I \le 12$. Combined with equation 14, the resultant linear algebra statement of the finite element penalty algorithm for the PNS equation system, becomes

$$\left\{FI\left(k,\ \lambda,\ \theta,\ \Delta x,\ \{QI\}\right)\right\} = \{0\} \tag{15}$$

Equation 15 is a highly non-linear algebraic equation system, the character of which is largely determined by the choice of the arbitrary solution parameters k, λ, θ, and Δx. Equation 15 does not readily admit a useful linearization, even for $\theta = 0$ which corresponds to explicit integration. Hence, the appropriate solution statement is the (Newton) matrix solution form,

$$\left[J\left(\{FI\}\right)\right]^p_{j+1}\{\delta QI\}^{p+1}_{j+1} = -\{FI\}^p_{j+1} \tag{16}$$

where p is the iteration index at step x_{j+1}, and

$$\{QI\}^{p+1}_{j+1} \equiv \{QI\}^p_{j+1} + \{\delta QI\}^{p+1}_{j+1} \tag{17}$$

$$\left[J\left(\{FI\}\right)\right] \equiv \frac{\partial\{FI\}}{\partial\{QJ\}} \tag{18}$$

Equation 17 defines the fully-discrete approximation to the dependent variable set at the nodes of UR^2_i, hence also $\tilde{q}^h(x_j)$ throughout R^2, see equation 10. Equation 18 defines the (Newton) Jacobian of the non-linear algebraic equation system, equation 15.

Some Basic Decisions

Equation 15 delineates the basic decisions to be made regarding implementation of the penalty algorithm into a computer code. In addition, for $\theta > 0$, a decision is required regarding approximate construction of the Newton algorithm Jacobian $[J]$, equation 18, since it's size for the twelve dependent-variable PNS statement is unwieldy on present computers. The decision on k, equation 11, of course impacts considerably on the "size" of $[J]$.

The multiple free jet analyses reported herein were conducted using the CMC:3DPNS computer program.[5-10] Each of the basic decisions have been made and evaluated for this code. The discretization of R^2 is defined as the union of triangular cross-section finite elements spanned by the linear (k=1) natural coordinate cardinal basis. The trapezoidal rule is employed for the integration algorithm, $\theta = \frac{1}{2}$ in equation 14. The penalty parameter λ, following extensive numerical experimentation, is defined as the diagonal matrix,

$$\lambda^p \rightarrow [\lambda]^p \equiv C\ \Delta x\ [UI]^p_{j+1} \tag{19}$$

where C is a constant of order unity, and the elements (on the diagonal) of $[UI]^p_{j+1}$ are $\{UI\}^p_{j+1}$, the nodal distribution of $\{QI\}$ computed at each iteration p at x_{j+1}.

The functional form of the penalty term, equation 13, involves definition of an auxiliary dependent variable ϕ^h, as

$$L(\tilde{p}^h) = \frac{\partial}{\partial x_j}\left(\tilde{p}^h\tilde{u}^h_j\right) \equiv \frac{\partial^2\phi^h}{\partial x_j^2} \tag{20}$$

The boundary conditions for ϕ^h are a linear combination of homogeneous Dirichlet and Neumann constraints, defined according to required flow porosity on various segments of ∂R. Hence, $\tilde{q}^h$ is augmented for one additional entry, the solution of

$$L(\phi^h) = \frac{\partial^2\phi^h}{\partial x_j^2} - \frac{\partial(\tilde{p}^h\tilde{u}^h_j)}{\partial x_j} = 0 \tag{21}$$

The Galerkin weighted-residuals algorithm statement for equation 21 is the algebraic equation system $\{F13\} = \{0\}$, which is added to equation 15, hence equations 16-18. Therefore, the explicit form of the complete penalty term in equation 13 is.

$$\lambda \int_{R^2} \frac{\partial (N_k)}{\partial x_i} L(\bar{p}^h) d\tau \equiv S_e \left[C\Delta x \int_{R^2_e} [U] \frac{\partial (N_k)}{\partial x_j} (N_k)^T \{\phi\}_e d\tau \right] \quad (22)$$

Regarding the Newton algorithm Jacobian, equation 18, is replaced with two sparse matrices, yielding a corresponding compromise on overall convergence rate while significantly reducing the matrix rank. The initial-valued dependent variables $(\bar{u}_i^h, k, \varepsilon)$ are sequentially solved as multiple right side substitutions to equation 16, using the $\bar{u}_i^h$ Jacobian, $[J11]_{j=1}$, where

$$[J11] \equiv \frac{\partial \{F1\}}{\partial \{U1\}} \quad (23)$$

The Poisson field variables $(\bar{p}^h, \phi^h)$ are solved sequentially as multiple right side substitutions using the $\bar{p}^h$ Jacobian [J66]. The scalar components of $\bar{u}_i \bar{u}_j$ are determined using an elemental averaging and assembly procedure, equivalent to solving equation 16 using [J77] for multiple right side substitutions. The algorithm timing utilizes the sequence [J11], [J66], [J77], with update of the Jacobians occurring at every iteration. Details of the formation of these Jacobians is given in reference 7.

IV. Results and Discussion

Benchmark Tests

The PNS finite element penalty algorithm, as operational in the CMC:3DPNS computer code, is well documented for subsonic aerodynamic problem definitions involving semi-bounded and fully bounded solution domains [1,11]. Additional documentation is reported[12] for an unbounded aerodynamic wake-type flow. Each of these includes detailed comparisons between algorithm prediction and experimental data, including the complete Reynolds stress tensor for two- and three-dimensional geometries. These comparisons serve to quantitatively verify the appropriateness of the "standard" turbulence model constants C_α, equation 6, which are used for the free-jet analyses.

As the typical case in three-dimensional, turbulent aerodynamic flow prediction, quality experimental data to initiate solutions is usually non-existent. Hence, tests were conducted to evaluate self-generation of initial conditions for the free-jet configuration. The basic assumption was that the sole available initial data is the dominant velocity scalar component $\bar{u}_1(x_1, x_2)$ on the PNS solution initiation plane. Figure 2 illustrates a two-dimensional slot jet test problem thus characterized by $\bar{u}_1^0(x_2) \equiv \bar{u}_1^0$, within and exterior to the jet. Since a non-zero background level of dissipation function is a computational requirement (ε^{-1} appears throughout equations 4-6), background levels of both $k^0 > 0$ and $\varepsilon^0 > 0$ are defined to yield a background "turbulent viscosity" level $\nu_t^0 = C_\mu k^2/\varepsilon$ of the order of the laminar viscosity ν. Numerical experimentation indicates $k^0 = O(10^{-4})$ and $\varepsilon^0 = O(10^{-9})$ yield adequate algorithm stability. At the knee of the profile in $\bar{u}_1^0$, Figure 2, the initial level of turbulent viscosity is assumed known, e.g., $10 \leq \nu_t^0/\nu \leq 10^2$. Since the nominal extremum order of k is $O(10^{-2})$, this can be achieved by setting $k^0 = O(10^{-2})$ and $\varepsilon^0 = O(10^{-7})$.

Figure 3 summarizes the PNS penalty algorithm prediction for the symmetric-half slot jet problem, for $\bar{u}^0_{lower} \equiv 0.02\ \bar{u}^0_{jet} \equiv u^0_{upper}$ and $\nu_t^0 = O(10^2)$, on the span $0 \leq x_1/H_f \leq 1.0$, where H_f is the slot jet half-width. The initial condition for $\bar{u}_1^0$ was interpolated as a step function on the nodes of the discretization of x_2, yielding the spiked initial conditions for k^0 and ε^0 shown as solid lines. The maximum levels of k and ε increase by a factor of 2-4, by $x_1/H_f = 0.5$, and thereafter decrease monotonically as the enhanced level of ν_t diffuses into the velocity defect region. The jet potential core is eroded by about 25% by $x_1/H_f = 1.0$.

Figure 3b) summarizes the entrainment action predicted by the penalty algorithm. By definition, $\bar{u}_2 \equiv 0$, as shown by the solid line. Since the order delta $\bar{u}_2$ momentum equation is homogeneous, the sole source for $\bar{u}_2 \neq 0$ is the action of the penalty constraint in equation 13. The PNS solution indicates a large entrainment at $x_1/H_f = 0.5$, where $\bar{u}_2 = -0.1$ in the farfield, which progressively moderates as the solution proceeds further downfield. The boundary conditions for ϕ for this geometry are $\phi = 0$ at the farfield and $\partial\phi/\partial x_2 = 0$ on the symmetry line.

The second basic test is the three-dimensional problem of a single jet of initially circular cross-section. For this case, $\bar{u}_{jet} = \bar{u}_1^0$ (= 30 m/s) and $\bar{u}^0_{exterior} = 0.1\ \bar{u}_1^0$. Figure 4 summarizes the PNS prediction of transverse half-plane velocity field at $x_1/H_f = 1.0$, where H_f is the radius of the initial jet, for laminar flow and for turbulent flow with $\nu_t^0 = 10$. Both solutions exhibit the required symmetries and predict essentially radial entrainment. The plot length of each individual velocity vector is the measure of the relative magnitude of $\bar{u}_2$, scaled to the local predicted extremum magnitude $\bar{u}_2^m$. For the laminar flow prediction, $\bar{u}_2^m = 0.0017$, while $\bar{u}_2^m = 0.044$ for the turbulent case. Thus, the measure of magnitude of entrainment for the turbulent case is approximately 20 times that for the laminar case, in qualitative agreement with expected behavior. The boundary conditions for ϕ for this case are $\phi = 0$ everywhere in the farfield and $\partial\phi/\partial x_2 = 0$ on the symmetry plane. As in the two-dimensional test, $\bar{u}_2^0 \equiv 0$, and the penalty term in equation 13 is the sole causal mechanism initiating and maintaining the computed transverse plane velocity field.

Multiple Free Jet PNS Prediction

The multiple jet case of main interest corresponds to a symmetric four-jet geometry with the jets located in close proximity and of small initial diameter. This configuration is verified, using experimental smoke flow visualization techniques, to rapidly induce a substantially large transverse plane velocity field which efficiently pumps fluid, initially interior to the circumference of the jets, into the exterior region. Figure 5a) illustrates the persistant unidirectional flow of smoke obtained with the multi-jet system inoperable. Figure 5b) shows the rapid smoke dispersal promoted by the multiple jet system operating at design conditions.

Figure 6 is a layout sketch of the multiple jet device indicating characteristic dimensions. Operating on design, free air is induced to flow down each vent channel, of length 0.02 m, at a nominal velocity $\bar{u}_j = 12$ m/s. The locator radius of the jets is R = 0.004m, and the initial hydraulic diameter of each jet is d_j = 0.001 m. In the region interior to R, $\bar{u}_1^o = 0.02\ \bar{u}_\infty^o$ while in the essentially unbounded exterior region $\bar{u}_1^o = 0$. The characteristic Reynolds number for the jet flow is $Re = 10^6$/m, and the vent channel walls are quite rough.

The symmetry of this multiple jet geometry permits the majority of PNS calculations to be performed on the symmetric quarter domain with boundary OABC, Figure 6. Figure 7 graphs this domain showing the nodal coordinates of the basic M = 19 x 19 non-uniform computational mesh. The lateral extent of the domain spans twice the locator radius R. Segments OA and OB are symmetry planes, upon which the normal component of velocity vanishes and all other variables possess vanishing normal derivatives. Boundary segment ACB is assumed sufficiently remote, such that all dependent variables have vanishing normal derivatives except ϕ, which vanishes identically since the boundary is porous.

For the basic assessment, the sole specified initial conditions are $\bar{u}_1^o(x_1, x_\ell)$, and the levels of ν_t^o in the air jet and background flows. Since the PNS predicted secondary vortex flow field develops very rapidly, a relatively large (20%) background $\bar{u}_1^o$ velocity field was used for efficiency. (The PNS algorithm stability was marginal using a 10% background flow specification. Small, but not significant differences were predicted in $\bar{u}_1(x_1, x_\ell)$ distributions at various stations downstream of the injector face. The assumed initial level of ν_t exerts a much more significant influence.) Therefore, within the air jet, $\bar{u}_1^o = 1.2\ U_\infty$, where U_∞ = 12 m/s, the design velocity. Everywhere exterior to the locator radius, $\bar{u}_1^o \equiv 0.2\ U_\infty$, and interior $\bar{u}_1^o \equiv (0.2 + 0.02)\ U_\infty$. Hence, the $\bar{u}_1^o$ velocity strain-rate distribution on the initial surface plane was on-design. Further, within the air jet $k^o \equiv 0.005$, with ε^o defined such that $\nu_t^o/\nu = 35$. Everywhere exterior to the jet, $k^o = 0.0001$ and $\nu_t^o/\nu = 3$.

Figure 8 is a composite of the multiple vortex secondary velocity field predicted by the PNS algorithm at $x_1/R = 1.5$, ie., 6 mm downstream from the plane of solution initiation. As in Figure 4, each velocity vector length is scaled to the extremum predicted level $(\bar{u}_\ell/U_\infty)_{max} \equiv u_T^m = 0.067$. The original location of each air jet coincides with the clustering of large radial velocities, and the net action of the four-jet device is to induce a system of eight symmetrically disposed, counter-rotating transverse vortex pairs. At this x_1 station, the maximum axial velocity component within the initial jet region was $\bar{u}_1 = 0.35$, hence the local ratio $u_T^m/u_T^m = 0.19$ is quite substantial in comparison to the PNS ordering analysis.

Quarter-plane plots of the PNS predicted evolution of the transverse plane vortex flowfield in the near vicinity of the locator radius and air jet are shown in Figure 9. A substantial field exists by $x_1/R = 0.5$, which is 2 mm downstream from the initial condition plane, although the vortex pattern has not matured. However, by $x_1/R = 1.0$, Figure 9b), the counterrotating pattern is clearly evident and $u_T^m = 0.038$ has remained essentially constant. By $x_1/R = 1.5$, Figure 9c), the visual appearance of the $\bar{u}_\ell$ distribution is nominally unchanged, although the overall strength has increassed by about 13%, since $u_T^m = 0.067$. The visual appearance of the double counter-rotating vortex pattern shown in Figure 9c) persists essentially unchanged for distances up to $x_1/R = 11$ downstream of the initial condition plane.

A species continuity equation, similar in appearance to equation 7, was added to the PNS system, to permit tracking of the distribution of fluid initially interior to the locator radius R. Figure 10a shows the $Y^o = 100\%$ smoke distribution at the solution initiation plane; the four troughs correspond to the location of the four air jets. Diffusion processes dominate on $0 \le x_1/R \le 1$, Figure 10b), and the extremum smoke concentration Y_m remains 100%. By $x_1/R = 2.0$, $Y_m = 97\%$, at $x_1/R = 3.0$ $Y_m = 84\%$, and the first non-zero level Y_e occurs at the boundary ∂R of the PNS domain at $x_1/R = 5.0$, Figure 10c), where $Y_m = 63\%$. By $x_1/R = 11.0$, Y_m has decreased to 39% and $Y_e = 23\%$, Figure 10d). Hence, the counter-rotating vortex system has homogenized the initial smoke level within a distance of about 44mm. Of greatest significance, on ∂R at $x_1/R = 11.0$, $\partial Y/\partial x_j \cdot n_j > 0$ confirms that the material transport is dominated by convection, in qualitative agreement with the smoke flow visualization experimental data.

Figure 11 summarizes the PNS computed distribution of turbulent kinetic energy $k(x_\ell)$ on $0 \le x_1/R \le 1.5$. The initial condition is $k^o = 0.005$, Figure 11a), within the jets and $k^o = 0.0001$ elsewhere. Due to the rapid decay of the air jets, the extremum level of k at $x_1/R = 0.12$ has increased sharply to $k_m = 0.022$, Figure 11b). This has further increased to $k_m = 0.035$ at $x_1/R = 0.25$, Figure 11c), and the crater shape of each profile is clearly evident. Diffusional processes eventually smooth the distributions, Figure 11d), and the extremum level has been reached, $k_m = 0.039$. Continuing downstream, the distributions of k become further homogenized at nominally the same maximum level.

A series of computational experiments were conducted to ascertain importance of assumed initial turbulence level on the PNS prediction. For one test, k^o was halved to $k^o = 0.0025$ and ε^o held constant, yielding $\nu_t^o/\nu = 9$. A second test was conducted with the air jets assumed laminar. Figure 12 summarizes these predictions in terms of decay of the jet velocity extremum, $\bar{u}_1^m(x_1)$, and the extremum predicted vortex velocity component $u_T^m(x_1)$. For the laminar flow case, the air jet extremum does not decrease at all on $0 \le x_1/R \le 1.5$, and the induced transverse plane component hovers about $u_T^m = 0.01$. In distinction, halving the initial turbulence level simply displaces the jet decay curve to the right, a distance of $\Delta x_1/R = 0.25$, and yields an extremum transverse component that is only modestly smaller by about $\Delta u_T^m = 0.005$. In comparison to the experimental data, these predictions confirm the importance of the vent channel roughness in promoting the desired action of the multi-jet system. In the same sense, the assumed initial level for k^o does not appear critical, in terms of the PNS solution, predicting a qualitatively valid solution, provided ν_t^o is sufficiently large to permit self-generation of solutions to the k-ε equation system.

Additional experimental data confirms that sufficient protrusion of the locator radius surface beyond the multi-jet injector face can markedly reduce the level of visually apparent swirling motion. This geometry modification was modeled by assuming the locator radius R, Figure 7, was a solid surface for a specified distance $\Delta x_1/R$ downstream. Hence, the initial PNS solution domain is contained within the radius surface, and the boundary conditions on this surface are $\bar{q}^m = (0)$. After marching the prescribed distance, the PNS solution is

stopped, the locator radius surface is computationally removed and the remainder of the solution domain OABC added, and the PNS solution restarted using the current solution as initial conditions.

Figure 13 summarizes the resulting PNS prediction of $\bar{u}_t(x_1,x_t)$. Since the solid locator radius surface is a sink for momentum, one expects that a proportionally larger level of transverse plane velocity will result. Figure 13a) confirms this for a 1 mm extension. The nominally radial flow from the jet region is evident, it does not penetrate the radius boundary, and $u_t^m = 0.182$ is more than double the extremum predicted without the extension. Figure 13b) shows the $\bar{u}_t$ distribution computed at $x_1/R = 0.75$ with the solid surface appended. A weak vortex pair is barely discernable, and $u_t^m = 0.052$ has decayed by a factor of three. Figure 13c) shows the $\bar{u}_t$ distribution computed at $\Delta x_1/R = 1.5$, downstream of the 1 mm extension, which used the data of Figure 13a) as initial conditions. Comparing to the on-design solution, Figure 9c), a single vortex pair of much weaker strength has replaced the basic prediction. Even though the extremum of $\bar{u}_t^m = 0.055$ is only modestly decreased, the vortex pattern of Figure 13c) would be much less effective in promoting convection of material from within the interior region.

For a final computational experiment, the available smoke flow visualization data indicate that the multiple jet device efficiency is only modestly altered by partial blocking of one of the initial jets. Since this constraint destroys the inherent geometric symmetries, the PNS solution domain must now encompass a region that is a factor of four larger. Figure 14 graphs the transverse velocity distribution $\bar{u}_t$ at $x_1/R = 1.5$ on an M = 19 x 19 mesh that is twice as coarse as the base discretization, Figure 7. However, comparing Figure 8 and 14 confirms that the coarse grid full solution has captured the essential eight-vortex pair structure, and $\bar{u}_t^m = 0.084$ is within 20% of the finer grid extremum, Figure 9c).

Figure 15 graphs the PNS predicted transverse plane velocity distribution $\bar{u}_{t_n}$ at $x_1/R = 1.5$ obtained with the lower right jet completely shut off. A through-flow has resulted over the occluded jet, and the extremum level of $u_t^m = 0.12$ is about 50% larger than the design configuration. Figure 16 compares the computed distributions of smoke density at $x_1/R = 6.0$ for both coarse grid solutions. Figure 16a) compares visually with the finer grid solution, Figure 10c), and $Y_m = 53\%$ lies on the interpolation of trajectory extremum. The loss action of the occluded vent is clearly evident in Figure 16b), although $Y^m = 59\%$ is only 10% larger than the on-design solution. These PNS predictions thus agree qualitatively with the field data, and further permit a quantitative comparison measure of the action of design modifications.

V. Conclusions

The finite element penalty numerical solution algorithm for the three-dimensional parabolic Navier-Stokes equations, for subsonic turbulent flows, has been applied to prediction of secondary vortex flowfields induced by multiple free-jets issuing in close proximity. The combined action of rapid jet decay and discreteness of the multiple jet configuration has been quantitatively assessed regarding resultant entrainment and secondary vortex structures. No detailed experimental measurements are available for comparison of the numerical predictions. However, interpretation of inexpensively acquired video-graphic smoke flow visualization data has provided a basis for qualitative comparisons. Further, a range of computational experiments were conducted, involving parameter variations, that permitted further qualitative comparisons. The availability of the computer program embodiment of the theory, as a computational laboratory, has been verified of utility and of sufficient versatility to permit a range of experiments. It is fair to assume that this constitutes one small step towards the eventual realization of computational fluid dynamics as a diagnostic practice.

VI. References

1. Baker, A. J., and Orzechowski, J. A., "An Interaction Algorithm For Three-Dimensional Turbulent Subsonic Aerodynamic Juncture Region Flow," AIAA J., V. 21, 1983, to appear.

2. Dodge, P. R. and Lieber, L. S., "A Numerical Method For the Solution of Navier-Stokes Equation For a Separated Flow," Technical Paper AIAA-77-170, 1977.

3. Patankar, S. V., Numerical Heat Transfer and Fluid Flow, McGraw-Hill/Hemisphere, NY, 1980.

4. Briley, W. R., and McDonald, H., "Analysis and Computation of Viscous Subsonic Primary and Secondary Flows," Technical Paper AIAA-79-1453, 1979.

5. Mikhail, A. G. and Ghia, K. N., "Analysis and Asymptotic Solutions of Compressible Turbulent Corner Flow," Trans. ASME, J. Engr. Power, V. 104, 1982, pp. 571-579.

6. Cebeci, T., and Smith, A.M.O., Analysis of Turbulent Boundary Layers, Academic Press, New York, 1974.

7. Baker, A. J., Finite Element Computational Fluid Mechanics, McGraw-Hill/Hemisphere, NY, 1983.

8. Baker, A. J., "The CMC:3DPNS Computer Program For Prediction of Three-Dimensional, Subsonic, Turbulent Aerodynamic Juncture Region Flow-Volume I - Theoretical," NASA Technical Report CR- , 1982.

9. Manhardt, P. D., "The CMC:3DPNS Computer Program For Prediction of Three-Dimensional, Subsonic, Turbulent Aerodynamic Juncture Region Flow - Volume II - User's Manual," NASA Technical Report CR-165997, 1982.

10. Orzechowski, J. A., "The CMC:3DPNS Computer Program For Prediction of Three-Dimensional, Subsonic, Turbulent Aerodynamic Juncture Region Flow - Volume III - Programmer's Manual," NASA Report CR-165998, 1982.

11. Baker, A. J., and Orzechowski, J. A., "A Continuity-Constraint Finite Element Algorithm For Three-Dimensional Parabolic Flow Prediction," Proceedings ASME Sym. on Computers in Flow and Experiments, ASME/WAM, 1981, pp. 103-117.

12. Baker, A. J., Yu, J. C., Orzechowski, J. A., and Gatski, T. B. "Prediction And Measurement of Incompressible Turbulent Aerodynamic Trailing Edge Flows," AIAA Journal, V. 20, No. 1, 1982, pp. 51-57.

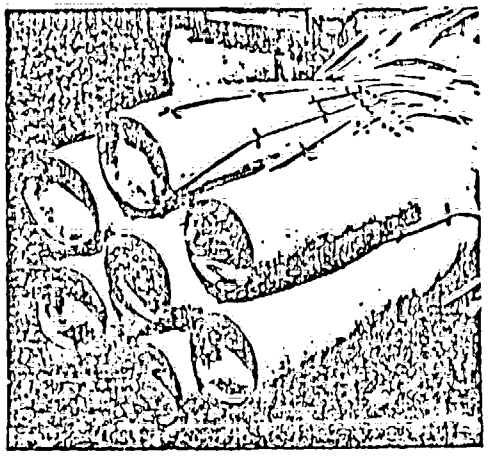

Figure 1. Illustration of a Multiple Jet Configuration.

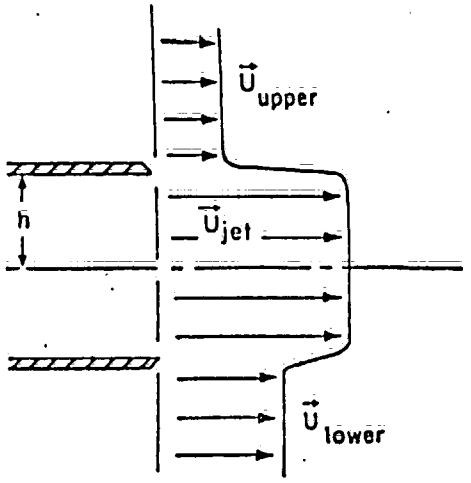

Figure 2. Geometry of a Two-Dimensional Slot Jet.

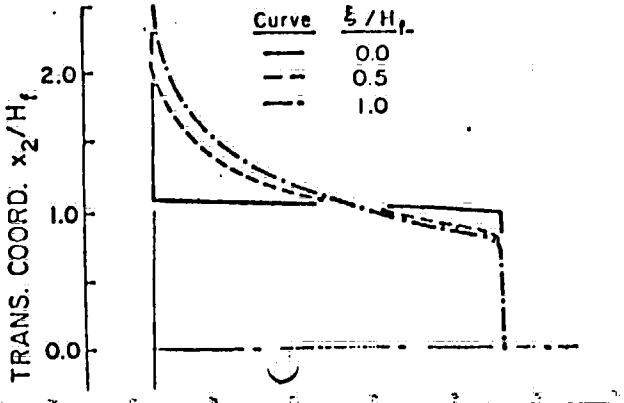

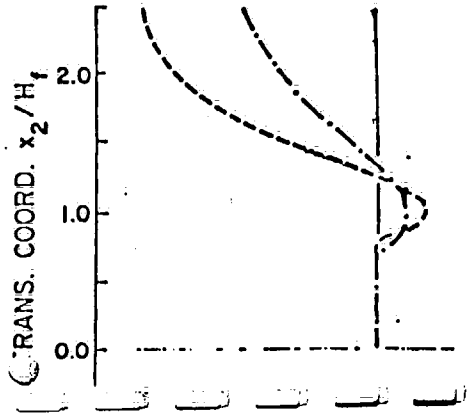

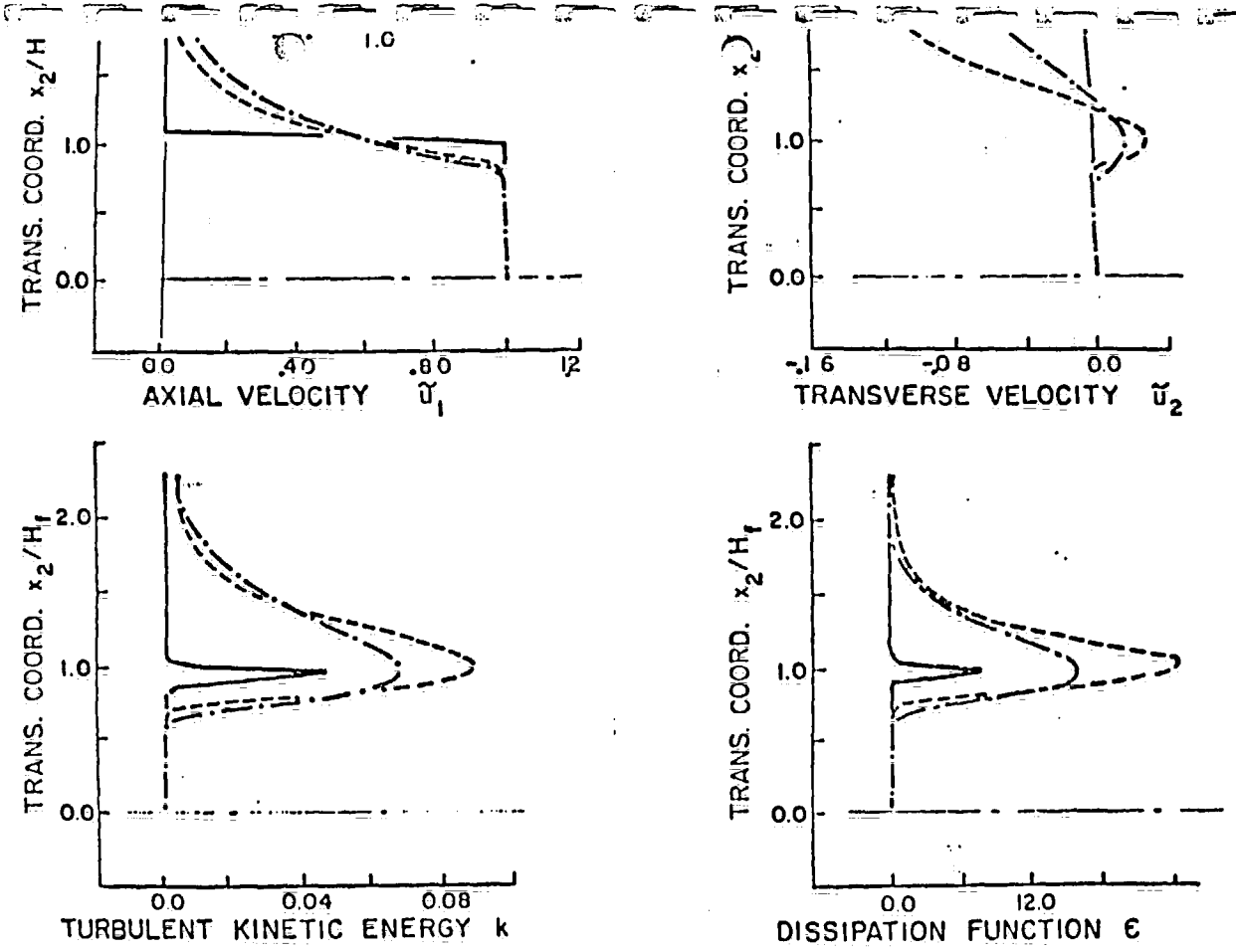

Figure 3. Penalty Algorithm Solution of Symmetric-Half Subsonic Slot Jet, $\bar{u}_1^o$ = 30 m/s, $0 \leq x_1/H_f \leq 1.0$, a) Axial Mean Velocity $\bar{u}_1$, b) Transverse Mean Velocity $\bar{u}_2$, c) Turbulent Kinetic Energy k, d) Isotropic Dissipation Function ϵ.

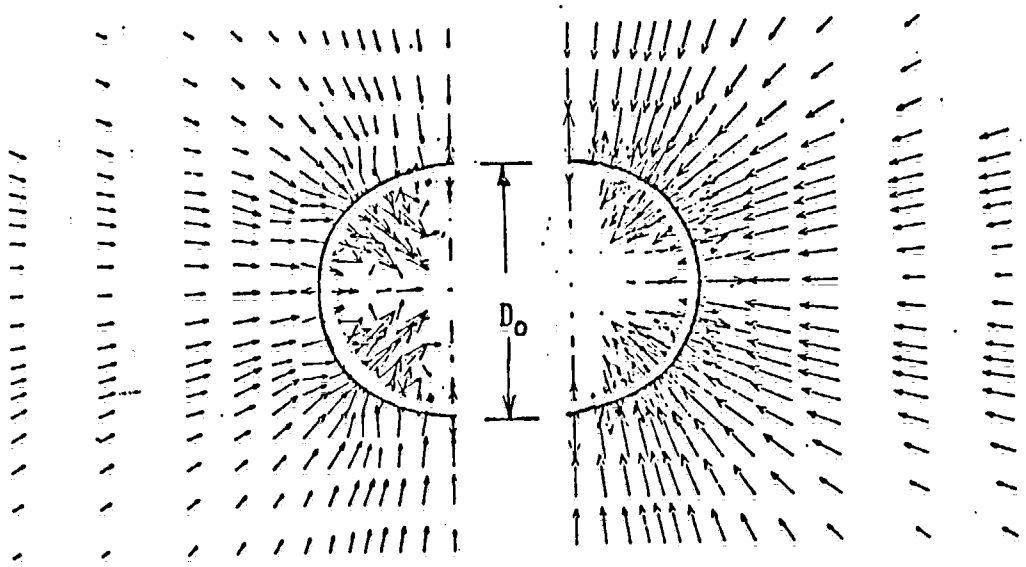

Figure 4. Penalty Algorithm Solution For Transverse Mean Velocity $\bar{u}_\ell$ Distribution, Symmetric-Half Circular Free Jet, $\bar{u}_1$ = 30 m/s, x_1/D_h = 1.0, a) Laminar Jet, u'_ℓ = 0.0017, b) Turbulent Jet, u'_ℓ = 0.044.

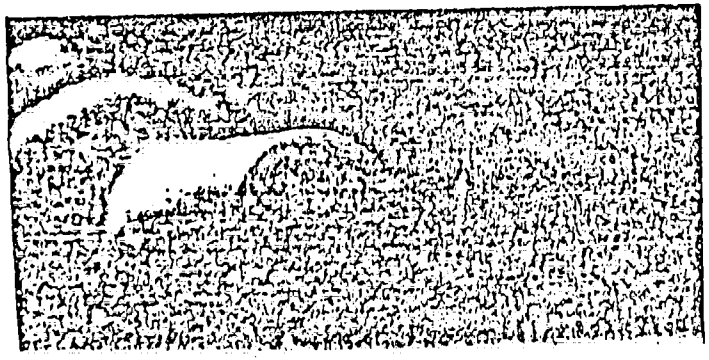

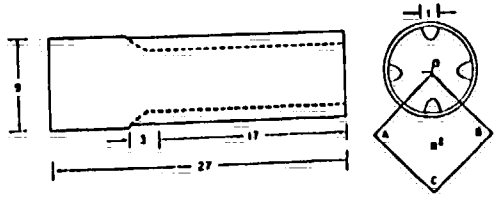

Figure 6. Engineering Layout of Multiple Jet

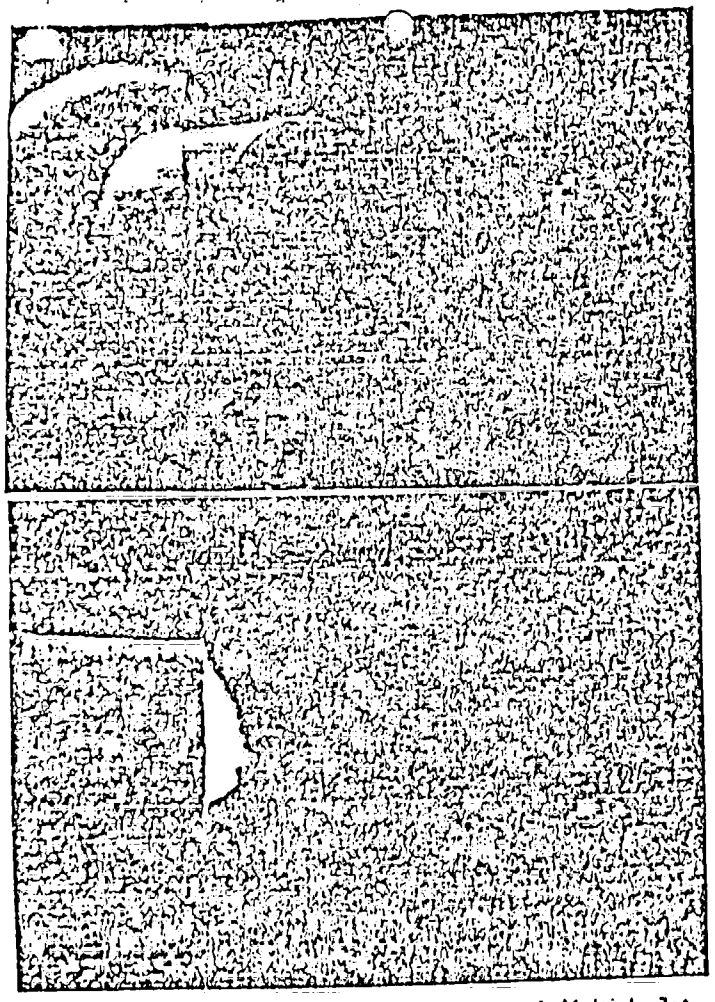

Figure 5. Smoke Flow Visualization of Multiple-Jet Configuration, a) Jet Flows Off, b) Jet Flows On.

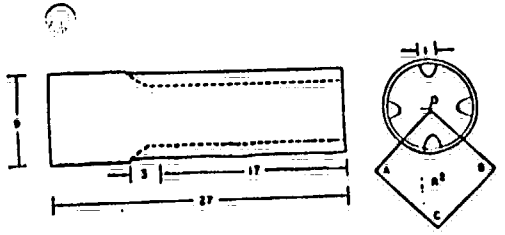

Figure 6. Engineering Layout of Multiple Jet Geometry, a) Plan-View, b) End View, Dimensions in mm.

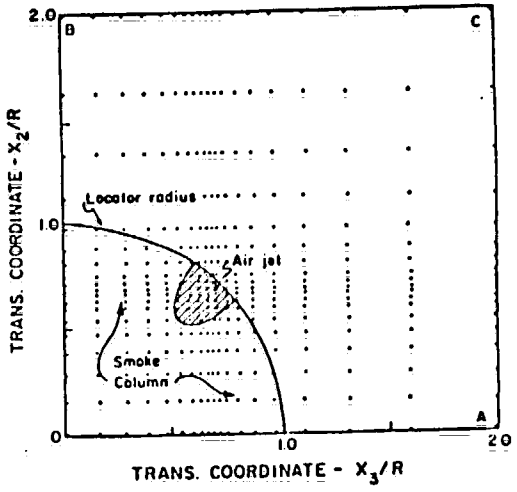

Figure 7. Penalty Algorithm Solution Domain For Symmetric Quarter Plane Prediction of Four Multiple Jet Configuration Including Nodal Coordinate Distribution of M = 19 x 19 Discretization.

1005062894

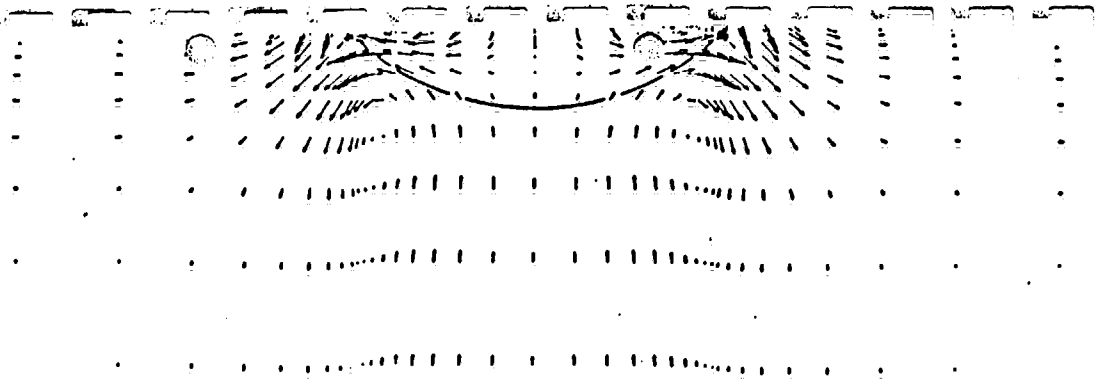

Figure 8. Composite Penalty Algorithm Prediction of Transverse Plane Velocity $\bar{u}_\ell$ Distribution, Four Multiple Jet Geometry, $\bar{u}_1 = 12$ m/s, $x_1/R = 1.5$.

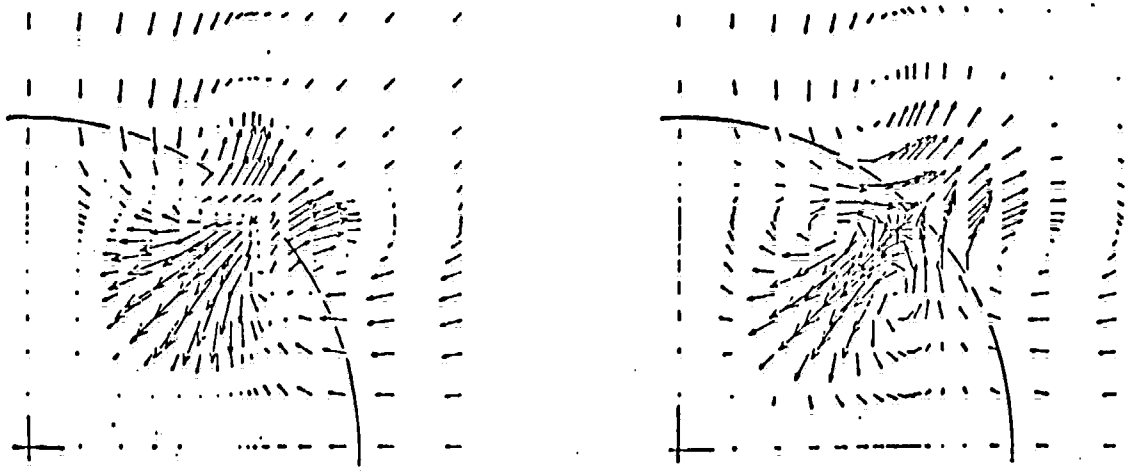

Figure 9. Nearfield Transverse Plane Velocity u_ℓ Distributions, Penalty Algorithm Prediction, $\bar{u}_1^p = 12$ m/s, a) $x_1/R = 0.5$, $u_\ell^{rp} = 0.058$, b) $x_1/R = 1.0$, $u_\ell^{rp} = 0.058$, c) $x_1/R = 1.5$, $u_\ell^{rp} = 0.067$.

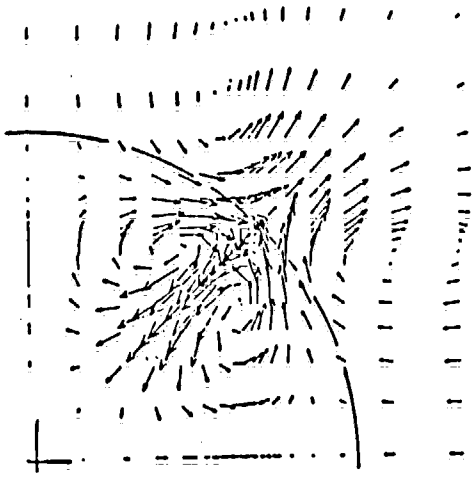

Figure 9. Nearfield Transverse Plane Velocity u_ℓ Distributions, Penalty Algorithm Prediction, $\bar{u}_j^o$ = 12 m/s, a) x_j/R = 0.5, u_ℓ^n = 0.058, b) x_j/R = 1.0, u_ℓ^n = 0.058, c) x_j/R = 1.5, u_ℓ^n = 0.067, Concluded

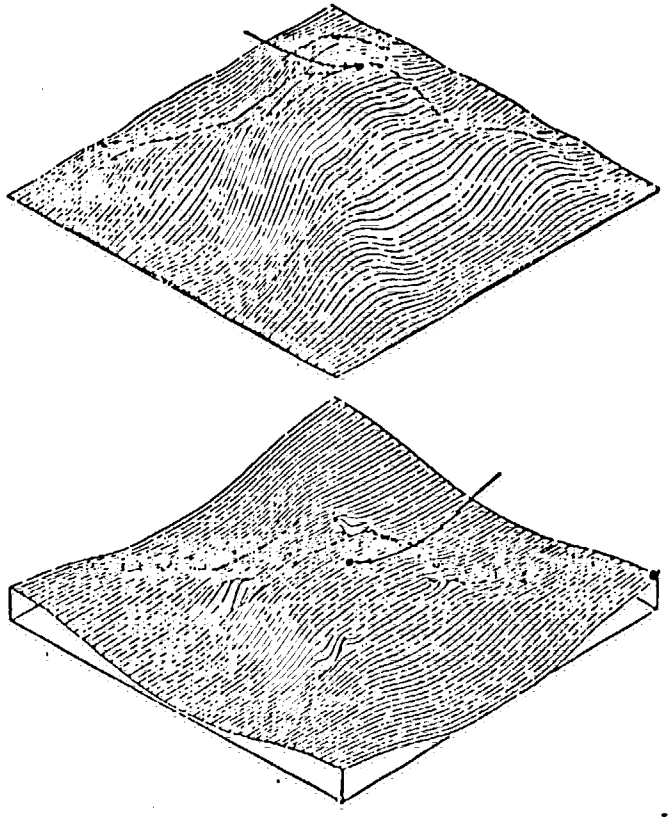

Figure 10. Penalty Algorithm Prediction of Smoke Visualization Distributions, Four Multiple Jet Geometry, $\bar{u}_j^o$ = 12 m/s, a) x_j/R = 0.0, Y_m = 100%, b) x_j/R = 1.0, Y_m = 100%, c) x_j/R = 5.0, Y_m = 63%, Y_e = 0.5%, d) x_j/R = 11.0, Y_m = 30%, Y_e = 23%.

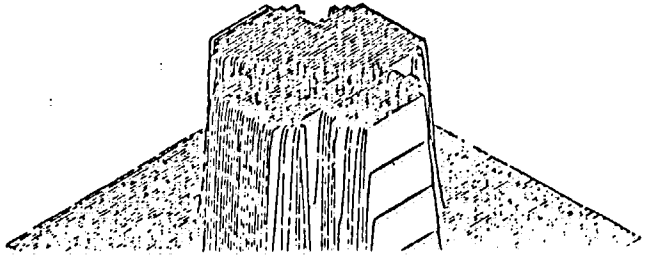

APPENDIX III

SENSORY ASPECTS OF THE BARCLAY CIGARETTE

by

William S. Cain, Ph.D.
John B. Pierce Foundation
Yale University
New Haven, Connecticut

DRAFT
COMMERCIAL IN CONFIDENCE

Sensory Aspects of the Barclay Cigarette

William S. Cain

John B. Pierce Foundation Laboratory and Yale University

My task today is to tell you about the flavor of the Barclay cigarette and to place its unique action into the context of human sensory perception. When asked how he chooses which brand of cigarettes to smoke, the smoker will customarily state "on the basis of flavor." Cigarette manufacturers accordingly devote considerable energy to the formulation of good tasting cigarettes. This task presents a particular challenge in the formulation of ultra-low delivery cigarettes. In that case, the manufacturer seeks to maintain flavor high but to deliver only small amounts of 'tar.'

How to Increase Flavor

There are fundamentally two ways to increase the flavor of a cigarette. One is to intensify the stimulus physically or chemically, i.e., to deliver a stronger product. The other way is to use the existing stimulus more effectively by taking advantage of certain principles of sensory functioning.

Barclay Produces Greater Flavor Than Its Ultralow Competitors

The Barclay cigarette has distinguished itself by its high flavor in comparison to other cigarettes of about the same

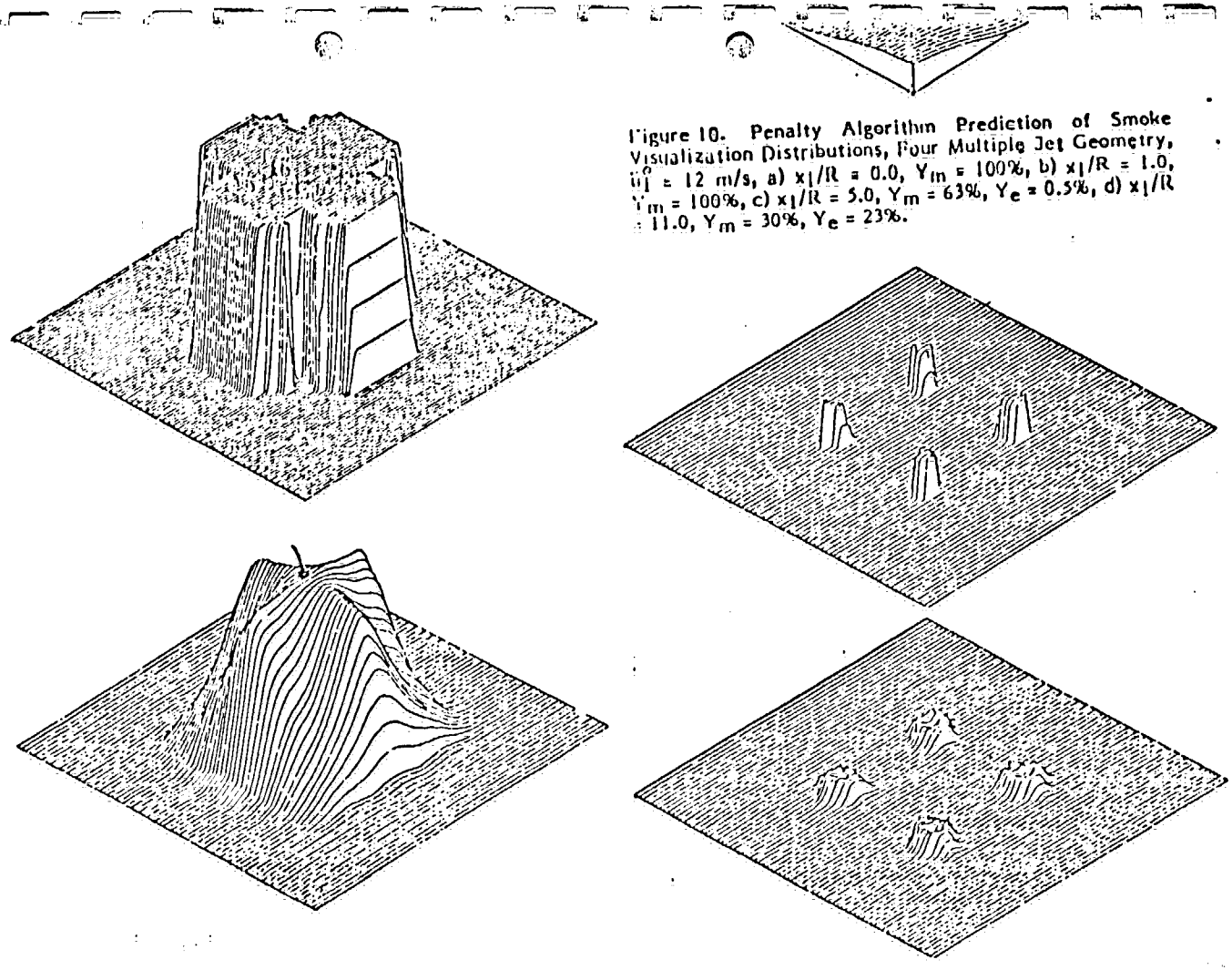

Figure 10. Penalty Algorithm Prediction of Smoke Visualization Distributions, Four Multiple Jet Geometry, $\bar{u}_j^o$ = 12 m/s, a) x_j/R = 0.0, Y_m = 100%, b) x_j/R = 1.0, Y_m = 100%, c) x_j/R = 5.0, Y_m = 63%, Y_e = 0.5%, d) x_j/R = 11.0, Y_m = 30%, Y_e = 23%.

Figure 1

How To Increase Strength

- Increase Stimulus Concentration
- Stimulate More Receptors (Spatial Summation)
- Increase Stimulation Time (Temporal Summation)

delivery of 'tar' and nicotine. Comparisons of Barclay to its ultralow competitors in the U.S. have demonstrated its flavor advantage time and time again. For illustrative purposes, I will show some results obtained from a panel of consumers who had no training in the judgment of cigarette flavor. This study has particular relevance because it reveals the contribution of Barclay's Actron filter to the maintenance of cigarette flavor. The study compared Barclay (1 mg 'tar', 0.2 mg nicotine, FTC values), Now (2 mg 'tar', 0.2 mg nicotine, FTC values at the time of the study in early 1981), and a hybrid composed of the Now tobacco rod fitted with the Actron filter. The panelists smoked four samples of each cigarette in random order throughout a day of testing. Most panelists smoked low delivery cigarettes customarily. Each panelist rated the strength and the draw of a sample on a graphic rating scale (a 23-cm line) that contained the letter R at its midpoint. This reference point represented the strength or draw of the panelist's customary brand. A sample perceived as stronger in flavor received a rating (a mark on the line) to the right of the R and a sample perceived as weaker received a rating to the left of the R. In Fig. 2, the average ratings of the three products appear on the ordinate as positive values (greater than R) or negative values (lower than R) expressed in centimeters (distance from R).

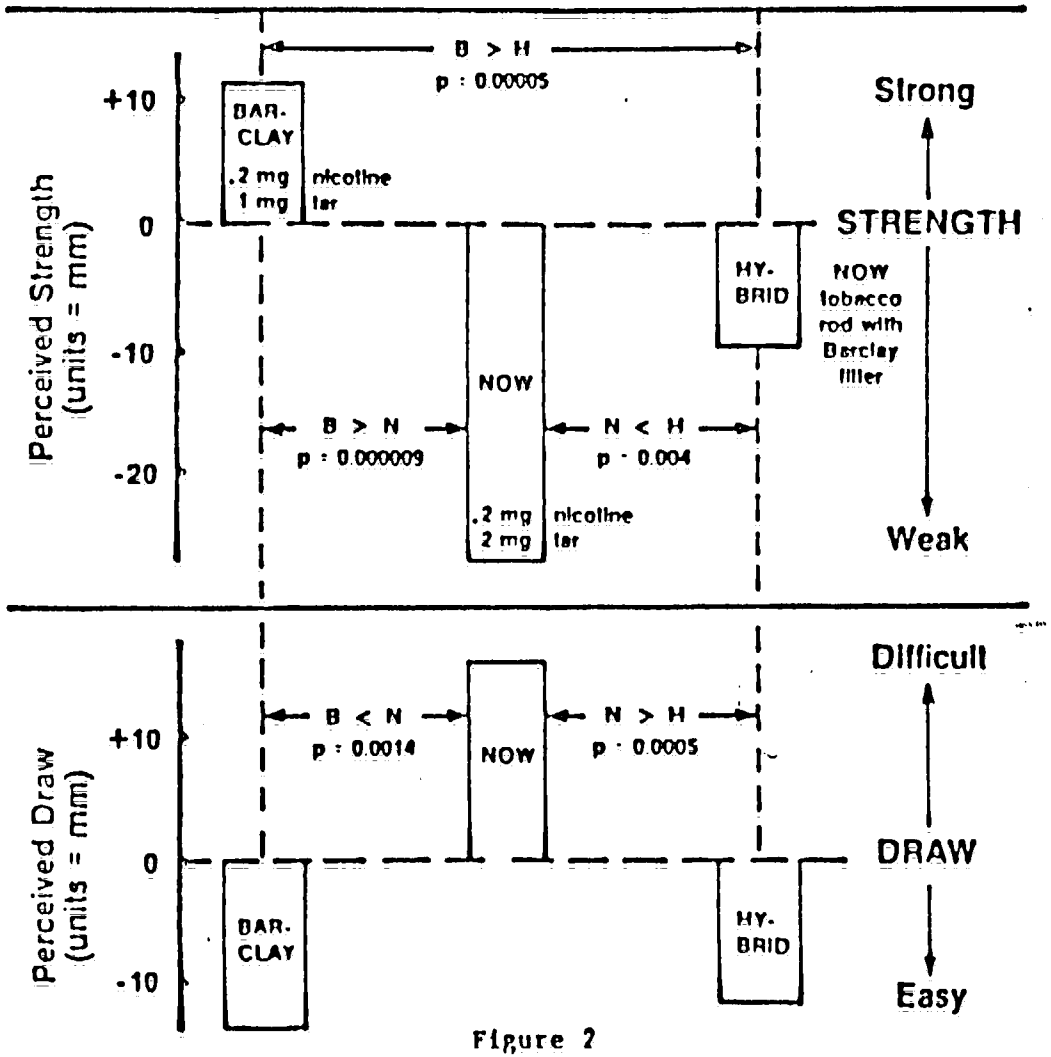

Figure 2

A comparison of the perceived strength and draw of Barclay, Now, and a hybrid composed of the Now tobacco rod fitted with Barclay's Actron filter.

The data and associated probability values in Fig. 2 leave little ambiguity about the flavor advantage of Barclay over Now. In addition to its high flavor, Barclay revealed itself to have a remarkably easy draw, a highly desirable characteristic in an ultralow delivery cigarette. The results obtained with the hybrid reveal the contribution of the Actron filter to both flavor and draw. When fitted to the Now tobacco rod, which contains a less rich blend of tobacco than Barclay, the Actron filter caused a significant increase in flavor over the unaltered Now. Both products with the Actron filter (Barclay and the hybrid) had easy draw, far below that of Now.

What is Flavor?

The terms flavor and taste, as used colloquially, actually refer to various types of sensations. These include odor aroused through stimulation of olfactory receptors located in the upper reaches of the nasal cavities and true taste aroused through stimulation of taste buds on the tongue. Both types of sensations play a role in the experience of cigarette flavor, but less of a role than another type of sensation, common chemical sensation. The common chemical sense gives rise to the experience of pungency, feel, impact, pain, and warmth and cold from chemical stimulation. This sense modality

forms our most primitive chemosensory channel. In the oral cavity and nose, its receptors arise from the trigeminal nerve, the glossopharyngeal nerve, and the vagus nerve. The smoker seeks a feel or impact from his cigarette and this comes about from the action of the smoke on the receptors of these nerves. The receptors are free nerve endings liberally distributed throughout the two nasal cavities, the mouth, the throat, and neighboring areas.

Fig. 3 depicts olfactory nerve fibers and trigeminal fibers that innervate the lateral wall of one nasal cavity. The olfactory fibers which arise from the olfactory bulb (see structure denoted 7) innervate only a small portion of the cavity. The trigeminal fibers innervate the rest of the cavity, the palate, and other areas not shown. The branches in the figure ramify again and again to form a fine grain of common chemical sensitivity throughout the cavity. Branches of the trigeminal nerve also innervate the anterior portion of the tongue. When we consider the endings of all three nerves (trigeminal, glassopharyngeal, and vagus), we find a sensory system of considerable areal extent (Fig. 4).

Spatial and Temporal Summation

Although the common chemical sense responds to chemical stimuli, it can also be considered a cutaneous sense modality. Investigators of the cutaneous senses have long known

Figure 3

A view of the neural innervation of the lateral wall of the nasal cavity and a portion of the palate. The neural branches that emanate from the structure denoted 7 (the olfactory bulb of the brain) represent the olfactory nerve. All other neural branches (1-6, 8, and 9) represent portions of the trigeminal nerve.

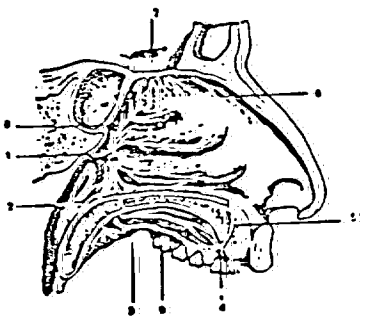

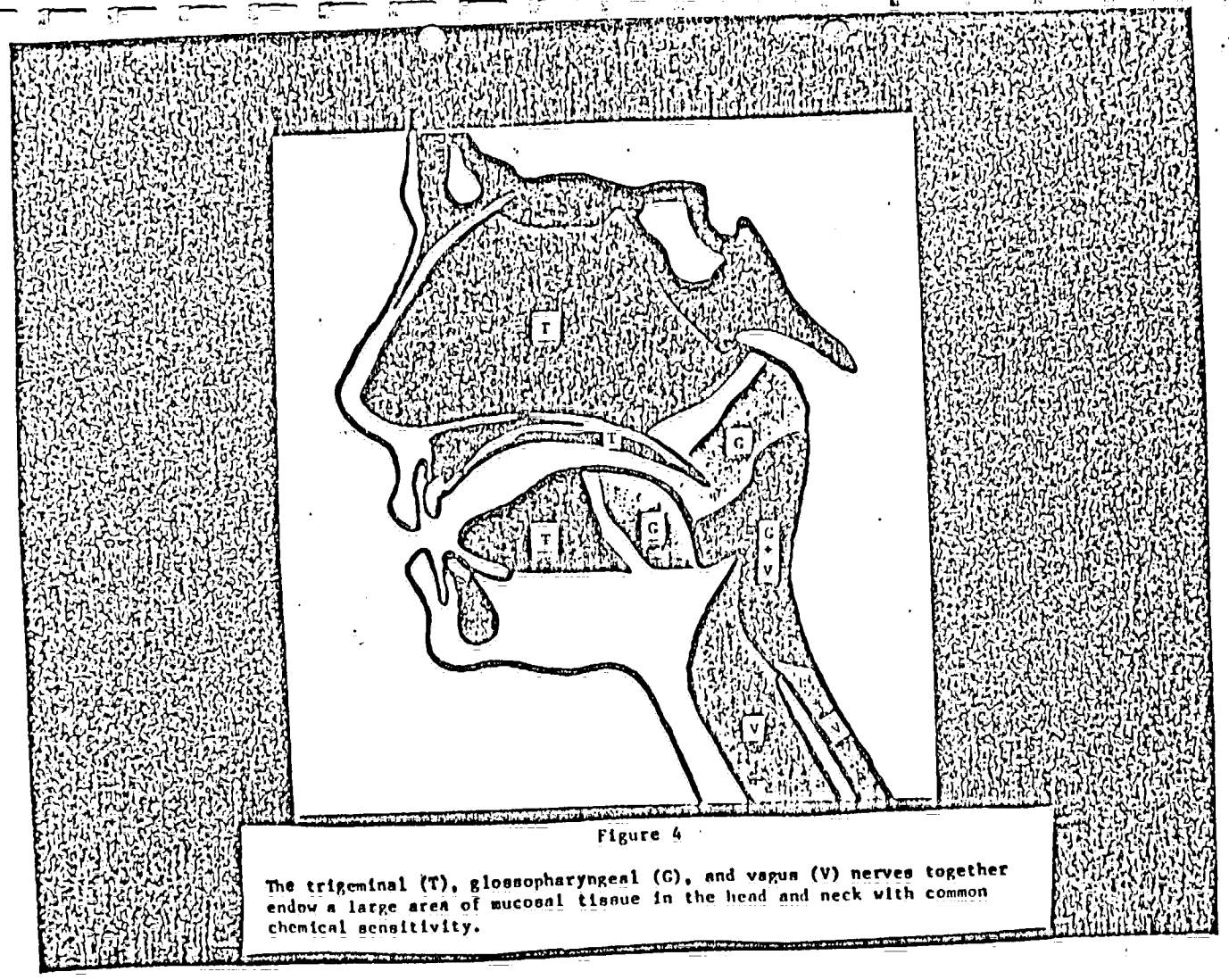

Figure 4

The trigeminal (T), glossopharyngeal (G), and vagus (V) nerves together endow a large area of mucosal tissue in the head and neck with common chemical sensitivity.

that these modalities, whether on the external or internal surfaces of the body, exhibit a common functional property, namely spatial summation. That is, the larger the area stimulated, the stronger will be the sensation. I can illustrate the phenomenon with an experiment on bilateral summation of the pungency of an inhaled stimulus, carbon dioxide. At concentrations above about 10% by volume, carbon dioxide produces pungency with virtually no accompanying odor. The lowest function in the family shown in Fig. 5 portrays the growth of pungency with concentration when carbon dioxide entered only one nostril. The other functions portray the growth of pungency when various combinations of concentrations entered the two nostrils (e.g., 20% to the left nostril, 28% to the right nostril). The dashed line portrays the case where the same concentration enters both nostrils. Bilateral (spatial) summation is evident throughout the family of functions.

Dr. Baker's paper on the aerodynamics of the Actron filter revealed that a primary feature of the filter is to disperse smoke throughout the oral cavity and thereby to maximize the probability of contact between the smoke and the areally extended receptor surface. Hence, the Actron filter offers a more efficient delivery of smoke to the receptors.

Another illustration of spatial summation, this time operating during actual cigarette smoking, appears in Fig. 6. Participants judged the overall strength of the cigarettes

Barclay and Triumph (3 mg 'tar', FTC value) and also the strength at various loci in the oral cavity. (The panel made graphic ratings on a scale that extended from 0 cm, or no strength, to 13 cm, or high strength.) The experimental manipulation of interest in the experiment entailed the application of a topical anesthetic to the anterior portion of the oral cavity (zones A-D as shown in Fig. 7) or to both anterior and posterior portions (zones A-F). In comparison to smoking with an unanesthetized mouth (denoted I in Fig. 6), smoking with anesthesia in the anterior portion (II) reduced overall strength somewhat and smoking with anesthesia in both the anterior and posterior portions (III) reduced overall strength even more. The ratings of the locus of sensation revealed to us that persons can decide that aspect of the sensory experience only vaguely. The primary impression of the smoker with a partially anesthetized mouth is just an overall reduction in the strength of the cigarette.

Another salient characteristic of the common chemical sense is temporal summation. It occurs over a time scale of many seconds. This can be demonstrated by the results of an experiment where subjects inhaled a nonpungent odorant, isoamyl butyrate, that stimulated primarily the sense of smell and a pungent stimulus, ammonia, that stimulated the common chemical sense (Fig. 8). Note that the longer the pungent stimulus was inhaled, the stronger was the sensation. It is noteworthy that

Figure 5

Perceived pungency of carbon dioxide for various combinations of concentrations presented to the two nostrils. The lowest function of the family depicts pungency aroused when one nostril received various concentrations (20-55%) and the contralateral nostril received just air (0% carbon dioxide). The next higher function depicts pungency aroused when one nostril received various concentrations and the contralateral nostril received a 20% carbon dioxide, and so on. The dashed line depicts the case where both nostrils received the same concentrations.

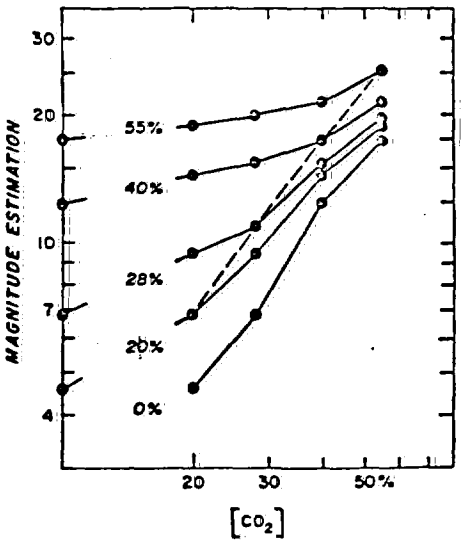

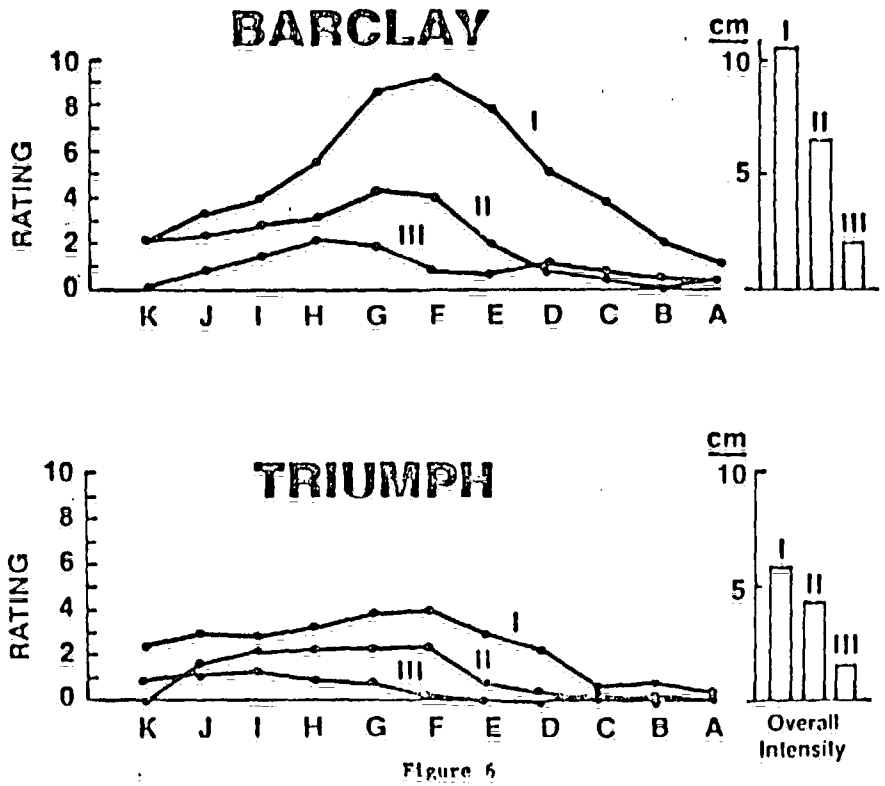

Figure 6

Right side shows ratings of overall strength when panelists smoked Barclay and Triumph with the unanesthetized normal mouth (I), the mouth anesthetized in the anterior portion (II), and the mouth anesthetized in both anterior and posterior portions (III). Left side shows ratings of strength at the various loci shown in Figure 7.

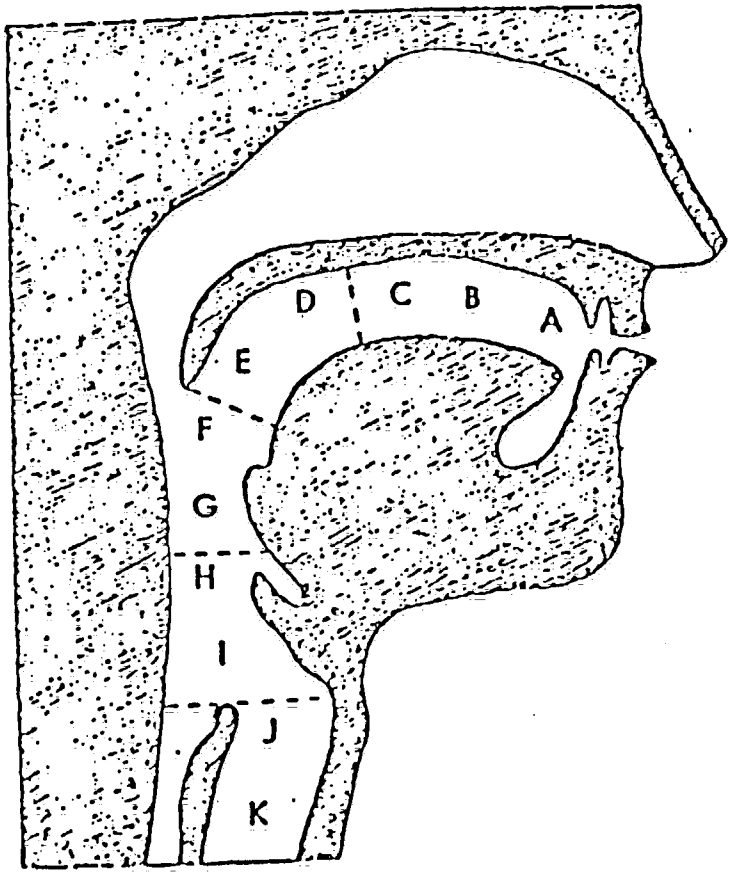

Figure 7

Division of the mouth and neighboring regions into zones for the purpose of judging the locus of sensory experience during smoking.

Figure 8

Upper part shows the perceived strength of three concentrations of a benign odorant, isoamyl butyrate, at two durations of inhalation. Lower part shows the perceived strength of four concentrations of the pungent substance ammonia at three durations of inhalation.

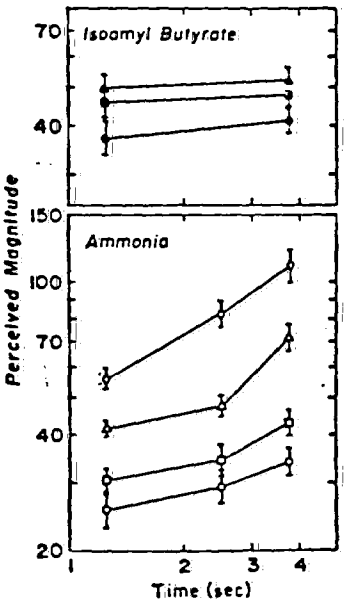

an important action of the Actron filter is to increase the time of contact between the smoke and the receptors. This presumably gives the smoke the opportunity to produce a greater sensory effect. I have concluded that both temporal and spatial factors can therefore cooperate to increase the effectiveness of smoke that emanates from the Actron filter.

The Influence of Sleeves

It would be valuable to show in a direct way that it is actually the dispersion aroused by the Actron filter that enhances the flavor of the Barclay. One way to do this would be to alter the dispersion and to measure any corresponding alterations in flavor. As Dr. Baker has shown, placement of a thin plastic sleeve over the filter provides one way to alter dispersion. According to Dr. Baker's computations, as the end of a sleeve protrudes more and more from the face of the filter, there is a progressive reduction of dispersion. Even a protrusion (i.e., creation of a recess between the sleeve and the filter) of only 0.5 mm impairs dispersion. Sensory judgments made on a 9-point rating scale confirm that an impairment of dispersion will reduce the strength of the flavor. Fig. 9 shows that protrusions up to 3 mm cause a progressive reduction in the strength of the Barclay. The addition of sleeves to the brands Merit, Cambridge, Carlton, and Now had no systematic effect on their flavor intensity.

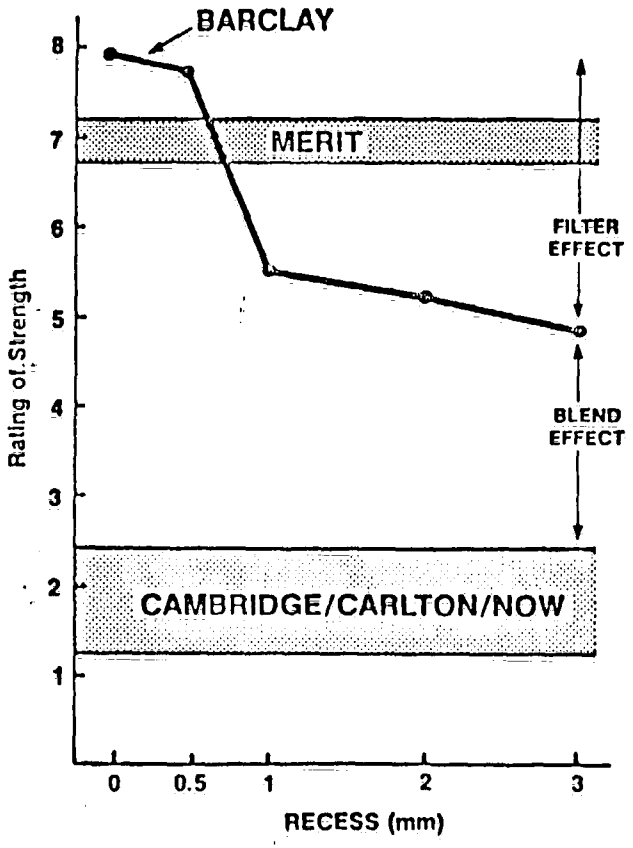

Figure 9

Perceived strength of Barclay and other brands fitted with thin plastic sleeves over the filters. The abscissa shows the degree of protrusion of the end of the sleeve from the face of the filter. A 1-mm recess, for example, represents a 1-mm protrusion or overhang.

Even though a 3 mm protrusion virtually destroys the dispersive action of the Barclay, its flavor did not fall to a level as low as that of its ultralow delivery competitors Cambridge, Carlton, and Now. The blend of the Barclay is richer than that of these other brands and we have therefore indicated both a filter-effect and a blend-effect in Fig. 9. Part of what we call the blend-effect, however, may occur because of Barclay's unmatched ease of draw shown previously in Fig. 2 above. It is our common experience that smokers find an easy drawing ultralow delivery cigarette more flavorful than one that offers high resistance.

Conclusion

The Barclay cigarette is, to our knowledge, the first cigarette to employ known features of sensory functioning, particularly spatial and perhaps temporal summation, to achieve high flavor. This occurs without intensification of the cigarette itself beyond the addition of a blend rich in nicotine. Barclay represents a step forward in cigarette technology, perhaps one of various steps that will ultimately allow the principles of sensory functioning to aid in the design of ultra-low delivery cigarettes of high flavor.

Figure 10

How To Increase Strength

- Increase Stimulus Concentration
- More Effective Stimulus Delivery
  — by using known principles of sensory perception

APPENDIX IV

MEASUREMENTS OF LIP PRESSURE EXERTED ON A CIGARETTE DURING NORMAL SMOKING

by

Roger D. Kamm, Ph.D.
Massachusetts Institute of Technology
Cambridge, Massachusetts

DRAFT
COMMERCIAL IN CONFIDENCE

MEASUREMENTS OF LIP PRESSURE EXERTED ON A CIGARETTE DURING NORMAL SMOKING

Roger D. Kamm, Ph.D.

Massachusetts Institute of Technology

Cambridge, MA 02139

ABSTRACT

Measurements were made of the pressure exerted by human lips on the filter of a cigarette during normal smoking conditions using a small, fluid-filled bulb attached to a low-compliance pressure transducer. In two series of measurements, the mean lip pressure and standard error were 34.2 (± 3.0) and 35.2 (± 2.9) torr, respectively. These pressures compared favorably with those applied by the Cambridge holder (used in the standard FTC testing procedure), but were much lower than the pressures exerted by two different holders (Filtrona and Borgwaldt) both of which are constructed from a rigid cylindrical housing with a segment of latex tube mounted inside. Pressures measured by these two holders were in close agreement with the pressures predicted by a nonlinear theoretical model for the distention of latex rubber tubes.

INTRODUCTION

Although factors relating to smoking behavior have been the subject of considerable study, interactions between the smoker's lips and the cigarette filter have received relatively little attention. This is no doubt due to the fact that, for most brands of cigarette, the lip-filter interaction has little effect on what the smoker receives in the way of tar and nicotine. While this has generally been assumed in the past, the lips may actually play a significant role in all cigarettes that are ventilated to reduce the levels of tar and nicotine in the smoke. If the lips impair the normal flow of ventilation air, the delivery of these substances could be considerably increased from that indicated by the accepted testing procedures. Obviously, if either the lips or the fingers of the smoker cover the ventilation holes, then the smoker will, in effect, be smoking a much stronger cigarette. Finger blockage has, in fact, been observed in as many as 40% of all ventilated cigarette smokers according to a recent study [Kozlowski (1982)].

Recently, a new type of filter has been introduced that could be susceptible to a somewhat different type of 'sabotage'. This filter also has ventilation perforations at approximately the same location on the filter as other conventional filters, but these perforations directly communicate only with four small grooves that run beneath the filter paper to the end of the filter. If these grooves were to become collapsed due to pressures exerted by the lips during smoking,

then once again the smoker would receive more smoke than would a testing machine and the machine figures would, in fact, be misleading to the consumer. This presumes, of course, that the holder used during testing does not compromise the flow of ventilation air in any way due, for example, to pressures that are unrealistically high. Clearly, the pressures exerted by human lips as compared to those applied to the filter by the various filter holders used in cigarette testing, becomes an important factor.

I have conducted a series of tests under conditions simulating normal smoking in which the contact stress acting between the smoker's lips and the cigarette filter has been measured. The pressures exerted by three different types of cigarette holder have also been measured and compared to the measurement of lip pressure. These measurements will be presented and their import for the ventilation reaching the smoker will be discussed.

Since measurements of this type have not been made in the past, it was necessary to develop a new measurement technique for this purpose. The technique devised for these tests draws upon methods that have been used to measure contact stress in other situations, but differs both in the size of the sensing element and the sensitivity required.

Various methods have been employed in the past to measure the contact stress acting between two solid surfaces. These methods generally measure the force applied to a known surface area by way of the deflection of a diaphragm or the change in electrical properties

of a piezoelectric or piezoresistive device. Although these methods are reliable and accurate in most applications, they fail in this situation either because they lack the necessary sensitivity or because they cannot be sufficiently miniaturized to ensure that the act of measurement will not significantly influence the pressures we wish to determine. To ensure reliable measurement of lip pressure, a device is required which is small compared to the cigarette diameter and which conforms to the smoker's lips when contact is made. The device must be sensitive and capable of measuring pressures, accurately, down to 10 or 20 torr (1 torr = 1 mm Hg).

Somewhat similar measurements have been made inside the mouth. In these, the purpose has been to determine the pressures exerted between the lips and the teeth or the tongue and teeth. Intra-oral pressures have been measured both by a technique similar to that employed in these tests, and by using a sensitive strain gage mounted on the tooth surface or in a small plastic housing. In such tests, pressures in the range of 20 to 150 torr have been observed in normal activities such as speaking and swallowing [Proffit (1975)].

EXPERIMENTAL METHODS

Measurement Apparatus. In order to satisfy the stringent requirements stated above, a miniature pressure sensing element was developed. This miniature probe consists of a thin-walled, latex rubber bulb, nearly spherical in shape (dia. = 1.5 mm) with a narrow throat to allow attachment to a segment of hypodermic needle tubing (L = 1 cm, I.D. = 0.01 cm). The needle tubing is connected to a teflon catheter (L = 50 cm, I.D. = 0.05 cm) that leads to a low compliance pressure transducer. The entire system (bulb to transducer) is filled with water to eliminate the compliance due to fluid compressibility and, therefore, maximize the usable pressure range of the device.

The bulb was mounted on the cigarette filter in one of two ways. In one set of experiments (Series I) the bulb was attached directly to a small exposed segment of the cellulose filter material at a distance of 7 mm from the tip of the filter using a fast-acting contact adhesive. In the other set (Series II) the bulb was first mounted onto a 1 cm long segment of thin-walled latex tube (nominal I.D. = 0.79 cm) which could be slipped over the end of the filter to the desired position. The latter modification was adopted merely to facilitate the mounting of the probe.

The assembled apparatus is shown in Figure 1. When mounted in the fashion shown, a smoker's lips or filter holder would press on the sensing probe causing the internal fluid pressure to increase. This is immediately sensed by the pressure transducer and can be displayed on an oscilliscope screen.

Due to the properties of the bulb and to the distribution of stresses on the bulb, the recorded pressure (P_{rec}), in general, differs from the applied pressure (P_{app}). To illustrate, consider a general functional relationship between the volume of the sensing bulb (V_{bulb}), the pressure difference acting across the bulb ($P_{app}-P_{rec}$), and the distribution of pressure acting on the external surface of the bulb [$D(\vec{r}_s)$],

$$V_{bulb} = V_{bulb}[P_{app}-P_{rec}, D(\vec{r}_s)] \quad (1)$$

where $\vec{r}_s$ denotes position on bulb surface]

Because the volume of <u>incompressible</u> fluid within the measurement system is constant, changes in bulb volume (ΔV_{bulb}) and changes in transducer and tubing volume (ΔV_{trans}), must be of equal magnitude but of opposite sign. Therefore, we can write:

$$V_{bulb} = V_{bulb,i} + \Delta V_{bulb} = V_{bulb,i} - \Delta V_{trans} \quad (2)$$

We further note that ΔV_{trans} is a function only of the internal pressure and can therefore state:

$$\Delta V_{trans} = \Delta V_{trans}(P_{rec}) \quad (3)$$

Combining (1)-(3), we can deduce the following functional relationship:

$$P_{app} = h[P_{rec}, D(\bar{r}_s)] \quad (4)$$

Therefore, to the extent that the distribution of external pressure is either relatively constant or unimportant, P_{rec} will be directly related to P_{app}.

Since the exact form of the function h is not known, a calibration apparatus was developed and used with each individual test. The device (Figure 2) was designed so as to mimic as closely as possible the distribution of pressure produced by the lips, thus maintaining $D(\bar{r}_s)$ roughly constant. The calibration device consists of two rigid Plexiglas plates, each machined to accept a cigarette, and a 10 cm length of thin-walled latex rubber tubing. When assembled, the latex tube is positioned directly over the sensing bulb and any pressure applied inside the tube is directly exerted on the sensing bulb. A calibration curve was obtained by inflating the latex tube to approximately 5 or 6 levels of pressure within the range of interest. The relationship was plotted as E_{rec} vs. P_{app} (E_{rec} is the output voltage of the transducer associated with P_{rec}) as in the sample curve given in Figure 3.

Protocol for Lip Pressure Measurements. In preparation for an experiment, the sensing probe was mounted onto a cigarette in one of the two ways described above. The smoking panelist was then brought into the room and was seated at a table on which the instrumented cigarette had been placed. Each panelist was asked to smoke in a normal fashion and at a normal pace, taking care to position the small sensing probe squarely against their lip. For each test, we obtained approximately ten pressure measurements: five with the bulb positioned against the lower lip and five with the bulb positioned against the upper lip. The pressure excursions during each puff were monitored using an oscilliscope and the maximum deflection for each puff was recorded.

During the course of measurement, it was occasionally necessary to guide the panelist with regard to bulb position. Observing the pressure on the oscilliscope, it was immediately evident when the panelist's lip had missed the bulb. All cases in which the bulb was missed were ignored.

Each cigarette was calibrated using the procedure described above either prior to or following the test. In several cases the calibration was performed both before and after the lip pressure measurements to ensure consistency of the calibration relationship.

In the two series of tests, usable data were obtained on 12 and 18 subjects, respectively. Three sets of data were not used due to one of two problems -- either the bulb ruptured during the test, or the teflon catheter came too close to the burning ash and melted. All the results are summarized in Table 1.

Filter-Holder Measurements. The measurements of pressure exerted on the three filter holders were all conducted with the same instrumented cigarette,+ calibrated in the manner described above. In each case, several pressures were recorded at the position of peak pressure within the holder and are summarized in Table 2. The three holders tested are sketched in Figure 4. They are:

1) Cambridge. This holder, the FTC standard, is comprised of a rigid plastic holder on which a latex rubber sheet can be mounted. The latex sheet used in this test was the industry standard, 0.20-0.23 mm thick with a 3 mm dia. hole. When stretched onto the holder, the hole diameter increases to 3.9 mm.

2) Borgwaldt. This holder is made from a rigid, cylindrical housing with a latex tube slipped inside and stretched over the two ends. The standard latex sleeve used in our tests had dimensions: O.D. = 7 mm, wall thickness = 0.36-0.43 mm.

3) Filtrona. This holder consists of a cylindrical housing with a latex sleeve inside, mounted on the two ends. It differs from the Borgwaldt mainly in terms of the tube dimensions: (O.D. = 6 mm, wall thickness = 0.38 mm).

+ The diameter of a cigarette filter is 8 mm.

DISCUSSION OF RESULTS

Lip pressure measurements. The objective of this study was to measure the pressures exerted by human lips during normal smoking and to compare these pressures to those produced by various types of cigarette holders used for testing purposes. The values of lip pressure presented in Table 1 are seen to fall in a wide range with a mean value of 34 torr. This was lower than any of the filter holders tested, but was closest to the pressures produced by the Cambridge holder.

The scatter in the data reported in Table 1 can be attributed to a variety of factors. First, there are obvious differences in jaw structure, muscle tone and smoking behavior between individuals. Even the same individual will exhibit a wide degree of variability from one draw to the next. In this regard, it is useful to look at a comparison between the overall mean pressure and the maximum pressure for each subject (Table 1). Typically, the maximum pressure was about twice as high as the overall mean. Five subjects, however, exhibited values of P_{max} greater than four times as high as the mean. We suspect that this was due to the panelists' teeth coming into contact with the sensing bulb. Another source of variability is in the positioning of the bulb between the panelists' lips. Clearly, the contact stress acting between the filter and lips will be distributed non-uniformly both along the axis of the cigarette and around the circumference. By instructing the panelist to place the bulb squarely

against either the upper or lower lip, we attempted to obtain a measurement near the maximal point of this distribution. Due largely to the considerable variability of insertion depth from smoker to smoker, however, this was often difficult to accomplish. This was most vividly demonstrated by the total absence of signal when the panelist's lips missed the probe altogether. Therefore, these measurements must be viewed as approximate peak pressures and that, based on the variability of our measurements, the actual peak pressure during any particular puff may typically be two to three times as large as the mean value given in Table 1.

The pressures we observed are in approximate agreement with measurements of pressure in a region lingual to the maxillary molars during the act of speaking, for example. Using measurement probes mounted in plastic, Proffit (1975) found contact stresses to lie in the range of 10 to 60 torr for teenage caucasian subjects.

All the measurements reported thus far pertain to the maximum pressure excursion for each individual draw on the cigarette. The peak is recorded during a pressure history that typically has the appearance of the trace shown in Figure 5. Although deflections in this trace are not linearly related to lip pressure, we can still draw broad inferences from its general shape. Characteristically, the signal would rapidly deflect and reach an early maximum as the smoker placed the cigarette into his or her mouth and began to draw. Sometimes we observed a single plateau during this rising phase corresponding to a short pause between cigarette insertion and the onset of draw. The pressure would fall more or less rapidly as the

draw progressed, level off at the end of the draw, and then fall to zero as the cigarette was removed from the mouth. From traces like these, we are able to conclude that the pressure maximum is of very short duration and that the time-mean pressure during the draw is on the order of half the peak value.

Filter-holders. The three filter-holders were found to exhibit grossly different characteristics both in terms of the values of peak contact stress, and also in the distribution of that stress upon the filter.

Of the three filter-holders tested, only the Cambridge holder came close to exerting pressures comparable to those produced by the lips. The pressures exerted by the Borgwaldt and Filtrona holders were about 4 and 15 times larger than lip pressure, respectively. The differences between these two can be attributed entirely to the proportion and dimensions of the tubing used as demonstrated in the Appendix.

The pressures are not only lower with the Cambridge holder, but also act over a smaller surface area as compared to either the Borgwaldt or Filtrona holders. The region of contact in all cases is symmetric around the filter circumference but ranges in length from about 3 mm in the Cambridge to about 10 mm in the Borgwaldt and Filtrona.

These measurements of filter-holder pressure provide us with an additional check on the validity of our measurement technique. By the analysis described in the Appendix, it is possible to predict the approximate pressure exerted by either of the tube-in-cylinder holders (Borgwaldt or Filtrona). Accounting for an axial strain imposed during the mounting procedure of about 15% and for the effects of finite deformation and wall thickness, we come up with predicted pressures of around 520 torr for the Filtrona and 150 torr for the Borgwaldt holder (see Figure 6). These are in close agreement with the measurements reported in Table 2, suggesting that our measurements are, indeed, correct and accurate.

SUMMARY

Using a pressure probe developed specifically for the measurement of lip pressure and calibrated using a device which was designed to simulate the action of human lips, the pressures exerted by the lips of a smoker and by various types of cigarette holder have been measured. I found that the contact stress exerted between the lips of a smoker and the cigarette filter were comparable to those exerted within the mouth as measured by other techniques, but were generally lower than those produced by the various types of cigarette filter-holders used for testing purposes. Only the Cambridge holder (currently recommended by the Federal Trade Commission) produces pressures that are close to lip pressures.

APPENDIX -- PREDICTION OF FILTER-HOLDER PRESSURES

The measurement of filter-holder pressure proved to be useful, not only for comparison to lip-pressure but also as an independent means of calibration. Because the geometry of the two latex tube holders (Filtrona and Borgwaldt) is symmetric and relatively simple, the pressure they exert on a filter of known diameter can be predicted with reasonable accuracy.

The elastic tubes used in these two holders are subjected to both axial and circumferential strain denoted by ε_x and ε_θ, respectively. If the tube wall is assumed to behave as a homogeneous and isotropic thin-walled membrane, then these strains are related to the circumferential tension through [Tomoshenko and Woinowsky-Krieger (1969)]:

$$T = Eh(\varepsilon_\theta + \sigma\varepsilon_x)/(1 - \sigma^2) \qquad \text{A-1}$$

where E is the Young's modulus of the material, σ is Poisson's ratio and h is the tube wall thickness. The axial stress satisfies:

$$Q = Eh\,(\varepsilon_x + \sigma\varepsilon_\theta)/(1 - \sigma^2) \qquad \text{A-2}$$

The pressure difference across the membrane is related to the membrane tension and local radius of curvature in two mutually perpendicular planes and is given by:

$$\Delta P = P_{int} - P_{ext} = T/R_\theta - Q/R_x \qquad A-3$$

where, R_θ and R_x are the radii of curvature of the surface in a cross-sectional and axial plane, respectively.

When the tube is mounted but before a cigarette is inserted into the holder, $P_{int} = P_{ext}$ and

$$T/R_\theta = Q/R_x$$

When the cigarette is in place, $R_x = \infty$ and

$$T = R_\theta \Delta P = Eh\,(\varepsilon_\theta + \sigma\varepsilon_x)/(1 - \sigma^2) \qquad A-4$$

Moreover, since the volume of tube wall remains constant:

$$hRL = h_o R_o L_o \qquad A-5$$

where h_o, R_o, and L_o are the thickness, radius and length of the unstressed tube. Changes in radius and length are related to the circumferential and axial strain according to:

$$\varepsilon_\theta = (R - R_o)/R_o$$

$$\varepsilon_x = (L - L_o)/L_o$$

These expressions can be combined with (A-5) to yield:

$$h = h_o(\varepsilon_\theta + 1)\ (\varepsilon_x + 1)$$

Substituting into A-4 we obtain:

$$\Delta P = Eh_oR_o(1 + \varepsilon_x)[((R-R_o)/R_o) + \sigma\varepsilon_x]/[R^2(1-\sigma^2)] \qquad \text{A-6}$$

Of the parameters on the right in A-6 only ε_x is unknown. Rough estimates suggest that it is roughly equal to 0.15 for both filter-holders tested. Plotting ΔP as a function of axial strain, we obtain Figure 6.

The above analysis assumes both that the wall is very thin and that the stress-strain behavior of latex rubber is linear. This is,

however, only an approximation which is decreasingly valid for large strains. An analysis that relaxes both of these constraints has been performed by Taylor and Gerrard (1977) for the case of zero axial strain. Their result can be written:

$$\Delta P = \frac{2}{3}\frac{Eh_o}{D_o}\left(1 - \frac{R_o^4}{R^4}\right)\frac{\left(1 + h_o/2R_o\right)}{\left(1 + h_o/R_o\right)^2} \qquad \text{A-7}$$

The value of ΔP computed by this equation is also shown in Figure 6. If we assume, without proof, that changes in axial strain affect ΔP similarly for both cases, we obtain the approximate relationships indicated by the dash-dot lines in the figure.

REFERENCES

Taylor, L. A. and Gerrard, J. H., Pressure-Radius Relationships for Elastic Tubes and Their Application to Arteries; Part I - Theoretical Relationships, Med. and Biol. Eng. and Comput., Vol. 15, pp. 11-17, 1977.

Timoshenko, S. and Woinowsky-Krieger, S., Theory of Plates and Shells, Eng. Soc. Monograph, 1969.

Kozlowski, L. T., British Journal of Addiction 77 (1982) 159-165.

Proffit, W. R., Angle Orthodontics, Vol. 45, (1) pp. 1-11, Jan. 1975.

TABLE 1. DATA SUMMARY: LIP PRESSURE MEASUREMENTS

SERIES I

Subject	Upper Lip (P_u) (Torr)	Bottom Lip (P_b) (Torr)	Overall ($\bar{P}$) (Torr)	Lighting (P_L) (Torr)	$\frac{P_{max}}{\bar{P}}$ (Torr)
1	(no useful data -- see text)				
2	87	110	98.5	100	1.7
3	40	16	28	53	1.9
4	2.5	2.9	2.7	13	4.8
5	60	71	65	100	1.5
6	53	6.0	29	11.3	2.7
7	57	3.9	30	10[a]	8.5
8	88	4.4	46	3.4[a]	5.3
9A	10 > 7.5	16 > 13.2	13 > 10.4	8.8[a] > 13.2	3.1
9B	5.1	10.4	7.8	17.5[a]	1.5
10	16.7	15.5	16.1	12.5[a]	1.6
11	51.3	3.3	27.3	3.8[a]	4.0
12	18	25	21.5	7.5[a]	2.3
Average (s.d.)	43.7 (29.7)	24.7 (34.4)	34.2 (32.9)	55 (44.0)/8.4 (4.2) 29.8 (37.2)[b]	

(a) Lighting with bulb on lower lip.
(b) Upper lip/Lower lip. Overall average directly below.

TABLE 1. DATA SUMMARY: LIP PRESSURE MEASUREMENTS

SERIES II

Subject	Upper Lip (P_u) (Torr)	Bottom Lip (P_b) (Torr)	Overall ($\bar{P}$) (Torr)	Lighting (P_L) (Torr)	$\frac{P_{max}}{\bar{P}}$ (Torr)
1	7.9	18.8	14.0	(a)	2.1
2	(calibration error)				
3	7.0	6.7	6.8	(a)	1.5
4	59.5	4.8	32.1	6.4 (b)	6.3
5	4.4	3.5	4.0	2.54 (b)	1.6
6	27.5	2.1	14.8	(a)	3.4
7	124	144	133	135 (c)	1.3
8	10.7	37.5	22.6	(a)	2.6
9	9.5	2.6	5.7	1.0 (b)	1.6
10	14.9	6.7	9.7	4.1 (b)	2.1
11	51.8	1.5	26.6	(a)	3.7
12	(bulb rupture)				
13	(bulb rupture)				
14	54.0	22.4	35.1	20.3 (b)	2.3
15	63.5	115	82.9	57.1 (c)	2.1
16	57.5	31.5	44.6	(a)	2.8
17	138	31.6	80.5	7.6 (b)	2.2
18	97.4	27.9	54.0	5.1 (b)	1.9
19	7.0	6.8	6.9	12.7 (c)	1.8
Average ± s.d.	45.8 ± 43.1	29.0 ± 41.4	35.8 ± 36.1	25.1 ± 41.9	2.79 ± 1.68

(a) Bulb not against lip.
(b) Lighting with bulb against bottom lip.
(c) Lighting with bulb against upper lip.

TABLE 2

FILTER HOLDER PRESSURE MEASUREMENTS

Filter Holder	Contact Pressure (Torr)	No. of Observation
Cambridge	47	2
Borgwaldt	118	3
Filtrona	500	15

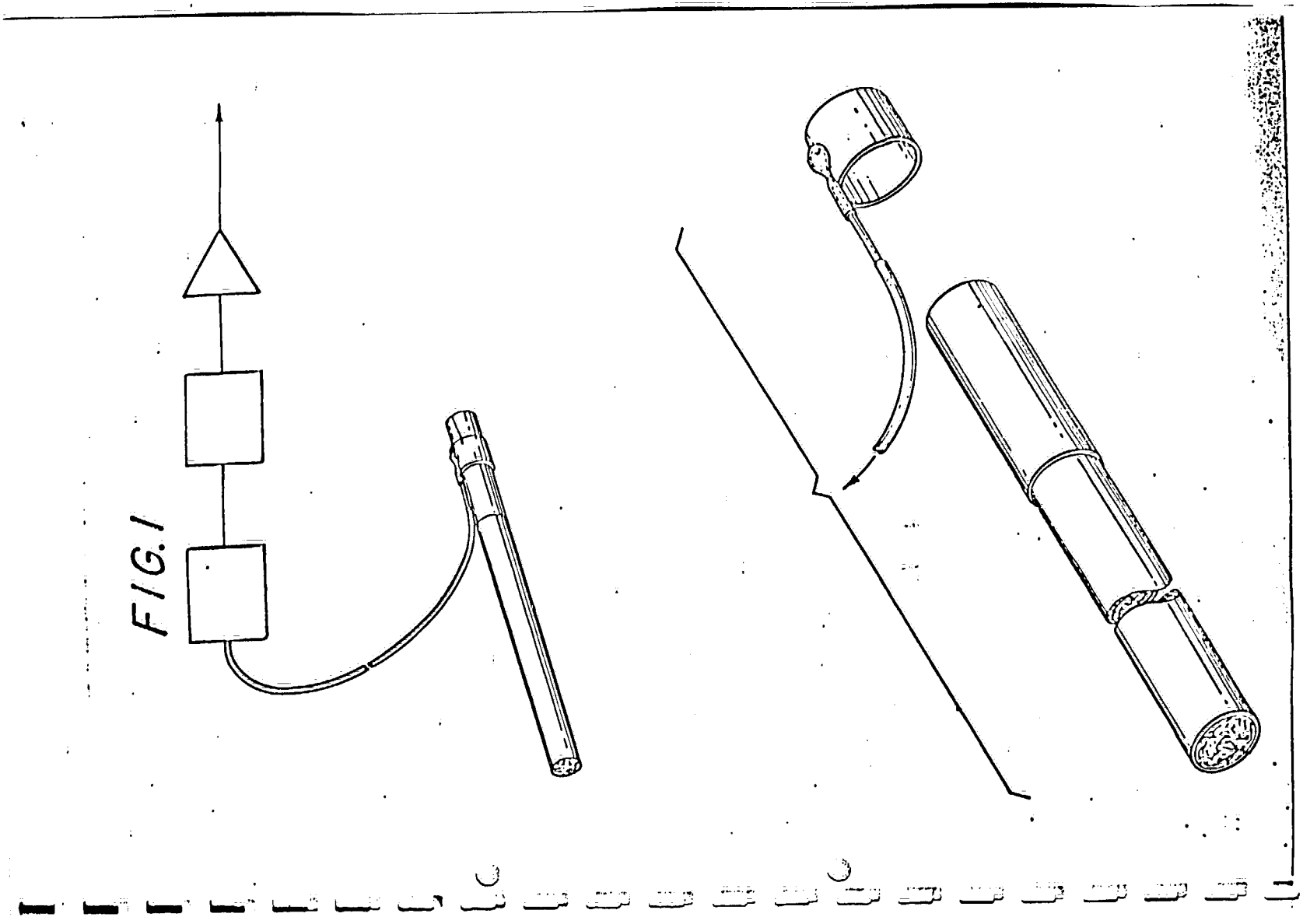

FIG.1

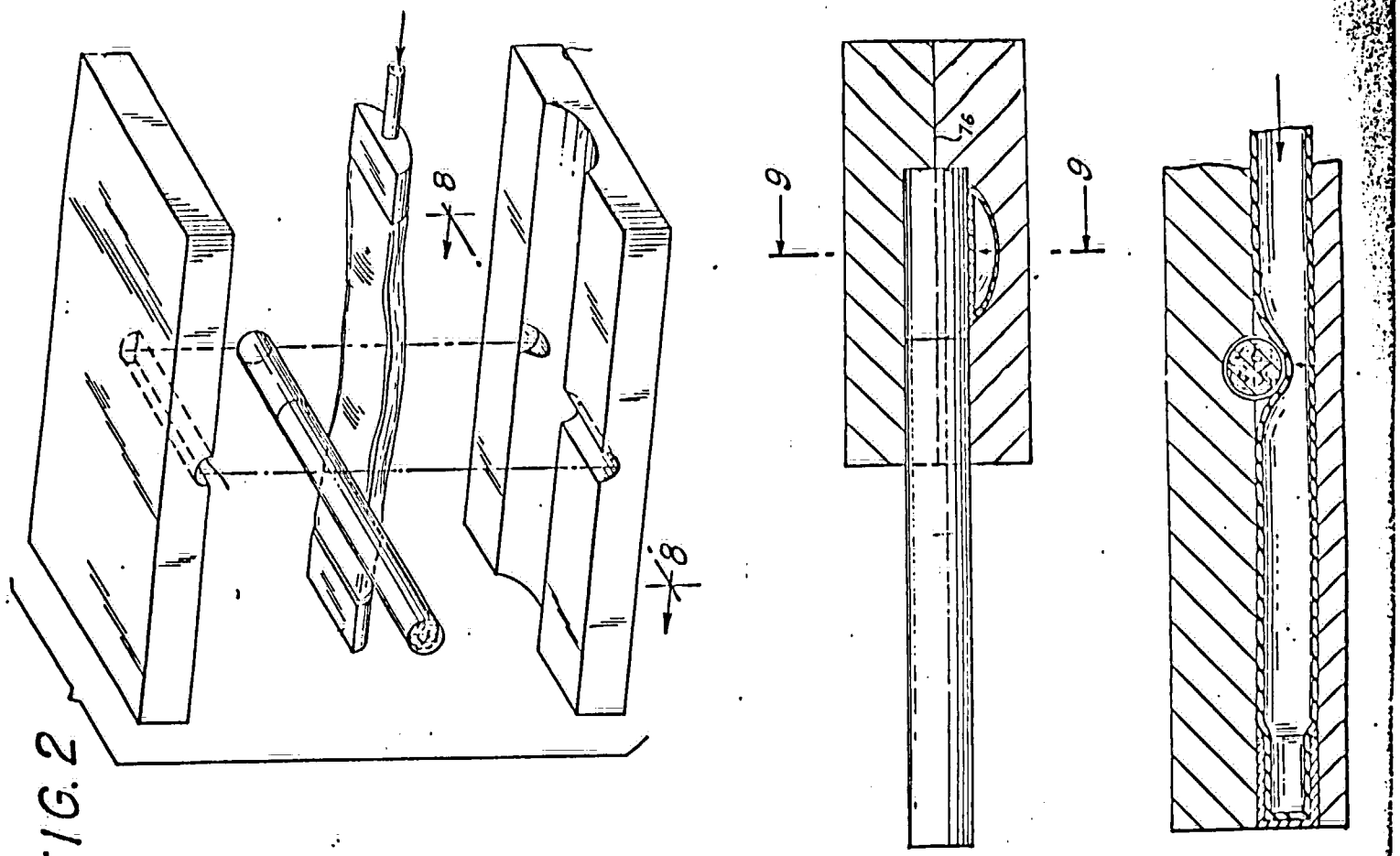

FIG. 2

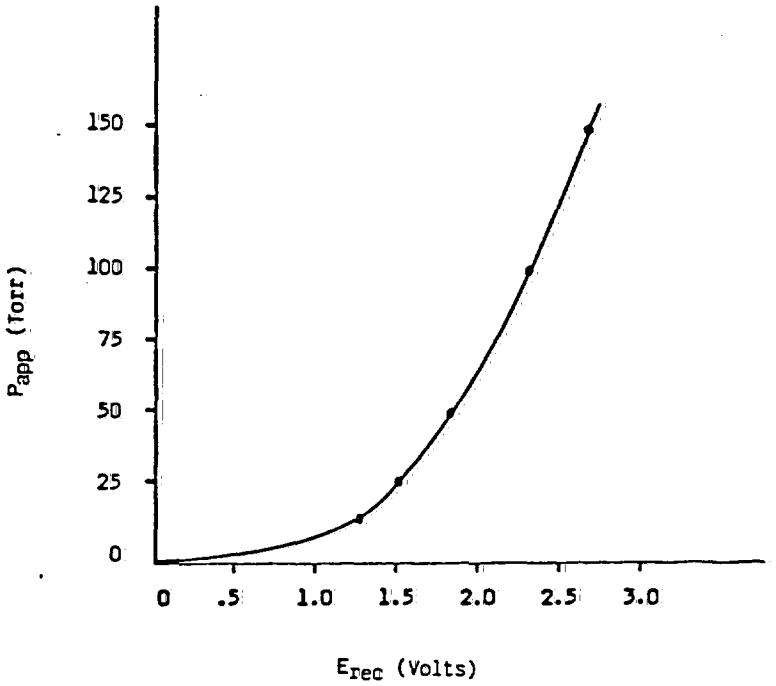

Figure 3. Sample Calibration Curve

(a)

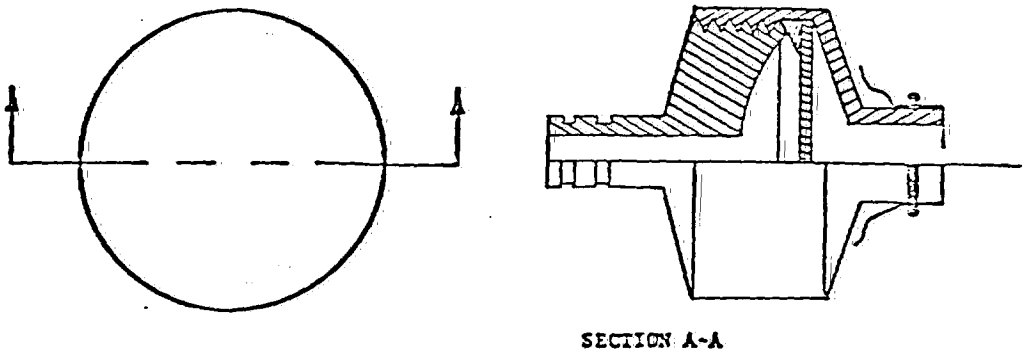

(b)

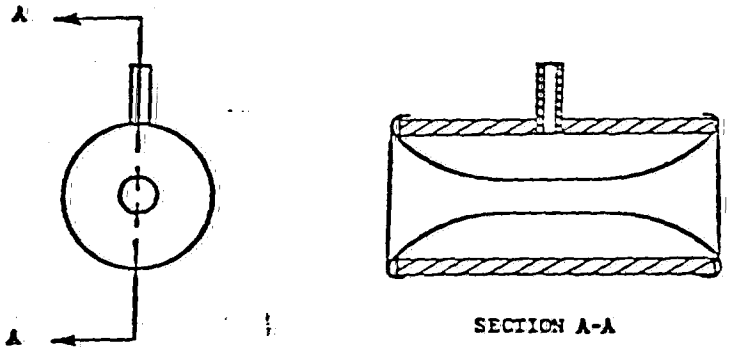

Figure 4. The Three Filter-Holders Tested: (a) Cambridge, (b) Borgwaldt, and Filtrona.

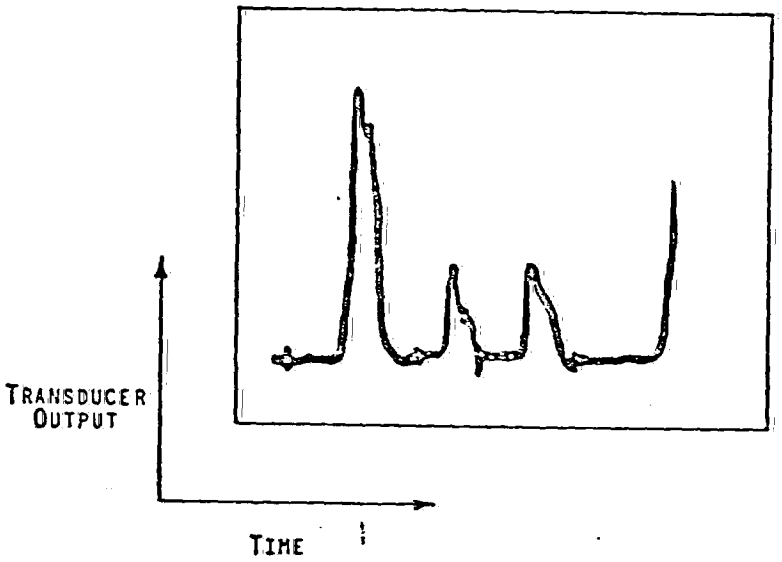

Figure 5. Oscilliscope Trace Showing The Voltage Output from the Pressure Transducer During Three Consecutive Puffs.

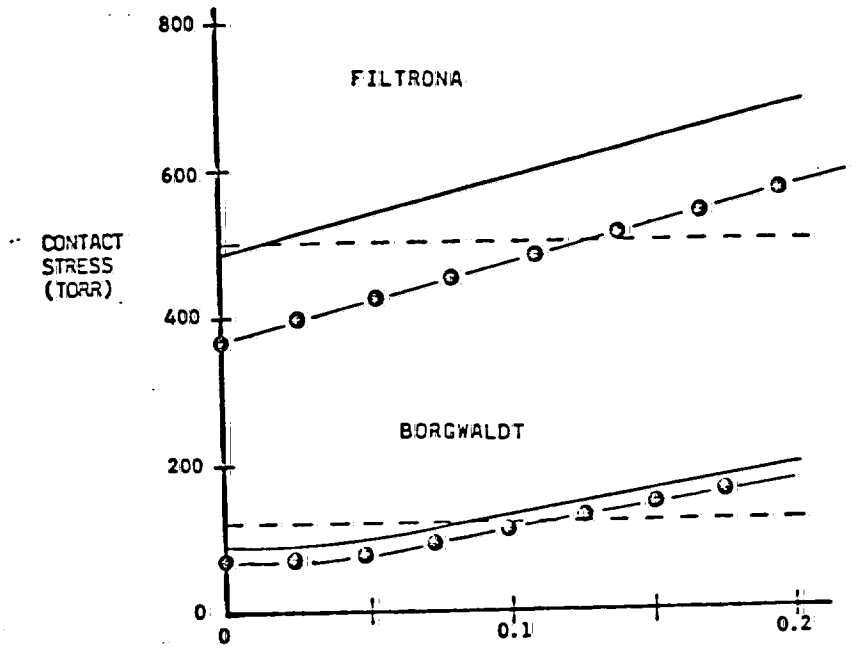

Figure 6. Predicted values of contacted stress for the Filtrona and Borgwaldt holders as a function of applied axial strain.

APPENDIX V

FILTER INTERACTION WITH LIP MUCOSA

by

Louis Fine, Ph.D.
University of Chicago
Chicago, Illinois

DRAFT
COMMERCIAL IN CONFIDENCE

Filter Interactions with Lip Mucosa

by Dr. Louis Fine

Zoller Clinic University of Chicago

A. Introduction

The three aspects covered were:

1. The videotapes of intra oral viewing, which by the use of a fiberoptic system demonstrated the interaction between the human lips and filter end in both "normal" and "abnormal" smoking - Abnormal smoking is caused by the design of the Puff Parameter Analyzer, hence forth termed the P.P.A. device.
2. A brief explanation of the anatomical variation in the oral area to better understand (a) the mechanism of smoking and (b) how these variables can effect measurements during experimental procedures.
3. The P.P.A. device and our concerns regarding its use as a means of measuring air dilution.

B. Video Tape Viewing

The first tape demonstrated the interaction of the lip mucosa to the filter end from both posterior and lateral viewing angles. Obstruction of the vents was not obvious.

The second tape enabled viewing of the limited surface area of the filter available to the lips when the P.P.A. device was used. This resulted in an observable alteration in the interaction between lips and filter end causing excessive mucosal coverage of the filter end.

C. Anatomical Variations

1. By use of 3 color slides, the 3 types of dental occlusion, Class I, II, and III were demonstrated.
2. A slide of the musculature in the facial area illustrated the composition of the orbicularis oris - a sphincter like muscle - which through its innervation from the VIIth cranial nerve, the facial nerve, contracts to form a seal around the filter.

Through demonstration, each attendee was able to experience the different pressures elicited in the oral area when swallowing and sucking. The downward movement of the lower jaw to form a negative pressure, which enables smoke intake into the mouth, was also demonstrated.

The nervous system connection between the higher brain centers, hypothalamus, and facial nerve were discussed to stress the importance of behavioral effects on measurement in an experimental environment.

The Vth nerve, the trigeminal nerve, being the necessary nerve of the facial area, is concerned with proprioceptive sensation in the tongue, lips and to a lesser extent the teeth. This sensation especially strong on the vermillion border of the lips and in the fingers is important for filter insertion depth perception. In smoking with the P.P.A. device, the important role of the fingers is lost.

Slides were used to demonstrate anatomical variation in the lips and to introduce terms of importance; e.g., inter-labial gap, incompetent lips, muscle tone, normal and abnormal paths of closure of the lower jaw and lips. These variations, especially in the Class II person, result in varied surface area contact and pressure between the lips and filter.

D. P.P.A. Device

Slides demonstrated how the decreased available surface area of the filter, when using the device, limits the insertion depth thereby altering the lip to filter end relationship. This altered relationship, together with the awkwardness of the device, behaviourable influences, and artificiality of smoking affect the ventilation system of the Barclay filter. Unfavorable abutment of the

lips behind the filter, angulation of filter between the lips, increased base line lip pressure, reactive inward pressure, increased pressure directed towards the end of the filter due to the decreased surface area on the filter are the major problems which arise in testing with a device like the P.P.A.

Conclusion

1. Fiber optic studies in 20 real Barclay smokers did not demonstrate any obvious occlusion of the filters' vents.
2. The P.P.A. device causes interference with the Barclay ventilation system.
3. This interference can be further exaggerated by anatomical variations, expecially in the Class II patient.
4. For these reasons, extrapolations from laboratory measurements using the P.P.A. to measure tar delivery are unreliable and misleading.

A more valid approach to measuring smoker-cigarette interaction is the consideration of the pharmacokinetic fate of nicotine in the smoker and the use of cotinine as a marker in plasma.

APPENDIX VI

PHARMACOKINETICS OF NICOTINE AND COTININE

by

Jacques van Rossum, Ph.D.
Medical School, University of Nijmegen
Nijmegen, The Netherlands

and

T. D. Darby, Ph.D.
University of South Carolina
Columbia, South Carolina

DRAFT
COMMERCIAL IN CONFIDENCE

PHARMACOKINETICS OF NICOTINE AND COTININE

Bioavailability of nicotine inhalation by smoking under steady state conditions

Jacques M. VAN ROSSUM, Ph.D., and Thomas DARBY, Ph.D.

INTRODUCTION

Cigarettes, cigars and pipes are devices by which nicotine present in the tabacco can be taken up by the body as a result of smoking. Different types or brands of cigarettes may produce different amounts of nicotine in the smoke. The amount of nicotine in the smoke is being determined by standard procedures with smoking machines (FTC method). As a consequence different amounts of smoke are offered to the upper respiratory tract and the lungs, leading to different quantities of nicotine taken up by the body.

Information on actual uptake can be gained by measuring a) the nicotine concentration in the blood, in the urine or other tissue fluids, b) the concentration of a metabolite of nicotine as, e.g. cotinine, or c) the pharmacological effects.

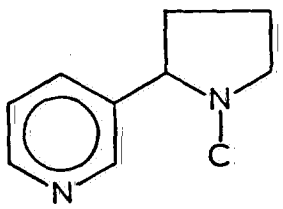

Nicotine

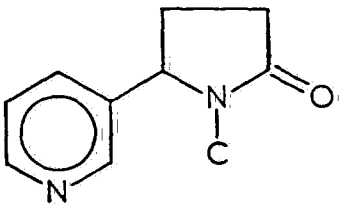

Cotinine

FIG 1. Nicotine and Cotinine Structures

In order to derive the intake of nicotine from the nicotine concentration or metabolite concentration in the blood, knowledge about the disposition and biotransformation of nicotine in the individual subject should be acquired. That is, pharmacokinetic and biopharmaceutic aspects of nicotine and cigarettes should be elaborated.

PHARMACOKINETICS OF NICOTINE INTAKE: BIOAVAILABILITY

It is possible to study the intake of nicotine or of drugs in general from the output (plasma nicotine, metabolite concentration, etc) if the so-called body transport function of the drug is known. Such studies require large amounts of data, both following i.v. injection and inhalation of nicotine from smoke and are therefore practically not feasible.

It is, however, possible to design the experiments in such a way that a limited number of data per individual are sufficient to answer the relevant questions. These questions are: a) the amount of nicotine taken up by the body, b) the rate at which it occurs and c) eventually the profile of the input function of nicotine.

The study of nicotine intake concentrates on the amount that is taken up (the absolute bioavailability) or in case of brand comparison on the relative amount or uptake ratios (relative bioavailability). The study of the intake of different brands of cigarettes compares to the study of the particular drug in the same dose in various dosage forms as capsules and tablets or different types of tablets.

Since nicotine is rapidly and also to a considerable amount converted into cotinine this metabolite is a candidate for bioavailability measurements (see Figure 1).

PHARMACOKINETIC SYSTEMS DYNAMICS OF NICOTINE

The kinetics of a substance as nicotine in the human body is determined by the physicochemical properties of nicotine and the properties of the various organs and tissues of the body.

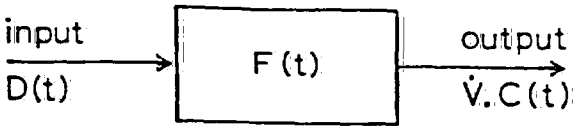

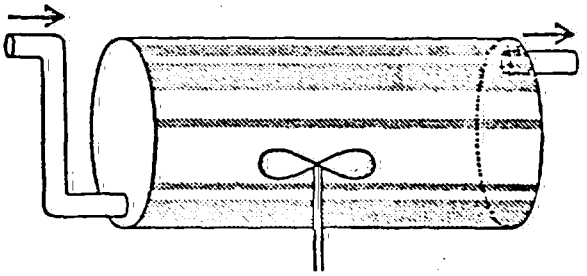

FIG. 2

TABLE 1

SUBSYSTEM: TRANSFER FUNCTION WITH EXTRACTION

$C(t) = \frac{D.(t)}{\dot{V}} * F(t)$ or $C(s) = \frac{D(s)}{\dot{V}} . F(s)$
pulse input (inj.) : $C(t) = \frac{D}{\dot{V}} . F(t)$
step input (infusion): $C(t) = \frac{\dot{D}}{\dot{V}} . \int_0^t F(\lambda)\, d\lambda$
any input : $C(t) = \frac{1}{\dot{V}} . \int_0^t D(t-\lambda).F(\lambda)\, d\lambda$
areas : $AC = \frac{AD}{\dot{V}} . AF \rightarrow AUC = \frac{(1-E)}{\dot{V}} .$ dose
mean times: $TC = TD + TF$ or $MTT = TF$
symbols: $AF = \int_0^\infty F(t)dt$ and $TF = \int_0^\infty t.F(t)dt/AF$

Subsystems

A tissue or organ may be regarded as a subsystem that receives a drug on the arterial side. Each molecule has a probability to remain in the subsystem for some time, so that a frequency distribution of transit times fully characterizes the tissue. See Figure 2a. Such a tissue may be analogous to a flow vessel (Figure 2b). Then the frequency distribution of transit times would be a single exponential function.

In general, the mean transit time (MTT), the flow of blood through the tissue and its volume are important tissue parameters. They can be obtained by determining the statistical moments of the subsystem transport function. See Table 1.

The intact system

The various subsystems are arranged in series and parallel to each other. The parallel subsystems can be grouped together such that one obtains a positive feedback control system with extraction (see Figure 3). The overall system equation can at once be written down (see Table 2).

The input function, $D_L(t)$, describes the amount of nicotine in the smoke offered to the mouth, upper respiratory tract and the lungs. It will depend on smoking behaviour, the type of cigarette and the type of filter used.

The transport function, $H_L(t)$, from mouth to upper respiratory tract (fraction f_B) and from the bronchioli and alveoli (fraction f_A), describes transport from application site to the aorta. $H_L(t)$ strongly depends on smoking behaviour as depth of inhalation, puff frequency, puff duration etc. This implies that only a fraction (f_L) of the amount of nicotine in the smoke may enter the body.

INHALATION OF NICOTINE: SAMPLING OF NICOTINE

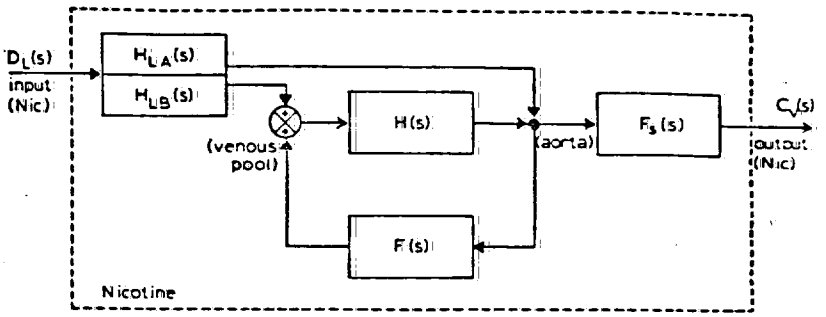

FIG. 3

TABLE 2 NICOTINE INHALATION KINETICS

Input : nicotine from smoke in mouth and respiratory tract

Output: nicotine concentration in venous blood

System equations:

$$C_V(s) = D_L(s) \cdot \frac{\{f_A.H_{LA}(s) + f_B.H_{LB}(s)\ H(s)\}}{\dot{V}_B} \cdot \frac{F_s(s)}{1-F(s).H(s)}$$

or

$$C_V(s) = D_L(s) \cdot H_L(s) \cdot \psi(s)/\dot{V}_{el} \quad \text{and} \quad C_V(t) = D_L(t) * H_L(t) * \psi(t)/\dot{V}_{el}$$

After a single dose ($D_L(t)$ = dose)

area : $AUC_V = \text{dose}.f_L/E.\dot{V}_B = \text{dose}.f_L/\dot{V}_{el}$

mean times: $MRT = TD_L + TH_L + MTT \cdot N_{rc} + TF_s$

During multiple dosing ($D_L(t) = \dot{D}_L$)

steady state: $\bar{C}_{V(pl)} = \dot{D}_L.f_L/\dot{V}_{el}$

$\psi(s)$ is the overall body transfer function for nicotine from aorta to sampling site.

$\psi(t)$ is the corresponding transport function in the real time domain, where * is the symbol of convolution

$H_L(s)$ is the overall transfer function from input site to aorta, where f_A is the fraction taken up in the alveoli and f_B is the fraction via mouth and the bronchi

TABLE 3

KINETIC SYSTEMS PARAMETERS OF NICOTINE AND COTININE IN MAN

drug	MRT (h)	clearance (l/h)	volume of distribution (l)	Extr. (%)	MIT (min)	N_{rc}
nicotine	2	60	120	20	24	4
cotinine	30	3	90	1	18	100

Nicotine follows input variation

Cotinine averages input variation

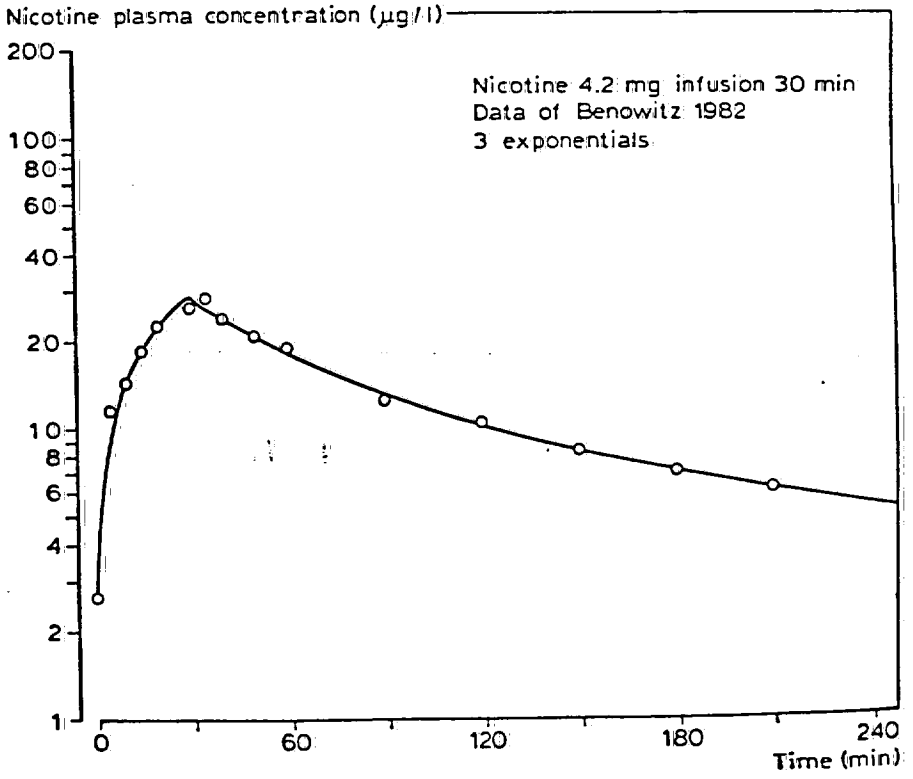

Fig 4

The function $F_s(t)$ gives the transport from aorta to sampling site (e.g. an arm vene). The function H(t) is the transport function from venous pool to aorta and the function F(t) is the transport function of all tissues of the body, except the heart-lung system. Since liver and kidney are included, extraction takes place here. The molecules that pass F(t) intact may again pass the system (recirculation) (van Rossum et al., 1982).

The relevant kinetic systems parameters: body MTT, extraction E, cardiac output $\dot{V}_B$, clearance $\dot{V}_{el}$ and body mean residence time MRT, with their interrelations are given in Table 2, again using statistical moments.

Total body transport function of nicotine

From plasma nicotine concentration curves following a known input of nicotine the total body transfer function of nicotine can be calculated. We have used i.v. nicotine studies by Benowitz et al. (1982) and Rosenberg et al. (1980) to calculate the body transport function $\psi(t)$ of nicotine in man (Figure 4).

The kinetic systems parameters of nicotine are given in Table 3. The average nicotine takes about 25 min for a single pass through the body. The extraction is about 20%, so that the average number of recirculations is 4 and therefore the mean residence time of nicotine is about 2 hrs. The clearance is about 60 l/h. As a consequence the dynamics of nicotine is fast, which implies that, according to control theory, the output (nicotine plasma concentration) follows the input. The bioavailability (here f_L) can be obtained from the area under the plasma concentration curve following a single dose or smoking a single cigarette, provided that the AUC of a known input has been determined. One does then, however, need to estimate the entire plasma nicotine curve which requires at least 10 data points per individual subject.

Steady state conditions

During a continuous intake of nicotine as occurs in very regular smoking after some time a steady state condition is reached. Then the average steady state concentration ($C_{V(pl)}$) directly relates to the intake (in mg/h or mg/day), the bioavailability f_L and the clearance $\dot{V}_{el}$ (see Table 2).

The dose depends on the type and brand of cigarette and the way the cigarette is smoked. The bioavailability f_L depends on the smoking behaviour (inhalation etc.) and the clearance merely on the individual (age, weight, etc.).

By comparing brands one should use cigarettes of the same class, since if a smoker is used to high tar cigarettes and switches over to low tar cigarettes, he may increase inhalation depth (behavioural adaptation).

NICOTINE LEVEL AS A MARKER OF NICOTINE INTAKE

From studies by Rosenberg et al. (1980), Benowitz et al. (1982), Russell and Feyerabend (1979, 1980, 1981) the body transfer function of nicotine can be calculated. See Figure 4. As pointed out, the dynamics of nicotine is fast, as its clearance is in the order of 60 l/h and its mean residence time is in the order of 2 hrs. Consequently, the nicotine level follows input variation as predicted by systems control theory. See Figure 5. In this figure 24 cigarettes of 0.2 mg nicotine are very regularly smoked during the day time, every 0.5 h one cigarette during 6 minutes (Fig. 5a). The nicotine transport function as calculated from Fig. 4 is used in Figure 5b. The result of 5a,b is the plasma curve of Figure 5c. Nicotine rapidly acquires a steady state with fluctuations around an average value. The result of five days of very regular smoking is given in Figure 7. It is evident that during the night practically all the nicotine is cleared from the body. Nicotine output (here the concentration) follows the input. Obviously, the variations in the steady

One day of regular smoking

24 cig/day, one every 1/2 h

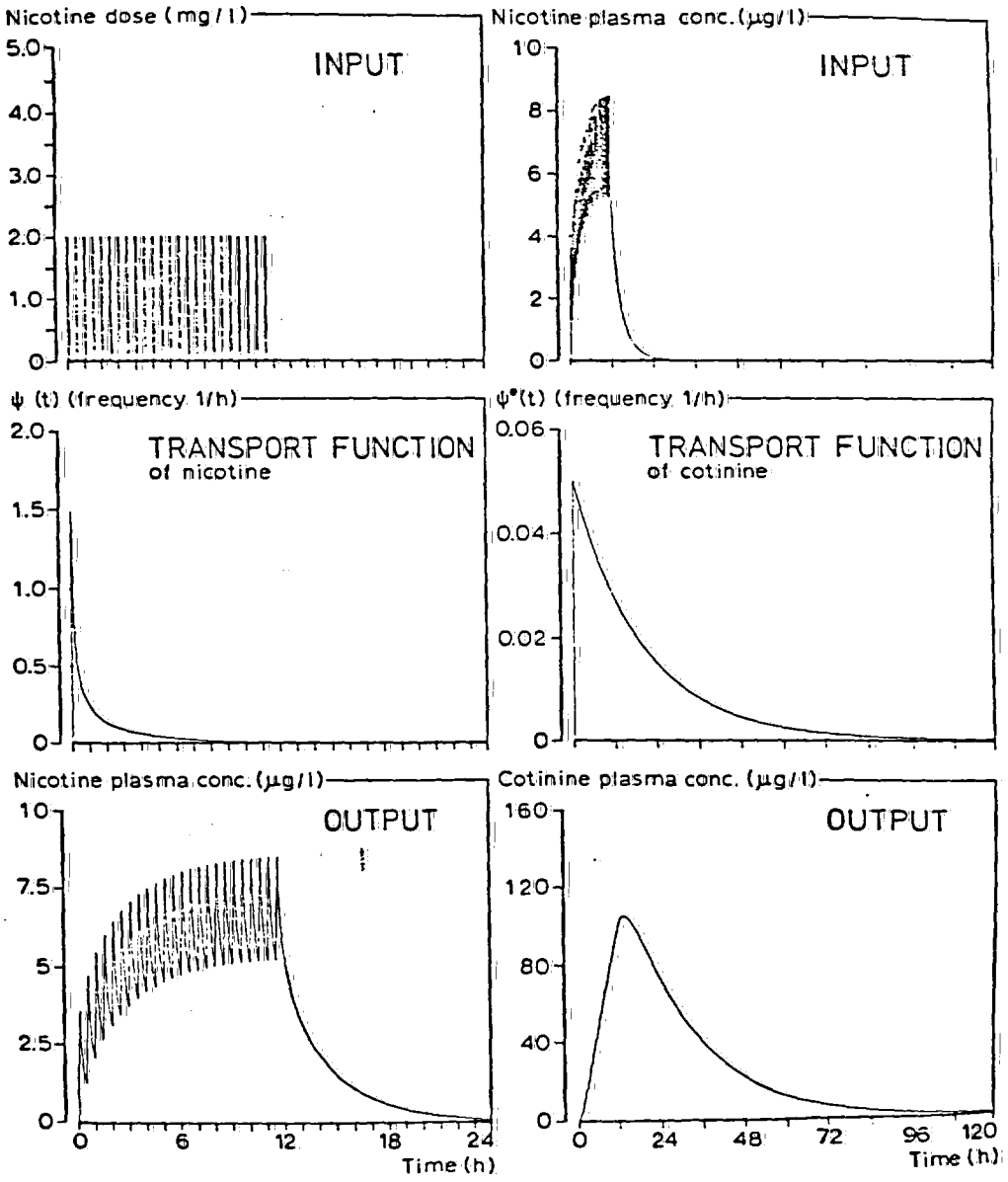

FIG. 5

state will vary much more when the input varies, as is the case in normal smoking. See Figure 8.

Nicotine can be used as a marker of nicotine input if sufficient blood samples are taken (minimum of 4 in 0.5 h) and the subject smokes regularly. For a drug with a slower dynamics fewer blood samples would suffice.

KINETIC SYSTEMS DYNAMICS OF COTININE

A major metabolite of nicotine is cotinine. The dynamics of cotinine is much slower as its clearance is in the order of 2 l/h and its MRT is in the order of 20 hrs.

The kinetics of cotinine is also according to a positive feedback control system (see Figure 6), but now the extraction is much less and therefore the number of recirculations is much greater. In case of intake of nicotine by smoking the nicotine in the blood is in fact the input for the cotinine. So, the total body transfer function for intake of nicotine and sampling of cotinine includes the transport functions of both drugs in succession. See Table 4.

The kinetic systems parameters of cotinine are given in Table 3. Although the overall transfer function from nicotine input in the respiratory tract to sampling of cotinine in the venous blood is very complex, the steady state level of cotinine again directly relates to the average intake of nicotine, D_L, the fraction of nicotine taken up, f_L, the fraction of nicotine eventually converted into cotinine, f_M^*, and the clearance of cotinine, $\dot{V}_{el}^*$. See Table 4.

Since the clearance of cotinine is much smaller than the clearance of nicotine the steady state level is higher, provided that f_M^* is not very small.

INHALATION OF NICOTINE: SAMPLING OF COTININE

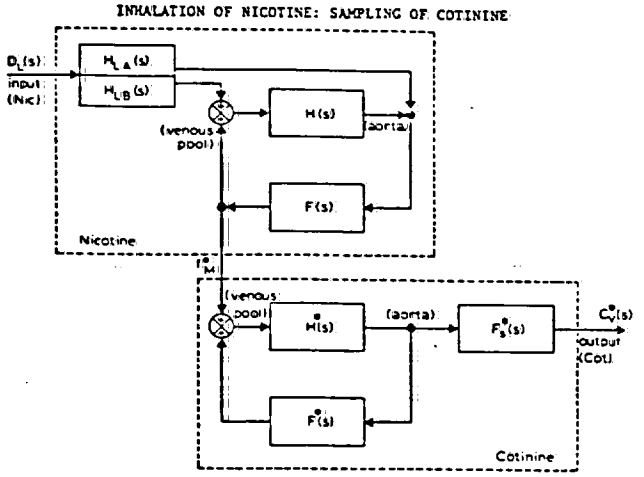

TABLE 4 NICOTINE, COTININE INHALATION KINETICS

FIG. 6

Input : nicotine from smoke in respiratory tract

Output: cotinine concentration in venous blood

System equations:

$$C_V^*(s) = D_L(s)\,\frac{H_L(s)}{\dot{V}_B}\cdot\frac{1}{1-F(s).H(s)}\cdot F(s).f_M^*\cdot\frac{F_s^*(s)}{1-F^*(s).H_s^*}$$

or

$$C_V^*(s) = D_L(s).H_L(s).\psi^*(s)/\dot{V}_{el}^* \quad \text{and} \quad C_V(t) = D_L(t)\circ H_L(t)\circ\psi^*(t)/\dot{V}_{el}^*$$

After single dose ($D_L(t) = D_L$ mg)

area : $AUC_V^* = dose.f_L.f_M^*/E.\dot{V}_B = dose.f_L.f_M^*/\dot{V}_{el}^*$

mean times: $MRT^* = TD_L + TH_L + MTT\,.\,N_{rc} + TF + MTT^*\,.\,N_{rc}^* + TF_s^*$

During multiple dosing ($D_L(t) = \dot{D}_L$ mg/h)

in steady state:

$$\bar{C}_{V(pl)} = \dot{D}_L\,.\,f_L\,.\,f_M^*/\dot{V}_{el}^*$$

$\psi^*(s)$ is the overall transfer function of nicotine in the aorta to cotinine in the sampling site

COTININE AS A MARKER OF NICOTINE INTAKE

The slower dynamics of cotinine also has important consequences for the stability of the steady state. In accordance with control theory the cotinine level is not sensitive to input variation, but on the contrary it averages the input.

In Figure 5 the intake of nicotine (a), the level of nicotine (c, d) and the level of cotinine (f) is given for a typical subject, that smokes very regularly 24 cigarettes per day. In contrast to nicotine, the next morning considerable levels of cotinine are still present.

The calculations for five days very regular smoking clearly show the steady state level of cotinine with peaks at the end of the day. See Figure 7. The calculations for normal smoking in Figure 8 show that cotinine is not sensitive to input variation.

CONCLUSIONS

In spite of the complex dynamics of nicotine and its metabolite cotinine, under steady state conditions the nicotine and cotinine level is directly proportional to the nicotine in the smoke of the cigarette in the same individual adopting a similar smoking behaviour. See Table 5. Under normal smoking conditions the input of nicotine varies, as e.g. the interval between cigarettes smoked is not constant.

The nicotine level follows input variation whereas the cotinine averages input variation. Cotinine is therefore a better marker of daily nicotine input than nicotine, provided that studies are done in the same individuals and under steady state conditions.

TABLE 5

STEADY STATE CONCENTRATIONS DURING CONTINUOUS NICOTINE INTAKE BY SMOKING

$$\text{Nicotine: } C_{pl} = \frac{\dot{D}_L \cdot f_L}{\dot{V}_{el}} \qquad \text{Cotinine: } C^*_{pl} = \frac{\dot{D}_L \cdot f_L \cdot f^*_M}{\dot{V}^*_{el}}$$

$\dot{D}_L$ = the dose of nicotine in the smoke (mg/h; dependent on type of cigarette)

f_L = the fraction of the nicotine absorbed (dependent on smoking behavior)

$\dot{V}_{el}$ = clearance of nicotine (dependent on the subject)

f^*_M = the fraction of nicotine converted into cotinine (subject-dependent)

$\dot{V}^*_{el}$ = clearance of cotinine (subject-dependent)

By smoking different brands of cigarettes of the same class by the same subject the steady state level of cotinine directly reflects the amount of nicotine in the smoke.

For the same individual ($\dot{V}_{el}$, V^*_{el}, f^*_m constant) with a a similar smoking behavior (f_2 constant) it holds that during steady state:

$$\frac{\textit{cotinine level on brand A}}{\textit{cotinine level on brand B}} = \frac{\dot{D}_L \textit{ brand A}}{\dot{D}_L \textit{ brand B}}$$

Five days of regular smoking

(24 cig. per day)

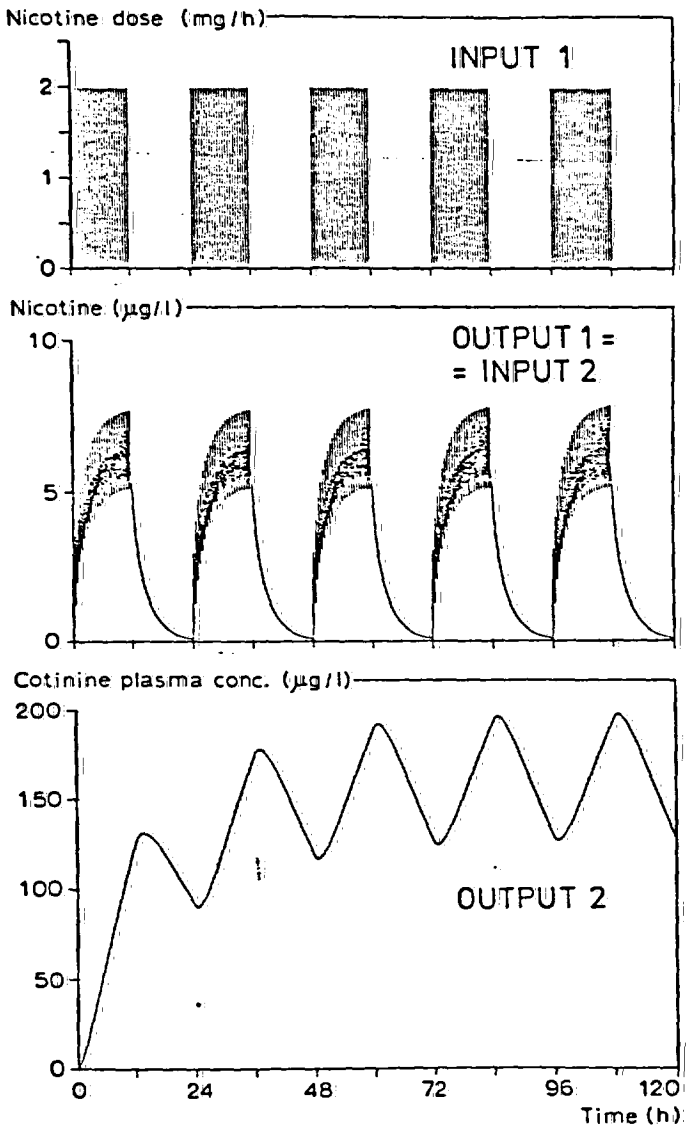

FIG. 7

Five days of normal smoking

(24 cig. per day)

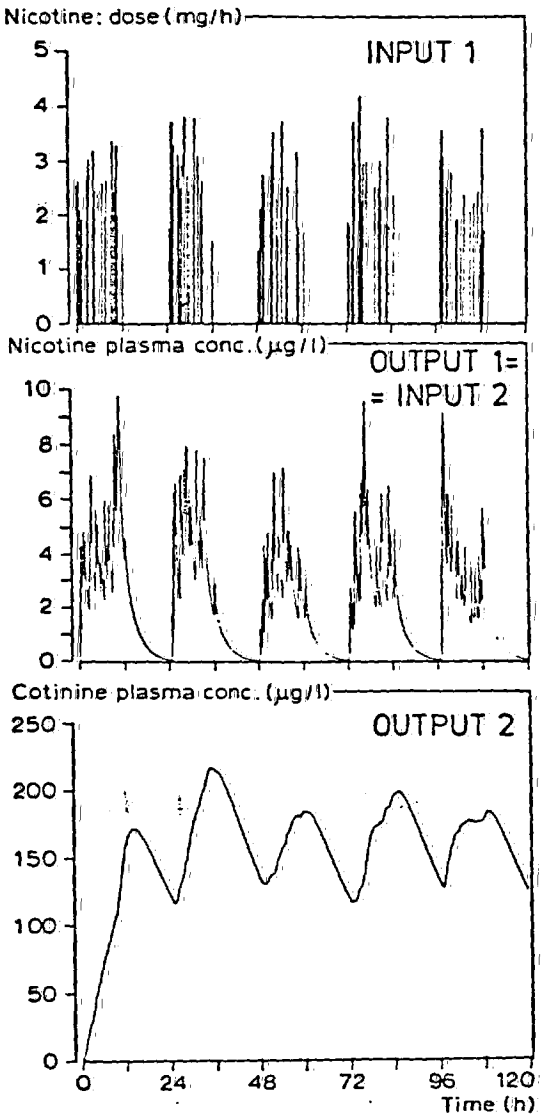

FIG. 8

REFERENCES

Benowitz, N.L., P.J.M. Reese, T. Jones and J. Rosenberg, Interindividual variability in the metabolism and cardiovascular effects of nicotine in man, J. Pharmacol. exp. Ther. 221, 368-372 (1982).

Isaac, P.F. and M.J. Rand, Cigarette smoking and plasma levels of nicotine, Nature 236, 308-310 (1972).

Rosenberg, J., N.L. Benowitz, P. Jacob and K.M. Wilson, Disposition kinetics and effects of intravenous nicotine, Clin. Pharmacol. Ther. 28, 517-522 (1980).

Rossum, J.M. van, J. Burgers, G. van Lingen and J. de Bie, Pharmacokinetics: a dynamic systems approach, TIPS, in press (1982).

Russell, M.A.H. and C. Feyerabend, Cigarette smoking: a dependence on high-nicotine boli, Drug. Metab. Res. 8, 29-57 (1978).

Russell, M.A.H., M. Jarvis, R. Iyer and C. Feyerabend, Relation of nicotine yield of cigarettes to blood nicotine concentrations in smokers, Br. Med. J. 1, 972-976 (1980).

APPENDIX VII

SMOKER INTAKE FROM CIGARETTES IN THE 1 MG TAR CLASS

by

Gio B. Gori, Ph.D.
Franklin Research Institute
Silver Springs, Maryland

and

Cornelius J. Lynch
Franklin Research Institute
Silver Springs, Maryland

DRAFT
COMMERCIAL IN CONFIDENCE

DRAFT

Smoker Intake from Cigarettes in the 1 mg Tar Class

Gio B. Gori and Cornelius J. Lynch

The Franklin Institute

Silver Spring, Maryland

October 8, 1982

Draft

Not for Release

DRAFT

ABSTRACT

In the U.S., cigarette yields are measured according to standard analytical procedures issued by the Federal Trade Commission (FTC). Concern has been raised that such measurements may not be sufficiently informative to consumers of low yield cigarettes, whose smoke intake may depend mainly on the aggressiveness of personal behavior and cigarette characteristics other than yield. This study determined relative smoke intake in smokers of cigarettes in the 1 mg tar class who switched brands. Intake was measured as plasma levels of cotinine, a direct metabolite and good indicator of nicotine intake. All brands tested resulted in cotinine levels over a similar range of values from non-detectable to some 900 ng/ml. However, the overall mean levels for each brand, as well as the brand differences in individual smokers, were closely proportional to the small analytical differences of FTC

DRAFT

nicotine yields for each brand smoked. The implication is that FTC values may not predict the absolute intake of individual smokers, a task they could not be asked to achieve; however, they appear to offer valid information about the relative intake that individual smokers may expect from different brands in the 1 mg tar class.

INTRODUCTION

Numerous studies of cigarette smoking indicate that the intensity of effects depends on the dose inhaled (1). On this basis, cigarettes of low smoke yield have been advocated as being less hazardous. Considerable epidemiologic and laboratory evidence supports this advice (2), although controversy has risen over the definition and ranking of less hazardous cigarettes.

DRAFT

In the United States cigarette yields are officially measured using a standardized analytical procedure adopted many years ago by the Federal Trade Commission (FTC) with wide concurrence (3). Similar methods are used in other countries. Lately, concerns over the differences of individual smoking behavior have questioned whether the standardization of the FTC methodology is relevant in providing the consumer with a ranking of commercial cigarettes (4, 5, 6, 7). The particular implication has been that intake variance may be more pronounced for smokers of low yield cigarettes, where it may be affected by cigarette characteristics other than tar and nicotine yields, e.g. resistance to draw, etc.

The problem of measuring natural intake during field smoking conditions is complicated by the imposition of any experimental schedule, especially when smokers are asked to switch brands of substantially

different yields. Here, their immediate behavioral changes are determined by a mixture of organoleptic (e.g. flavor), pharmacologic (e.g. nicotine), kinesthetic (e.g. draw resistance), and psychological (e.g. novelty), factors, some of which subside after some time, while others remain to define permanent adjustments to the new cigarettes. The time to reach a new equilibrium varies with individuals, but it is probably in the order of weeks (5, 8, 9). Because of this, experiments focusing on the immediate outcome of switching to and from brands of markedly different yields are unlikely to inform about those stabilized conditions that eventually take over.

The present study set forth to measure the range of smoke intake in individual smokers of three popular U.S. cigarette brands, advertised as nominally yielding 1 mg of tar by the FTC method. It also addresses the question of how smokers respond to small differences in FTC smoke yields, as they switch from one to another of these brands.

DRAFT

Testing these questions with smokers of cigarettes of the same FTC yield class, is likely to avoid significant distortions of compensatory behavior, and justifies an experiment of relatively short duration (9).

Evidence for compensation has been obtained by measuring the number of cigarettes smoked, extent of tampering with filtration and smoke dilution devices, or the observation of greater volume and frequency of puffs and inhalation (4, 5, 6, 7). Clearly, these inferential measures do not provide a direct indication of smoke intake.

At the present state-of-the-art, cigarette smoke intake in man can be measured directly only through suitable markers in the blood of smokers, thus bypassing the uncertainties of indirect assessments. Carbon monoxide (CO), nicotine, and cotinine have been utilized for this purpose. The first has been questioned because smokers are exposed to CO from automobile emissions and other domestic,

occupational and industrial sources. Also, CO could originate from endogenous physiologic processes (10). Correlations of expired CO and plasma nicotine values have been found in well controlled and limited experiments conducted in restricted laboratory settings, utilizing few subjects and cigarettes of relatively high CO yields (11). However, the confounding influence of exogenous sources can be expected to be severe when large numbers of users of low CO cigarettes are asked to smoke under free ranging conditions, as in the present study.

Nicotine is obviously a most specific marker of tobacco smoke, although it is present in insignificant amounts in tomatoes, peppers and eggplant. While measurements vary, an approximation of its terminal half life is some 40 - 100 minutes in the bloodstream. This is likely to make its determination sensitive to short-time sampling variables, and to reflect mainly the input from the last two or three cigarettes smoked (12, 13, 14, 16). Its excretion rate also depends partially on

DRAFT

urine pH, resorption and other transient factors (17, 18, 21, 22), although these can be expected to contribute negligibly to variance if blood sampling is close to the actual time of cigarette smoking.

Potentially, a more serious difficulty in using nicotine as a marker is that individuals smoke with different intensity at different times of the day, when satiation sets in, or under stress as, for instance, during an experimental blood sampling session. The ideal marker would give an average indication of the cumulative results of discrete intake episodes over a suitable period of time, and should not represent simply the momentary experience of smoking one or two cigarettes.

Several human and animal studies have shown cotinine to be a principal and direct metabolite of nicotine, from which it arises at predictable and defined rates (13, 14, 15, 16). This correspondence is confirmed by the good linear correlation of nicotine and nicotine plasma levels,

as reported later in this study and by others (14). A terminal half-life of some 20 - 30 hours makes cotinine insensitive to short-time sampling variables, and requires only that subjects be sampled during late afternoon and at fixed days during the week, to equalize weekly and circadian steady-state patterns (14). On this account, cotinine is probably a better indicator of overall cumulative intake during undisturbed smoking activities, not significantly affected by immediate experimental stress behavior as nicotine intake could be. It is also present in plasma at concentrations 10 fold higher than nicotine, and demands less strict analytical procedures.

It should be noted that the kinetics of nicotine excretion and metabolism are poorly understood. Variations in individual behavior, weight, lean body mass and urinary pH will result in a range of plasma nicotine and cotinine values in different individuals smoking the same cigarettes (12-18, 20, 21). The metabolism of nicotine in the liver,

its major site of detoxification, is mediated by microsomal enzymes that can be activated or depressed by a number of dietary components, alcohol, drugs, pathologic and physiologic conditions (12-16). Such reasons and others preclude reliable quantitative estimates of smoke intake from plasma nicotine and cotinine levels. Nevertheless, these sources of variance are clearly not sufficient to unduly affect the observed linear correlation of plasma nicotine and cotinine levels, nor the week by week stability of cotinine levels in the subjects of our study. This suggests that, while metabolic and excretion dynamics may be different among individuals, they are likely to remain more stationary in the same individual over a relatively short time when diet, health status, medication and stress conditions remain virtually unchanged. Thus it is reasonable to conclude that changes in the plasma nicotine and cotinine of individual smokers, switching from brand to similar brand over a controlled time span, represent their individual experience with each brand, and give a reliable indication of their relative intake from each brand.

DRAFT

Therefore, the experiment was designed so that it could also be analyzed as a sequential one, considering individual smokers as they switch brands. In this self-matching analysis, individual smokers provide their own control, and the ratios of cotinine levels generated by each brand give a measure of the relative position of that brand.

Significantly, nicotine is delivered in close physical association with tar particles (19). Only a negligible amount is delivered in the vapor phase, and at the average pH of cigarette smoke most of it is absorbed in the lungs and not in the upper respiratory tract (20). Upon contact with the lung surface nicotine is rapidly transferred to the bloodstream, while less soluble tar components are first absorbed on the surface. Because of this, nicotine and cotinine are also valid indicators of tar intake, once the ratio of tar to nicotine of a cigarette's smoke is known.

DRAFT

As a working hypothesis, we adopted the proposition that nicotine may be proportional to the FTC nicotine delivery of the cigarette smoked. Thus, plasma levels of cotinine would also be proportional to nicotine intake, to FTC nicotine yields and, by suitable transformation to FTC tar yields.

DRAFT

MATERIALS AND METHODS

Cigarettes

The study utilized three commercial brands (A, B and C) belonging to the 1 mg FTC tar class. All cigarettes were purchased from commercial distributors, each brand coming from the same production batch, to minimize input variance. Specific analytical data are summarized in Table 1.

Subjects

Behavioral distortions could bias the hypothesis testing, especially compensatory up-shifts that could be expected if the subjects had been habitually smoking high yield cigarettes (22, 23, 24, 25.) Therefore, the study was designed so that participants would continue to smoke as

DRAFT

closely as possible to their habitual practices. Subjects were selected who customarily smoked either A or B Brand cigarettes yielding 1 mg nominal FTC tar. They were allowed to smoke under natural free conditions, as contrasted to an artificial or quasi-controlled experimental setting. The subjects (288 smokers, 117 men and 171 women) were approached randomly in shopping malls and through notices in community newspapers in each of five cities. Accepted respondents were at least 21 years of age, had been smoking at least 20 cigarettes daily for at least three months, and engaged in no other smoking-related practices (cigars, pipes, snuff, chewing tobacco, nontobacco smoking products). Only individuals in good health under no medication were recruited. Subjects were dropped from the study if disease and medical treatment intervened. Individuals with obvious alcoholic problems were also excluded. Each subject was informed at the outset that participation in the study would require smoking specific 1 mg tar brands provided free of charge; they also were asked not to change consciously any of their customary smoking practices.

DRAFT

Schedule

On their first visit, the subjects completed a brief questionnaire on their smoking history and related factors, and provided a 10 ml sample of venous blood for baseline cotinine analysis. Subjects were sampled in late afternoon on Wednesdays or Thursdays, in order to equalize circadian and weekly behavioral patterns and pharmacodynamic conditions.

Each respondent was given a week's supply of his/her own customary brand of cigarettes to smoke for the following week, and a cigarette tally sheet to record the exact time for each cigarette smoked in the 48 hours preceeding sampling. They were also provided with special containers, to collect all butts of the cigarettes smoked during the tallying period. Respondents reported on the following week and provided venous blood samples, as before. These data comprised a second set of baseline values.

DRAFT

At this point smokers of Brand A were given Brand B and vice versa. Respondents stayed on the alternate brand for three weeks, reporting to the test center weekly to provide venous blood, to obtain additional supplies of cigarettes, and to turn in the completed cigarette tally sheets.

Starting with the fifth visit to one of the test centers, all respondents were given Brand C cigarettes to smoke for two weeks, once again reporting to the center each week for blood samples. The sequence of brands smoked is summarized in Table 2. All subjects received a nominal monetary compensation at each sampling.

Nicotine - Cotinine Correlation

A separate group of 45 male and 41 female smokers of 1 mg tar cigarettes (31 Brand A, 35 Brand B, 15 Brand C, 5 Brand D) was recruited for the purpose of validating plasma cotinine as a marker of

DRAFT

plasma nicotine and smoke intake. These subjects had general characteristics as for the main group above, but special precautions were taken to insure that daily steady-state conditions for plasma nicotine and cotinine were well standardized, as required by pharmacokinetic considerations and previous experiences (14). To this end, the subjects in this group habitually smoked at regular intervals during the day, and especially during the three hours preceeding the sampling. Blood withdrawal for this group occured at the first time the subjects presented themselves, and was performed usually on a Thursday betweem 5:00 and 7:00 pm. These precautions are absolutely necessary for a realistic correlation. Sampling indiscriminately during the week would give results that are distorted by the behavioral changes that most smokers experience on weekends. Morning sampling, on the other hand, will also distort the correlation, because of the different times required to reach peak steady-state levels of plasma nicotine and cotinine (14). A control group of 23 male and 26 female nonsmokers was also recruited and sampled for plasma nicotine and cotinine.

Blood Samples

Blood samples were drawn by a certified technician; plasma was obtained by centrifugation and frozen without preservatives within fifteen minutes of being drawn. Samples were blind coded, shipped and stored frozen at -20°C or below.

Cotinine and Nicotine Analysis

Cotinine and nicotine levels in plasma were determined using methods developed by Jacob et al. (25). Standard curves were constructed and repeated every 40 determinations, by adding internal standards (N-ethylnornicotine for nicotine, and N-(2 Methoxyethyl) norcotinine for cotinine) to blank plasma samples which were carried through the extraction procedure. The peak height correlation was linear over the

DRAFT

range 0 to 600 ng/ml for cotinine, and 0 - 100 ng/ml for nicotine. Throughout the procedure, precautions were taken to avoid exogenous contamination (27).

As a quality control check, 178 plasma samples were selected randomly for re-analysis of cotinine values. The average of the original values was 245 ng/ml, with SEM of 11.4 ng/ml. The duplicate values had an average of 258 ng/ml, with SEM of 11.9 ng/ml. The linear correlation coefficient between the original and duplicate values was 0.93, and the paired t-test was not significant at P = 0.05. For nicotine, 21 samples were selected at random for re-analysis. The average of the original values was 26.3 with SEM 2.5 ng/ml; the duplicate set had an average of 26.8 with SEM 2.3 ng/ml. The paired t-test value was not significant at P = 0.05. These statistics suggest a high level of consistency in the analytical methodology.

DRAFT

To exclude possible interferences from other compounds in the analysis of cotinine and nicotine, a random group of samples was analyzed by high resolution gas chromatography and mass spectrometry (GS/MS). Ten plasma samples, previously analyzed as above, were processed according to our analytical methodology for the determination of cotinine. Prior to GC/MS analysis the sample extracts were pooled and concentrated to a volume of 20 ul. A 1 ul aliquot was then analyzed by GC/MS. The GC/MS conditions were:

GC/MS: Finnagan 4000
AMU Range: 35-450
Scan Speed: 1 scan per second
Mode: Electron Impact
Column: Fused silica, 30M x 0.312 mm
Flow Rate: 2 ml/min
Liquid Phase: DB5, J & W Scientific
Temperature Program: 50°C (4 min) to 280°C at 8°C/min
Injector Temperature: 260°C
Injection Volume: 1 ul, splitless

No interfering molecules were found. The calculated concentration of cotinine was 594 ng/ml by GC/MS, comparing favorably with the 526 ng/ml measured by the GC analysis routinely used.

DRAFT

RESULTS

Subject characterisitcs

General characteristics of the subjects entering the study are summarized in Table 3 and Figures 1 and 2. The groups represented predominantly white collar occupations and housewives. Male - female differences are reflected throughout the results, thus requiring separate analysis of the data.

Plasma Cotinine

Mean values of plasma cotinine measurements are summarized in Table 4, broken out by the brand of cigarettes customarily smoked, by sex, and stratified into three baseline range levels in order to compare smokers

DRAFT

with similar intake habits and demand. Baseline values were averaged over the first two measurements taken, while each respondent had been smoking his/her customary brand. The alternate brand values are averaged over the separate measurements for each respondent, when Brand A smokers were smoking Brand B and viceversa (see table 1). The last set of values in Table 4 are averages over the two weekly spans when all respondents were smoking Brand C.

Table 5, summarizes the mean values and associated standard errors of the plasma cotinine measurements broken out by groups having homogeneous characteristics, i.e. by the brand of cigarettes customarily smoked, and by sex. Overall baseline values were averaged over the first two measurements taken, while each respondent had been smoking his/her customary brand. The overall alternate brand values are averaged over three separate measurements for each respondent. The last set of values in Table 5 gives overall averages over the two time

DRAFT

periods when all respondents were smoking Brand C. No statistically significant differences (P = 0.05) were noted between observed and expected values in a self-matching paired t test analysis, except in the two instances given in Table 5. Although significant, these two deviations are very small and do not affect the overall conclusion, namely that for the low yield cigarettes tested, individual smoker plasma cotinine levels and intake of nicotine are closely proportional to the small differences of nicotine yields among brands, as determined by FTC methods (Figure 3 and Table 5). Expected values were made to reflect the FTC nicotine yield ratios for the brands smoked (Table 1).

In a consolidated assessment, Table 6 summarizes the results for all respondents as they smoked the three brands tested. Because the level of cotinine partially depends on the number of cigarettes smoked daily, (figure 4), a normalization was carried out for each data point of each respondent, by dividing his/her plasma cotinine values by the number of

daily cigarettes used prior to that sampling. Averages of these normalized values are given in Table 6. The ratios of these averages agreed well with the ratios of the analytical nicotine yields of the cigarettes tested (Table 2). Maximum recorded values of plasma cotinine are also given in Table 6, indicating that each brand tested is capable of generating a similar range of values.

The sample coefficient of skewness was calculated for each experimental set of values. In all cases the coefficient was positive, suggesting a slight dispersion of values to the right of the mean. No coefficient was significantly greater than zero ($P = 0.05$), nor did any coefficient change significantly for any group, indicating that the mean values given in Tables 4, 5, and 6 are free of distortion from dispersed sample points.

DRAFT

Number of cigarettes smoked daily

As calculated from the respondent's tally sheets, Table 7 summarizes the average numbers of cigarettes smoked daily, broken out by the brand customarily smoked, and by sex.

In all four groups of respondents, the least number of cigarettes smoked was for Brand A. The men smoked the largest numbers of cigarettes while on Brand C and the women smoked the largest number of cigarettes while on Brand B. The average change was always below 10%. Paired t-tests for each individual experience, revealed no significant differences at P = 0.05, suggesting negligible compensation in the number of cigarettes smoked daily.

Figure 4 shows that baseline plasma cotinine levels are positively correlated with the number of cigarettes smoked daily.

DRAFT

Nicotine-Cotinine Correlation

Figure 5 gives all data from a group of 86 male and female subjects expressly sampled to explore the correlation of plasma nicotine and cotinine. The linear correlation coefficient $r = 0.84$ is significant at $P = 0.001$. In the control group of nonsmokers, no subject had a detectable level of plasma cotinine (25 ng/ml or greater). Plasma nicotine in the males ranged from 0.5 to 4.8 ng/ml, with a mean value of 1.9 ng/ml and a S.E.M. of 0.3 ng/ml. For the females, the plasma nicotine ranged from non-detectable to 7.7 ng/ml, with a mean value of 1.5 ng/ml and S.E.M. of 0.3 ng/ml. The male and female subjects combined had an average plasma nicotine level of 1.7 ng/ml, with a S.E.M. of 0.3 ng/ml. The correlation in Figure 5 does not include values for the nonsmoking controls.

DRAFT

Plasma Cotinine and Daily Available Nicotine

Figures 6 and 7 give male and female data relating baseline plasma cotinine to available daily nicotine (ADN), defined by the FTC nicotine yield of the cigarette smoked (FTC(N)), and the number (CPD) of cigarettes smoked daily: ADN = FTC(N) X CPD. A positive correlation is discernible, although - as expected - the variance is large, with r = 0.48 for males and r = 0.47 for females, both correlation coefficients being significantly greater than zero at $P \geq 0.01$. The correlation coefficients did not improve after adjusting cotinine values for subject weight indicating that behavioral and sampling factors are the more likely sources of variance, metabolic factors being probably stable on account of the good correlation of plasma nicotine and cotinine.

DRAFT

CONCLUSIONS

At present there is scant knowledge of the average pharmacodynamic parameters of nicotine to cotinine transformation, excretion and metabolism. However, two observations suggest that these parameters are relatively uniform and stable in our sample of comparable subjects, and at least within the range of plasma concentrations measured. One is the correlation of plasma levels of nicotine and cotinine (Figure 5), which must be considered exceptionally good in view of the many possible sources of variance. The other is the remarkable stability of individual plasma cotinine values week after week, while smoking the same cigarette. Thus, it may not be realistic to infer precise quantitative estimates of smoke intake from plasma cotinine levels, but they are valid estimates of relative intakes from the cigarettes tested in this study.

DRAFT

The validity of results is reinforced by the positive correlation and dose response between plasma cotinine levels (intake) and the daily quantity of available nicotine (smoke), as defined by the specific yield and the number of daily cigarettes smoked.

It is clear that any of the brands tested results in plasma cotinine levels over a similar range of values, depending on the behavior, metabolic and somatic characteristics of smokers. The virtually unchanging quantity of daily cigarettes smoked suggest that the same statement is valid for nicotine intake. In turn, the physical association of nicotine and tar in cigarette smoke, and the nearly equal tar to nicotine ratio of the brands tested, suggest that similar conclusions are probably valid for tar intake.

Previous studies found that compensation, at least under experimental conditions, is usually only partial (5, 9, 24, 25). In this study, and

DRAFT

for the nominal 1 mg FTC tar cigarettes tested, small absolute differences in analytical cigarette yield did not elicit significant compensatory shifts, and smokers displayed plasma cotinine levels proportional to the differences of FTC nicotine yields of the brands smoked (figure 4). For individual smokers this proportionality occurs within a limited segment of the overall range of observed values, high inhalers remaining high, and vice versa. This is likely to reflect consistent individual differences in the nicotine and smoke intake requirements (Table 4). The differences observed upon switching also suggest that individual smokers of 1 mg tar cigarettes may find satiation at different levels within their personal range of nicotine and smoke intake.

In conclusion, the weight of the observations in this study suggests that, although FTC values may be inadequate quantitative indicators of actual smoke intake, they appear to be a valid representation of the relative intake that individual smokers can expect from the 1 mg FTC tar class cigarettes tested, and probably from similar brands in that class.

DRAFT

References

1. The health consequences of smoking. The changing cigarette. Report of the Surgeon General. U.S. Dept. of Health and Human Services. Washington D.C. 1981.

2. A safe cigarette? Gori GB, Bock FG, Eds.: Banbury Report No. 3., Cold Spring Harbor Laboratory. 1980.

3. Pillsbury HC, et al.: Tar and nicotine in cigarette smoke. J Assoc Anal Chem, 52: 458-462, 1969.

4. Schachter S: Pharmacological and physiological determinants of smoking. Annals of Internal Medicine, 88: 104-114, 1978.

5. Russel MAH, Sutton SR, Iyer R, Feyerabendi C, Vesey CJ: Long term switching to low-tar-low-nicotine cigarettes. Br J Addiction, 77: 145-158, 1982.

6. Tobin MJ, Sackner MA: Monitoring smoking patterns of low and high tar cigarettes with inductive plethysmography. Am Rev Respir Dis, 126: 258-264, 1982.

7. Kozlowski LT, Rickert WS, Pope MA, Robinson JC, Frecker RC: Estimating the yield to smokers of tar, nicotine and carbon monoxide from the lowest yield ventilated filter cigarettes. Br J Addiction, 77: 159-165, 1982.

8. Turner JA, Sillett RW, Ball KP: Some effects of changing to low-tar and low-nicotine cigarettes. Lancet, 2: 737, 1974.

DRAFT

9. Ashton H, Stepney R, Thompson JW: Self titration by cigarette smokers. Br Med J, 2: 357-360, 1979.

10. Sjostrand T: The in vitro formation of carbon monoxide in blood. Acta Physiol Scand, 24: 314-332, 1951.

11. Ashton H, Stepney R, Thompson WJ: Should intake of carbon monoxide be used as a guide to intake of other smoke constituents? Br Med J, 282: 10-13, 1981.

12. Armitage AK, Dollery CT, George CF, Houseman TH, Lewis PJ, Turner DM: Absorption and metabolism of nicotine from cigarettes. Br Med J, 4: 313-316, 1975.

13. Benowitz NL, Jacob P, Jones RT, Rosenberg J: Interindividual variability in the metabolism and cardiovascular effects of nicotine in man. J Pharmacol Exp Ther, 221: 368-372, 1982.

14. Gritz ER, Baer-Weiss V, Benowitz NL, Van Vunakis H, Jarvik ME: Plasma nicotine and cotinine concentrations in habitual smokeless tobacco users. Clin Pharmacol Ther, 30: 201-209, 1981.

15. Pilotti A: Biosynthesis and mammalian metabolism of nicotine. Acta Physiol Scand, Suppl, 479: 13-17, 1980.

16. Gonrod JW, Jenner P: The metabolism of tobacco alkaloids. Essays in Toxicology, 6: 35-78, Academic Press, New York, 1975.

17. Matsukura S, Sakamoto N, Seino Y, Tamada T, Matsuyama H, Muranaka H: Cotinine excretion and daily cigarette smoking in habituated smokers. Clin Pharmacol Ther, 25: 555-61, 1979.

18. Matsukura S, Sakamoto N, Takahashi K, Matsuyama H, Muranaka H: Effect of pH and urine flow on urinary nicotine excretion after smoking cigarettes. Clin Pharamcol Ther, 25: 549-554, 1979.

19. George TW, Keith CH: The selective filtration of tobacco smoke. In: Tobacco and tobacco smoke. Wynder EL, Hoffman D, Eds., 577-622, 1967. Academic Press. New York.

20. Armitage AK: Some recent observations relating to the absorption of nicotine from tabacco smoke. In: Dunn WL, Ed., Smoking behavior: motives and incentives., pp. 83-91, Washington, V.H. Winston and Sons, 1973.

21. Beckett AH, Gornod JW, Jenner PA: Possible relation between pKa , and lipid solubility and the amounts excreted in urine of some tobacco alkaloids given to man. J Pharm Pharmac, 24: 115-120, 1972.

22. Creighton DE, Lewis PH: The effect of different cigarettes on human smoking patterns. In: Smoking behavior: physiological and psychological influences. Thornton, RE, Ed., Churchill and Livingstone, London, 289-300, 1978.

23. Hennifield JE, Griffiths R: Effects of ventilated cigarette holders on cigarette smoking by humans. Psychopharm, 68: 115-119, 1980.

24. Russell MAH, Sutton SR, Feyerabend C, Salooje Y: Smoker's response to shortened cigarettes: dose reduction without dilution of tobacco smoke. Clin Pharmacol Ther, 27: 210-8, 1980.

25. Sutton SR, Feyerabend C, Cole PV, Russel MAH: Adjustment of smokers to dilution of tobacco smoke by ventilated cigarette holders. Clin Pharmacol Ther, 24: 395-405, 1978.

26. Jacob P, Wilson M, Benowitz NL: Improved gas chromatographic method for determination of nicotine and cotinine in biologic fluids. J Chromatogr, 143: 203-206, 1980.

27. Feyerabend C, Russell MAH: Assay of nicotine in biological materials: sources of contamination and their elimination. J Pharm Pharmacol, 32: 178-181, 1980.

DRAFT

Aknowledgements

The authors are grateful for the assistance of:

Lauren B. Leveton, M.S., Franklin Institute, Silver Spring, Maryland, who coordinated the overall study.

Deborah A. Schneider, M.S., Elrick Lavidge Inc., Atlanta, Georgia, who supervised the recruiting of volunteers and sample collection.

Roger A. Novak, Ph.D., Borriston Research Laboratories Inc., Temple Hills, Maryland, who performed the analysis of plasma samples.

The Brown and Williamson Tobacco Corporation Inc., Louisville, Kentucky, where the tar and nicotine yield determinations were performed for the brands used in this study.

DRAFT

Table 1. Analytical Data of Cigarettes Tested
Milligrams Per Cigarette* and Standard Deviation

Brand	Batch Code	Tar	Nicotine
A	1XL	0.9 ± 0.2	0.18 ± 0.02
B	00025	0.5 ± 0.2	0.10 ± 0.02
C	EB	0.6 ± 0.2	0.11 ± 0.02

*All Cigarettes 85 mm length, filter, soft pack.

DRAFT

Table 2. Brand Smoking Schedule

	Week						
	1*	2*	3	4	5	6	7
	A	A	B	B	B	C	C
	B	B	A	A	A	C	C

*Respondents's customary brand. The sequence is in one week intervals.

DRAFT

Table 3. Respondent Characteristics at First Entry

Customary Brand of cigarette	Number of respondents		Average # of mos. smoking cust. brand		Avg. # of cigarettes smoked/day		Average Age	
	M	F	M	F	M	F	M	F
Brand A	67	75	6.4	7.4	30.6	29.9	35.3	38.0
Brand B	50	96	11.8	11.6	30.2	28.0	39.8	39.1

DRAFT

Table 4. Plasma Cotinine, ng/ml, Averages and (S.E.M.)

Customary Brand	Sex	Baseline Range	N	Brand A	Brand B	Brand C
Brand A	M		67	317 (8)	222 (11)	235 (17)
		< 225	20	150 (13)	130 (16)	124 (14)
		225-450	35	334 (11)	229 (16)	265 (26)
		> 450	12	544 (17)	348 (30)	327 (49)
Brand B	M		50	322 (16)	206 (9)	223 (19)
		< 225	29	242 (23)	123 (13)	151 (17)
		225-450	20	458 (18)	313 (13)	353 (43)
		> 450	1	535 (NA)	480 (NA)	327 (NA)
Brand A	F		75	328 (7)	207 (15)	203 (13)
		< 225	22	141 (14)	71 (10)	94 (16)
		225-450	37	344 (10)	223 (24)	244 (20)
		> 450	16	544 (17)	361 (38)	271 (33)
Brand B	F		96	284 (14)	189 (6)	185 (11)
		< 225	63	226 (17)	128 (8)	151 (13)
		225-450	31	399 (22)	297 (10)	253 (23)
		> 450	2	477 (NA)	460 (NA)	411 (NA)

DRAFT

Table 5. Plasma Cotinine, ng/ml. Averages and (S.E.M.)

	Customary Brand A		Customary Brand B	
Sex	M	F	M	F
Initial Subjects	67	75	50	96
Baseline Entry	334	312	228	201
Baseline First Week	308	333	176	178
Baseline Overall	317 (13.9)	328 (18.0)	206 (16.8)	189 (10.9)
Alternate Brand* First Week	209	207	305	291
Alternate Brand* Second Week	235	210	342	266
Alternate Brand* Third Week	228	201	320	273
Alternate Brand*, Overall	222 (13.9)	207 (18.5)	322 (24.5)	284** (15.4)
Brand C First Week	240	212	202	192
Brand C Second Week	230	197	238	179
Brand C Overall	235 (17.3)	203 (14.0)	223 (20.2)	185*** (11.6)

*Brand A for Brand B smokers and vice versa.

**Significantly lower than expected, $P \geq 0.05$.

***Significantly lower than expected, $P \geq 0.01$.

Note. Statistical significance was determined on a self-matching basis, paired t-tests (two tailed), after adjusting individual values for the number of daily cigarettes consumed.

DRAFT

Table 6. Plasma Cotinine Summary Results (S.E.M.)

Cigarette Smoked	Brand A	Brand B	Brand C
Average plasma cotinine, ng/ml	310 (10.1)	204 (8.2)	208 (8.2)
Maximum value recorded ng/ml	833	859	899
Average cigarettes smoked daily	29.0	30.5	31.1
Average Normalized Plasma Cotinine, ng/ml*	10.8	6.8	6.7
Ratio to Brand C**	0.16	0.10	0.10
Nicotine mg/cigarette	0.18	0.11	0.10

*For each respondent, plasma cotinine values were divided by his/her average daily cigarette consumption. Averages of overall results are reported.

**Ratios of the normalized plasma cotinine values taking the Brand C value as 0.10.

DRAFT

Table 7. Daily Cigarette Consumption, Units, Averages and (S.E.M.)

Customary Brand	Sex	Baseline Range	N	Brand A	Brand B	Brand C
Brand A	M	20-52	67	31 (0.4)	33 (0.7)	34 (0.7)
		< 25	14	21 (0.7)	22 (0.8)	25 (1.2)
		25-35	32	30 (0.5)	33 (0.9)	34 (1.3)
		>35	21	39 (0.8)	41 (1.5)	40 (1.2)
Brand B	M	20-51	50	30 (0.8)	31 (0.4)	33 (1.1)
		< 25	13	20 (0.6)	21 (0.4)	23 (2.0)
		25-35	17	28 (1.1)	28 (0.6)	29 (1.8)
		>35	20	39 (1.8)	40 (0.8)	43 (2.0)
Brand A	F	20-55	75	29 (0.3)	31 (0.6)	30 (0.8)
		< 25	23	21 (0.4)	22 (1.2)	22 (1.3)
		25-35	35	30 (0.4)	32 (0.9)	32 (1.3)
		>35	17	39 (0.9)	41 (1.3)	41 (1.7)
Brand B	F	20-47	96	27 (0.5)	28 (0.2)	29 (0.6)
		< 25	36	20 (0.7)	20 (0.4)	21 (0.9)
		25-35	42	29 (0.8)	30 (0.4)	31 (0.8)
		>35	18	38 (1.5)	38 (0.2)	40 (2.4)

DRAFT

FIGURES

Figure 1. Subject distribution according to daily cigarettes smoked at time of entry.

Figure 2. Subject distribution according to baseline plasma cotinine values.

Figure 3. Baseline plasma cotinine values as a function of FTC nicotine delivery of Brands A and B.

Figure 4. Baseline plasma cotinine as a functon of daily cigarettes smoked. Brand A and Brand B smokers.

Figure 5. Plasma cotinine values as a function of plasma nicotine values Males and Females.

Figure 6. Baseline plasma cotinine as a function of available daily nicotine (mg), defined as FTC nicotine/cigarette, multiplied by the cigarettes smoked per day. ADN = FTC (N) X CPD - Males.

Figure 7. Baseline plasma cotinine as a function of available daily nicotine (mg), defined as FTC nicotine/cigarette, multiplied by the cigarettes smoked per day. ADN = FTC (N) X CPD - Females.

FIGURE 1

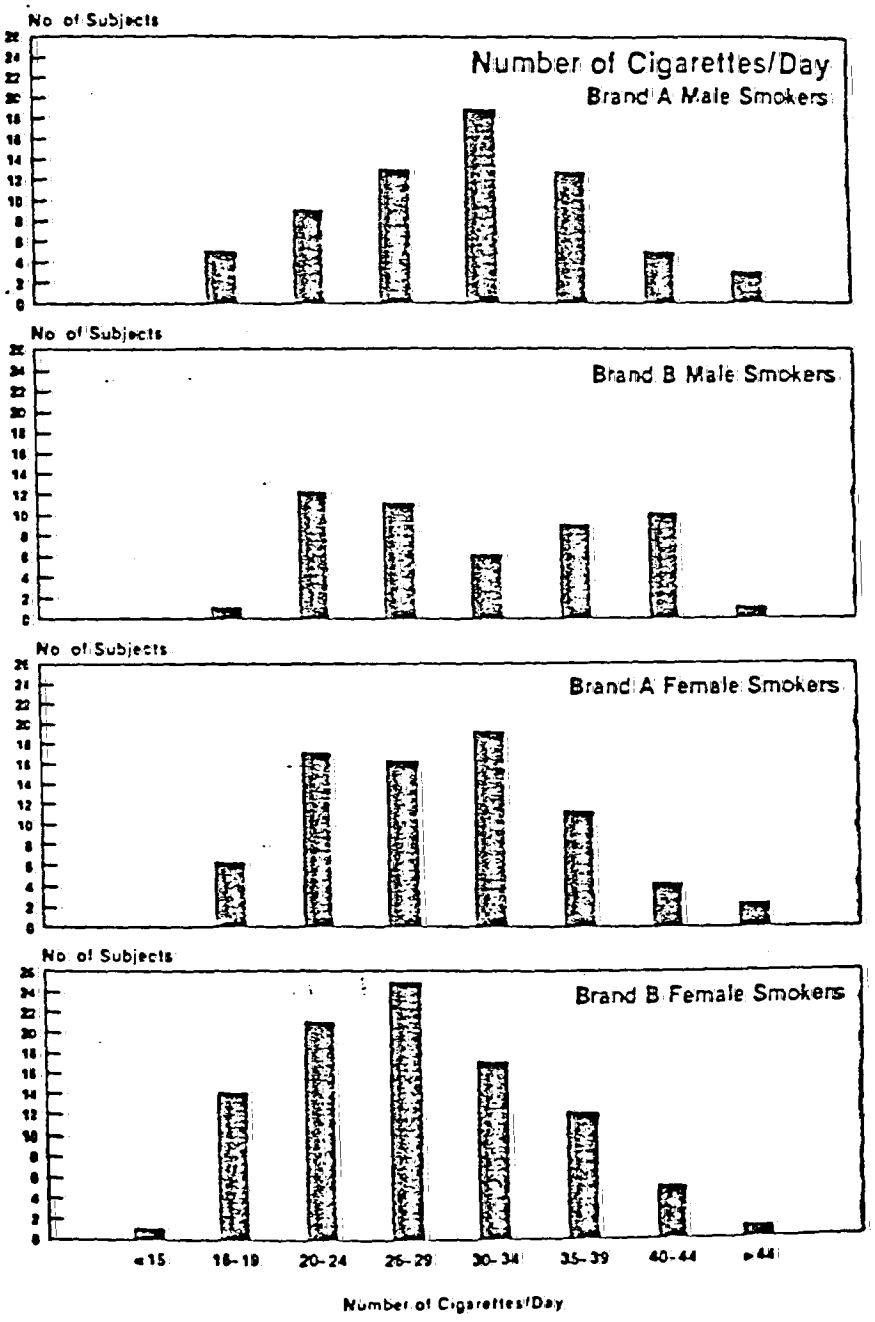

FIGURE 2

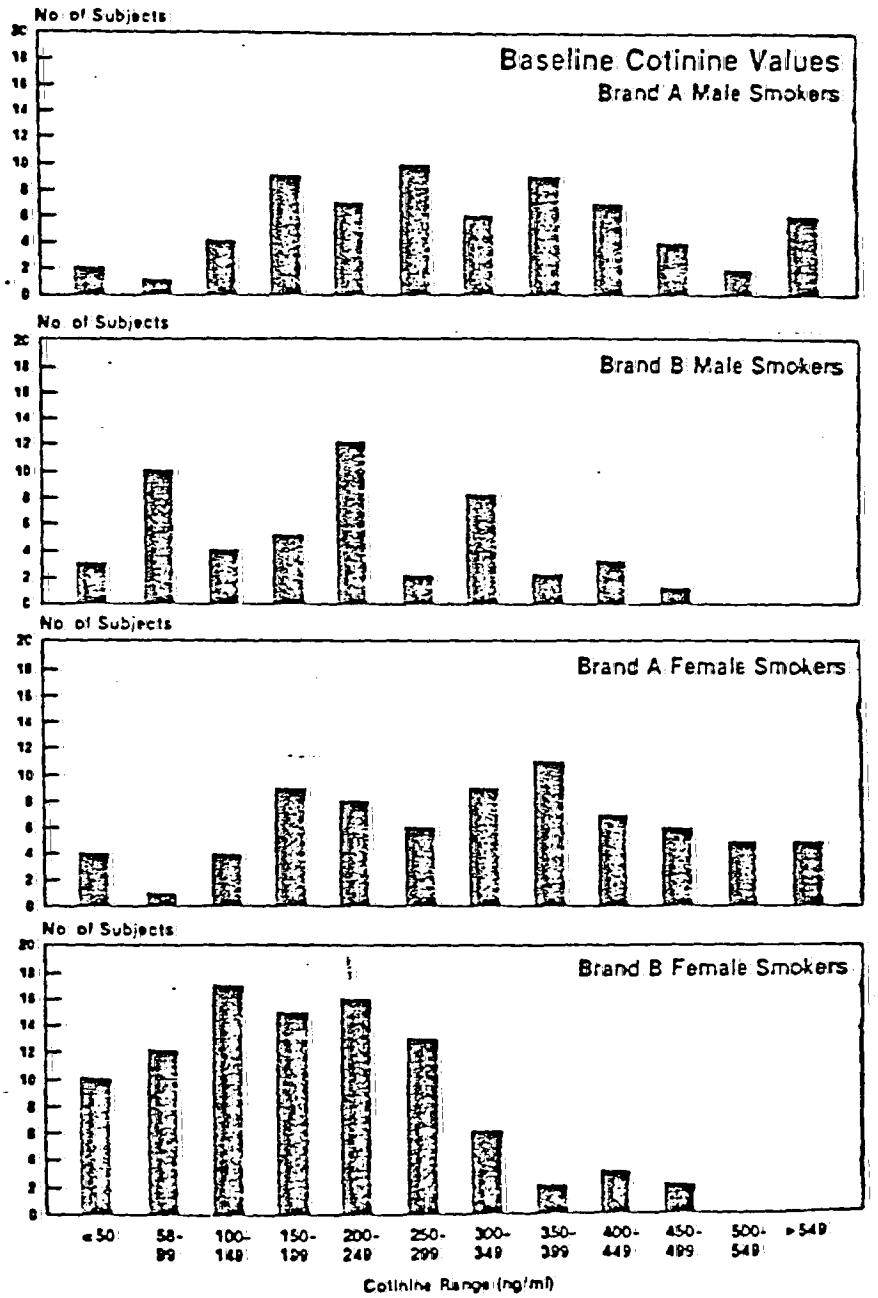

FIGURE 3

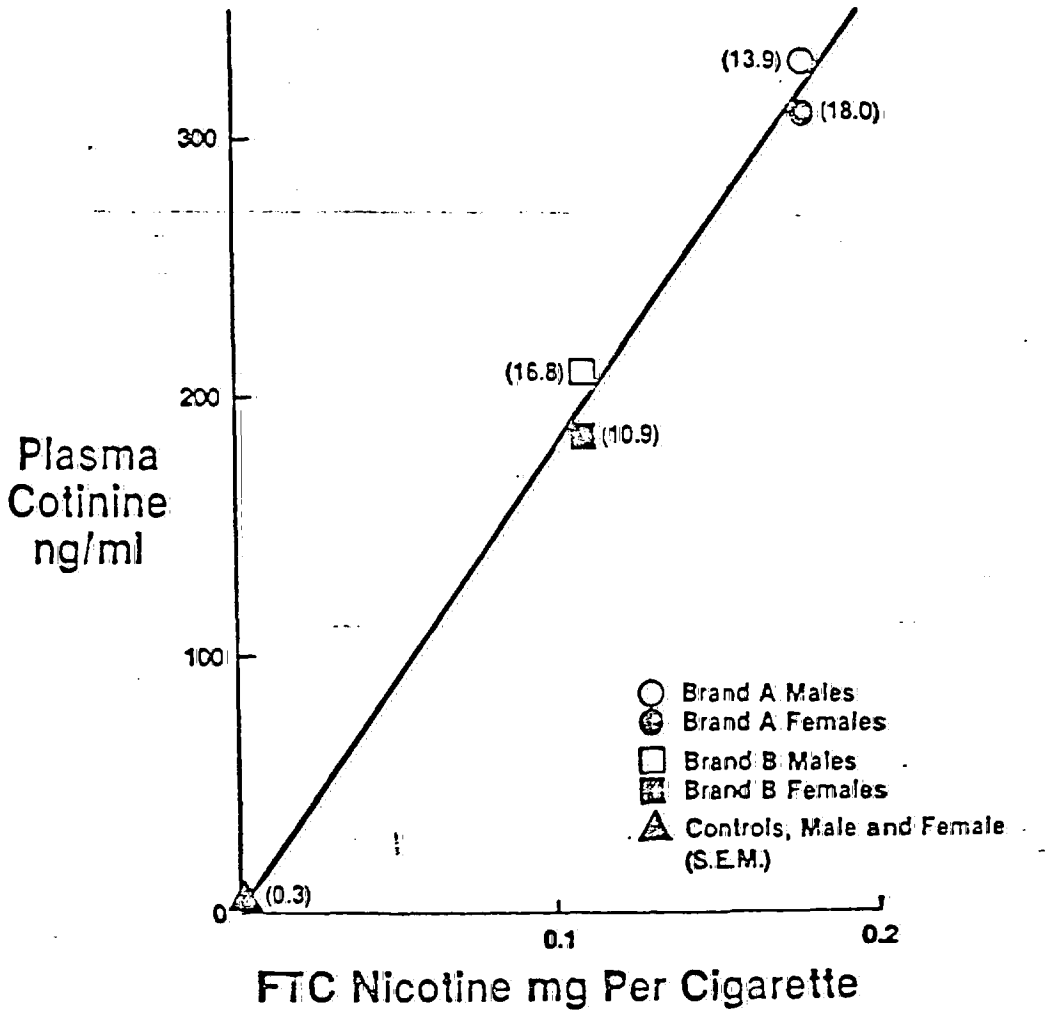

FIGURE 4

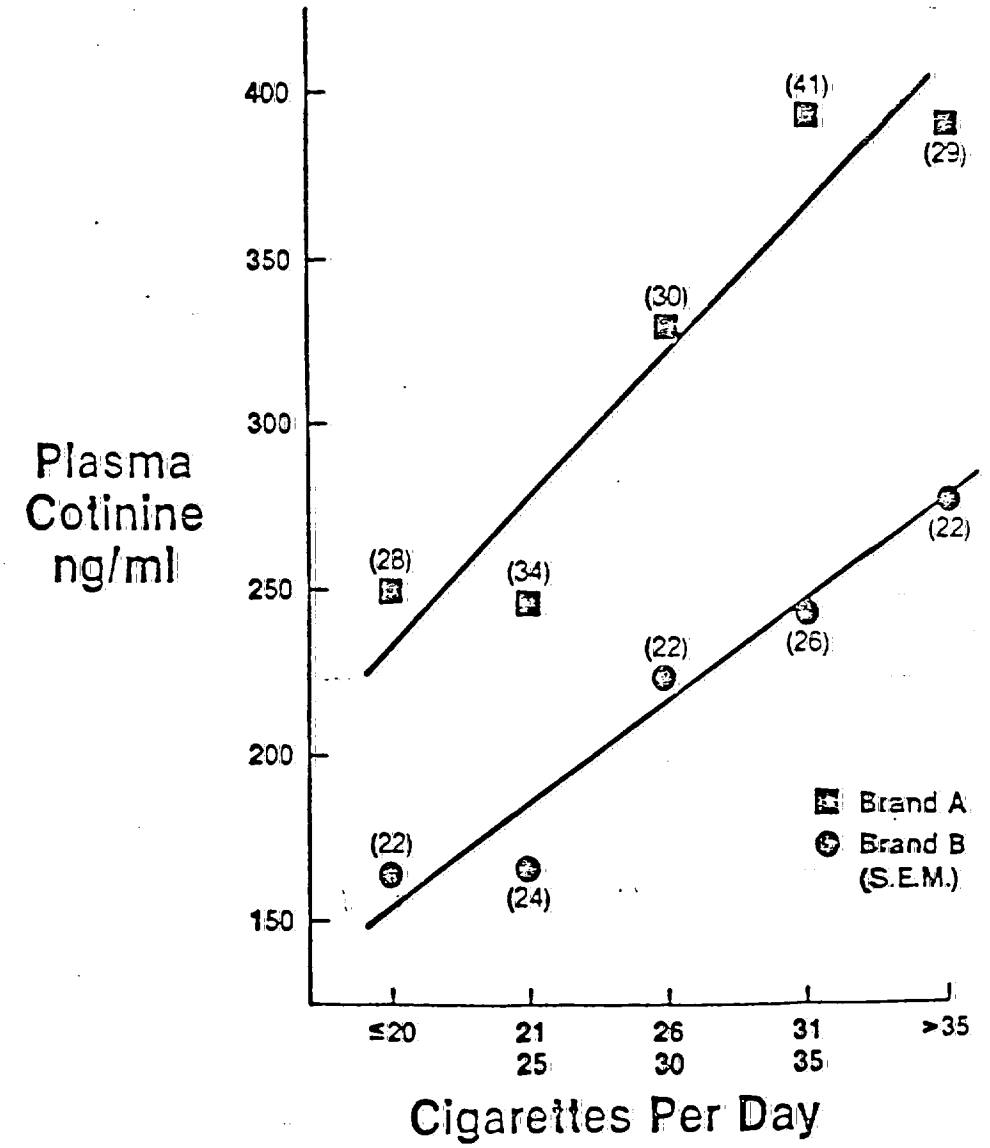

FIGURE 5

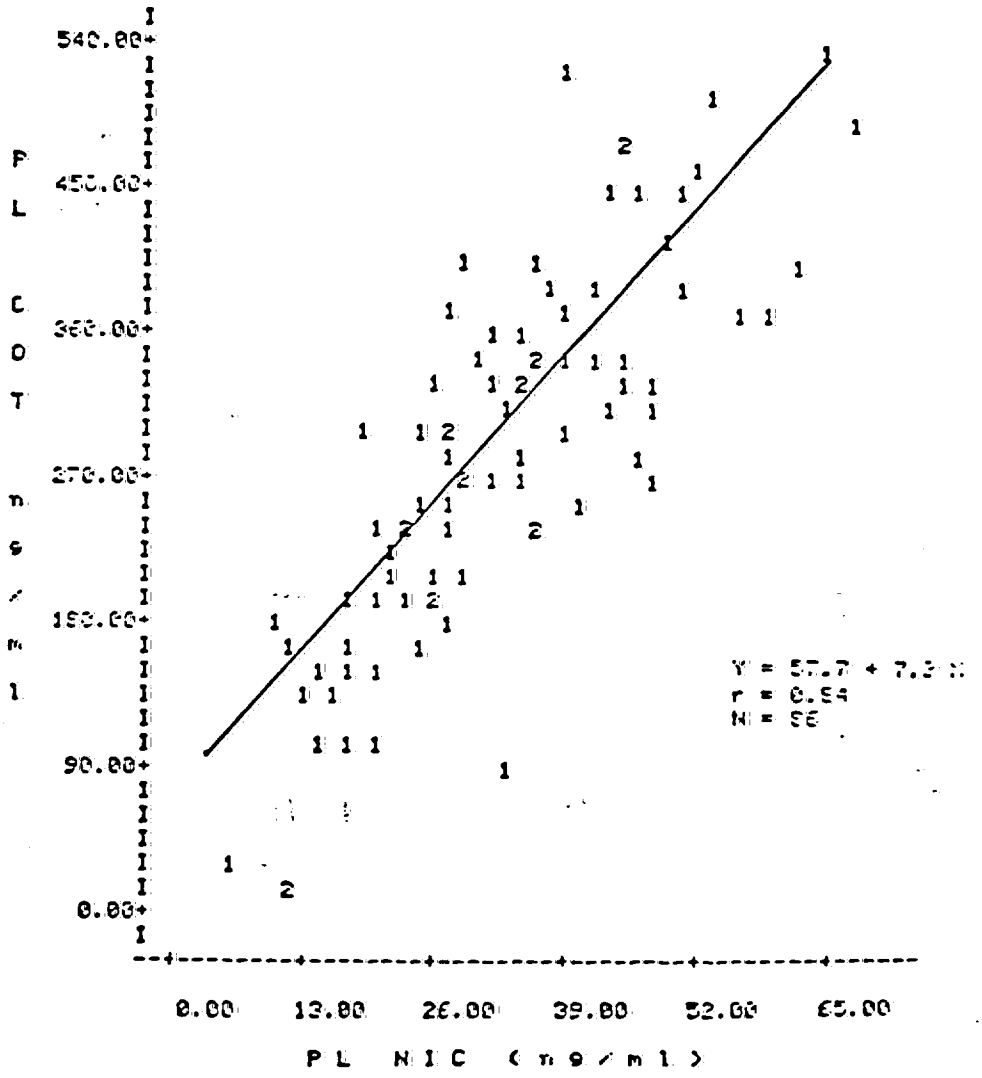

FIGURE 6

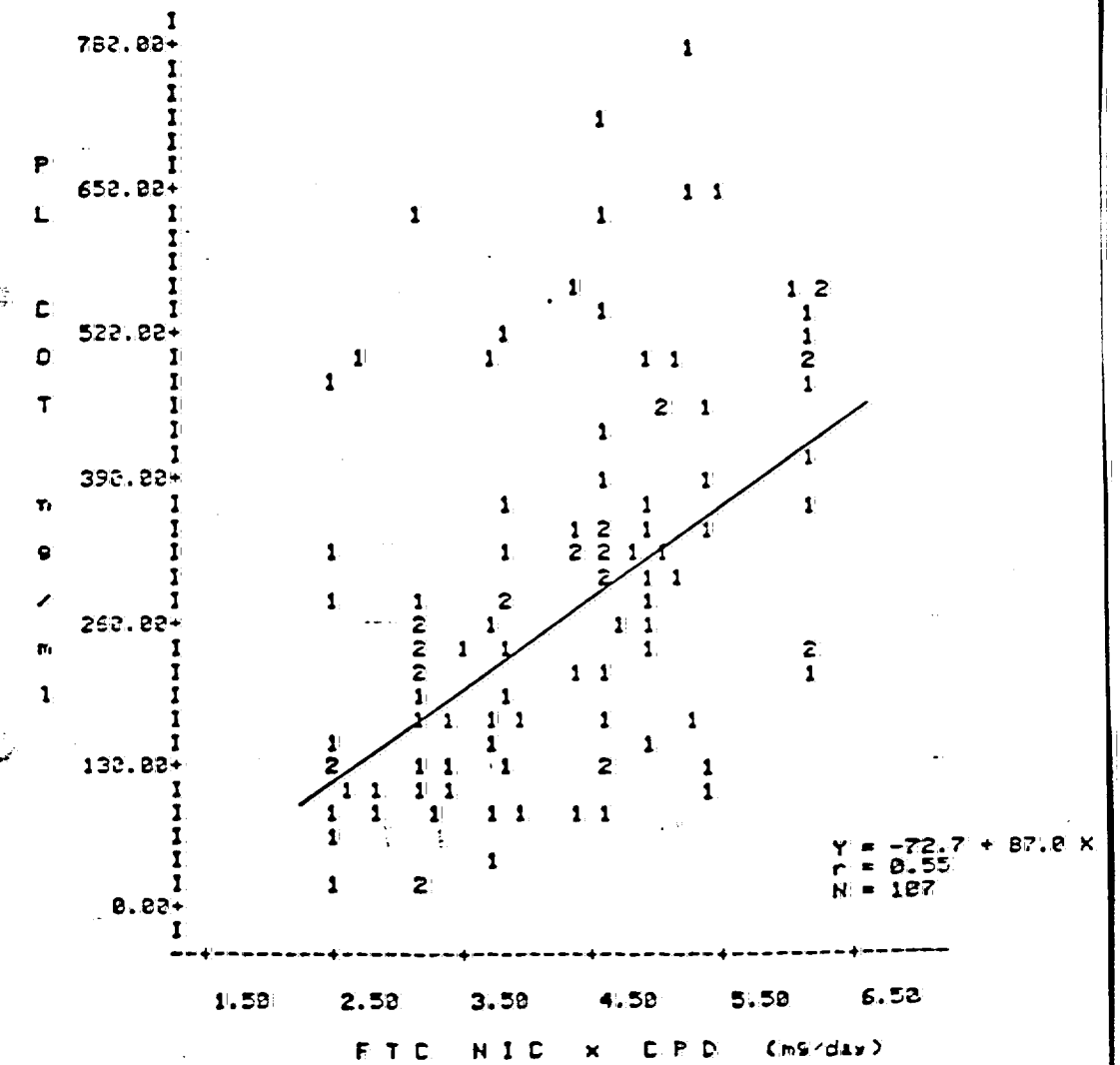

FIGURE 7

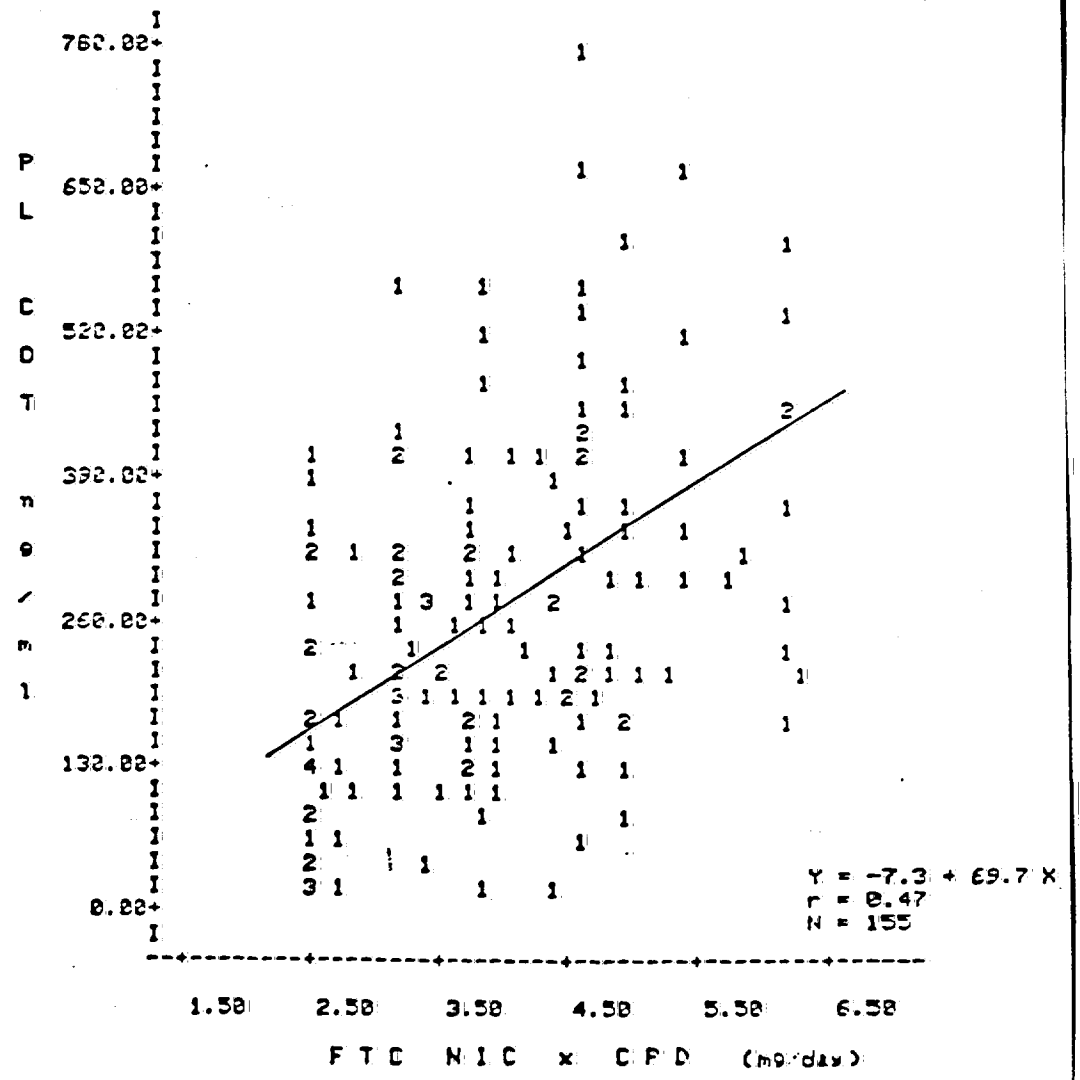

APPENDIX VIII

COMPARISON OF HUMAN UPTAKE AMONG CIGARETTE BRANDS RATED AS ONE MILLIGRAM TAR YIELD

by

T. D. Darby, Ph.D.
Medical School, University of South Carolina
Columbia, South Carolina

J. E. McNamee, Ph.D.
Medical School, University of South Carolina
Columbia, South Carolina

Jacques van Rossum, Ph.D.
Medical School, University of Nijmegen
Nijmegen, The Netherlands

DRAFT
COMMERCIAL IN CONFIDENCE

DRAFT
COMMERCIAL IN CONFIDENCE

COMPARISON OF HUMAN UPTAKE AMONG CIGARETTE BRANDS RATED AS ONE MILLIGRAM TAR YIELD.

T. D. DARBY, PH.D., J. E. McNAMEE, PH.D., AND J. VAN ROSSUM, PH.D.

SUMMARY

Several reports have shown the trend toward reduced carbon monoxide, nicotine, and tar yields of cigarettes over approximately the last 30 years. Concomitantly, reports of epidemiological studies have shown that individuals who have selected cigarette brands which standard smoking machine tests classify as ultra low yield brands have significantly fewer diseases related to smoking. While the smokers of the ultra low yield brands seem to benefit; the non-smoker benefits substantially from not smoking.

This report presents an analysis of data gathered from a large sample of regular smokers of ultra low tar yield cigarette brands. Since smoking behavior is recognized as a determinant of an individual smoker's uptake of both nicotine and tar, the large number of subjects studied greatly increases the value of the data derived from these studies. The experimental design allowed comparison of the plasma cotinine concentration obtained from smokers who were only minimally influenced by factors other than those normal to their own natural environment. Only those factors which normally affect smoking behavior and thus nicotine uptake would be expected to operate. Correction for daily cigarette consumption or for other factors which might alter nicotine uptake and thus tar intake on an individual cigarette basis were not included in the analysis. The plasma cotinine concentrations used in the analysis represent the total smoking experience of the individual during the period of smoking each brand represented in the study.

The major points made as a result of this analysis are:

1. Individuals differ greatly in their plasma cotinine concentration despite comparable consumption of numbers of cigarettes. Reasons are presented for this difference in the discussion section of the report.
2. Individuals with high plasma cotinine concentrations while smoking one brand tend to have high plasma cotinine concentrations on all brands investigated. The same statement is true for individuals with low plasma cotinine concentrations.
3. On the average a smoker's plasma cotinine concentration is proportional to the brand yield values obtained by measurement utilizing the standard smoking machine procedures.
4. If the individuals who obtain greater than average yield are considered to be a problem then these data support the conclusion that all ventilated filter cigarette brands share in the problem.
5. The large number of smokers who obtain lower than average plasma cotinine concentrations while smoking ultra low tar cigarette brands benefit from the reduced nicotine and thus tar intake.

DRAFT
COMMERCIAL IN CONFIDENCE

INTRODUCTION

The nicotine and tar rating of cigarettes as determined by a standard smoking machine method (FTC test method) are published for the various cigarette brands. Several brands are reported to be ultra low yield brands. These brands yield one milligram tar or less by the standard smoking machine test. The individual delivery of these brands is known to be affected by smoking behavior. It is generally accepted that increased cigarette consumption will increase nicotine and tar intake. The number of puffs taken per cigarette and the depth of inhalation are also recognized as factors that increase individual uptake of nicotine and tar.

Several reports, notably the report of Wald, Doll and Copeland, 1981, have shown the trend toward reduced carbon monoxide, nicotine, and tar yield of cigarettes over the past 30 years. Concomitantly, reports of epidemiological studies have shown that a significant reduction in the incidence of diseases related to smoking has accompanied the reported reduction in these substances. More recently filtration that includes air dilution has been used to markedly reduce potential cigarette delivery of nicotine, tar and carbon monoxide. Individuals who have selected cigarette brands which standard smoking machine tests classify as ultra low yield brands have statistically significant fewer diseases related to smoking than individuals who have remained as full flavor cigarette smokers. While the smokers seem to benefit from the reduced deliveries of cigarettes marketed today, the non-smoker benefits more as is evidenced by the very significant reduction in diseases related to smoking in the non-smoker population.

Investigators have reported that smokers who switch to the ultra low brands may increase their consumption or change their pattern of smoking to compensate for the reduced yield of the cigarettes. In addition questions have arisen as to the relative human uptake of nicotine and tar as a result of smoking the various brands which have different types of air dilution filters.

This report presents an analysis of data gathered from a large sample of regular smokers of air dilution filtered cigarettes which are classified as ultra low tar delivery cigarette brands by the FTC smoking machine method. The analysis presents evidence which supports the concept that inter-individual differences in nicotine uptake occur among smokers. The data supports the conclusion that there is no difference in the delivery of nicotine and thus tar to individual smokers as a result of changing brands from one type of air dilution filter to another type of filter.

METHODS

The investigation utilizes measurements of plasma cotinine concentration. Cotinine is a major metabolite of nicotine. Nicotine is a basic substance and like many amine compounds the concentration of the free base and the degree of ionization provides for rapid tissue or organ distribution of the compound. The intracellular ionization and low free base concentration prevents rapid redistribution of the compound to the

plasma compartment. Thus, measurement of plasma cotinine concentration made at a time other than at steady state, may not accurately reflect total body nicotine concentrations. Since distribution and excretion of nicotine are highly pH dependent, measurement of nicotine half-life and calculation of "apparent volume distribution" varies among individuals (Benowitz, N. L. et al, 1982). The substantial inter-individual difference in these parameters limits the usefulness of plasma nicotine concentration a a measure of nicotine uptake. The large apparent volume of distribution for nicotine greatly reduces the plasma concentration and adds to the complications associated with measuring plasma nicotine concentration.

Cotinine is more water soluble than nicotine and the apparent distribution is less affected by pH differences. Cotinine has a half-life that is said to be approximately 24 hours as compared to the reported two hour half-life of nicotine. Therefore, while the plasma nicotine concentration only reflects delivery of the last few cigarettes, plasma cotinine concentration determined under steady state conditions will be only minimally affected by the smoking experience with the last few cigarettes. Thus, measurement of plasma cotinine concentration provides a method for measurement of the nicotine and tar uptake as a result of an individual's smoking experience in the subject's natural daily environment. The data obtained includes both factors related to cigarette delivery and individual smoking behavior.

The determination of plasma cotinine concentration as a sensitive measurement of nicotine uptake is discussed in detail in a paper prepared by Doctor J. van Rossum.

This analysis includes data obtained from 288 smokers of ultra low tar cigarette brands. Individuals were recruited into the study by random sample interview in shopping centers and by newspaper advertisement. Only smokers who stated they smoked approximately 20 or more cigarettes per day were selected. An attempt was made to recruit equal numbers of males and females into the study.

STUDY DESIGN:* Smokers of either Barclay brand or Carlton brand cigarettes were selected for study since these two brands represented the preference of a majority of the persons interviewed. The Barclay brand cigarette is equipped with an Actron air dilution filter while the Carlton brand is equipped with a conventional air dilution filter. Baseline data included body weight and number of cigarettes smoked per day. A blood sample was obtained for measurement of plasma cotinine concentration.

The subjects continued to smoke their usual cigarette brand. At the end of 7 days blood samples were obtained for measurement of plasma cotinine concentration. During the period the subjects were asked to keep a diary which indicated number of cigarettes smoked and time of the day at which the cigarette was smoked. The subjects were asked to refrain from use of tobacco products other than smoking the brand they had been smoking for at least the last three months. On the average the subjects had smoked one brand of ultra low tar deliver for at least six months.

---

*These studies were carried out under the direction of Doctor Gio Gori at the Franklin Institute, Silver Spring, Maryland.

After the two week baseline period the Carlton smokers were switched to Barclay brand the Barclay smokers were switched to the Carlton brand. At the end of 7, 14, and 21 days on the new brand blood samples were obtained for determination of plasma cotinine concentration. During this three week period a diary was kept which indicated number of cigarettes smoked and the time of day at which the cigarette was smoked. On the average the smokers consumed 30 cigarettes per day for the three week period. The average of the three plasma cotinine concentrations for this three week period would be the result of smoking approximately 630 cigarettes.

After completion of the three week cross-over study, all the subjects were switched to Cambridge brand cigarettes. The Cambridge brand is equipped with a conventional air dilution filter. The smokers remained on Cambridge brand for two weeks. Blood samples for determination of the plasma cotinine concentration were obtained on days 7 and 14 following the switch to the Cambridge brand. Thus, the plasma cotinine concentration measured during this last two week period could serve for comparison with the plasma cotinine concentration measurement obtained from the subject during his baseline period and the data obtained during the cross-over period.

All cigarettes provided to the subjects were purchased from commercial distributors, each brand coming from he same production batch, thus minimizing variance. The data obtained from the standard smoking machine test (FTC method) for the batch of each brand used in the study are summarized in Table 1.

The plasma cotinine concentrations and other data were supplied to us by Doctor Gori and we were asked to provide an analysis of the data. The experimental design allowed comparison of the plasma cotinine concentration obtained from smokers who were only minimally influenced by factors other than those normal to their own natural environment. Those factors which normally affect smoking behavior and thus nicotine uptake would be expected to operate. The study design provided for the steady state conditions required for comparison of pharmacokinetic parameters as stressed by J. van Rossum, 1982. The cross-over and switch design allowed study of delivery of each brand in an individual smoker thus minimizing inter-individual differences in nicotine metabolism.

Our analysis included scattergram preparation which allowed comparison of plasma cotinine concentration obtained from individual smokers during their experience with each brand. Regression analysis and factor analysis were included in this study of the data. The figures that show the regression analysis also contain a line which provides for slope analysis that compares the maximum uptake of nicotine and thus tar for the individuals studied. Ninety percent of the smoker's studied gave uptake values less than the slope of this line times the uptake value obtained when the individual smoked the Cambridge brand.

The data are plotted as a log normal distribution. The cumulative percent of population sample providing a plasma cotinine concentration is plotted vs. the log of the value obtained for the plasma cotinine concentration. This log distribution plot was used to compare the deliveries of the cigarette brands equipped with the conventional air filter to the deliveries obtained from cigarettes equipped with the Actron filter.

RESULTS

The data showed wide inter-individual differences in plasma cotinine concentration. The number of cigarettes smoked per day averaged 30, and varied between less than 20 and more than 35. Neither daily cigarette consumption ($r^2 = 0.09$) nor the reciprocal of body weight ($r^2 = 0.01$) was significant in determining plasma cotinine concentration, over all smokers on all brands. There was a trend for increased plasma cotinine concentration to occur within individuals based upon daily cigarette consumption, however, variation in cigarette consumption was small and therefore the factor was of little use in the analysis.

Therefore, a method of analysis was used which allowed comparison of brand effects in a given individual, and thus inter-individual differences were avoided. The total smoking experience with each brand studied was included in the analysis. Corrections for daily cigarette consumption or other factors which might alter nicotine uptake and thus tar intake on an individual cigarette basis were not included in the analysis. The plasma cotinine concentrations shown in the figures represent the total smoking experience for that period of the study.

Figure 1. is a scattergram which indicates the plasma concentration differences for the individual smokers while smoking either Barclay or Carlton brand cigarettes. These data are derived from the cross-over period therefore the brand experience is new for each group. Table 2 provides the number of individuals and the percent of the total found in each of the four quadrants. The four quadrants were derived by providing a line at the average concentration obtained while smoking the brand indicated. Therefore, Quadrant I contains individuals who gave higher than average plasma concentrations of cotinine while smoking the Carlton brand and lower than average plasma concentrations of cotinine while smoking the Barclay brand. Quandrant II contains those individuals who gave higher than average cotinine plasma concentrations while smoking either brand. Quadrant III is composed of the individuals who gave higher than average concentration for plasma cotinine while smoking the Barclay brand and lower than average plasma concentrations for cotinine while smoking the Carlton brand. Quadrant IV contains the individuals with below average concentration of plasma cotinine while smoking either brand. It is interesting that more than three-fourths of the individuals tested are found in either Quadrant II or Quadrant IV. There was no difference in the number of individuals who showed a higher than average plasma concentration for cotinine while smoking either of the two brands. These data suggest that smokers who obtain high cotinine plasma concentrations while smoking one brand also obtain high plasma cotinine concentrations while smoking the alternate brand. While smokers who obtain low plasma cotinine concentrations on one brand also have low plasma cotinine concentrations on the alternate brand. This suggestion could be tested by use of regression analysis.

Since these smokers had smoked an ultra low yield brand for at least three months and the average period of smoking an ultra low yield brand was six months', adaptation to the delivery of the brands should have been a minimal factor. This appears to be the case since there was no obvious difference in the number of cigarettes smoked per day resulting in a higher delivery for one of the two brands during the cross-over period.

Figure 2 is a regression analysis comparison of the plasma cotinine concentration obtained with Carlton brand smokers who were switched to the Barclay brand. The figure shows the slope of the regression line (R) and the standard error of R is given below the figure. In addition, the slope of the line which will provide a result that assures that 90% of the smokers studied were below this value is shown on the figure. These data indicate that 90% of the subjects studied had plasma cotinine concentrations less than or equal to 2.77 times their plasma cotinine concentration while smoking the Cambridge brand cigarettes. The data from the standard smoking machine tests, shown in Table 1., provides nicotine yield values for the Barclay brand cigarettes that is 1.6 times greater than the nicotine yield for the Cambridge cigarettes. Thus, the slope for the regression line which intercepts at the origin of 1.34 is less than the delivery difference one might expect for delivery in the individual smokers. The line with a slope of 2.77 is the line which provides for an uptake that is greater than that experienced by 90% of the smokers in the study. Therefore the maximum uptake for the Barclay brand is no greater than 2.77 times the plasma cotinine concentration while smoking the Cambridge brand. This increased nicotine uptake can be partially explained based upon the increased yield of the Barclay brand which is 1.6 times greater than the yield obtained by the Cambridge brand. These individuals normally smoked Carlton brand cigarettes. Certainly these data do not support the contention that smokers of Barclay brand cigarettes, which are equipped with the Actron filters, receive 4 to 8 times the nicotine and thus tar yield they experience with a cigarette equipped with a conventional ventilated filter, the Cambridge brand.

Similar data are presented in Figures 3, 4, and 5 where Barclay brand smokers and Carlton brand smokers were switched to the Cambridge brand. The analysis shown in Figures 3 and 4 support the conclusion that smokers obtain a similar amount of nicotine from the Carlton and Cambridge brands. The slope of the regression line was 0.85 and 0.93 for the two comparisons of these brands. The effects of brand change from Carlton to Barclay and from Barclay to Carlton are illustrated by Figures 2 and 3 (labeled as Barclay new brand or Carlton new brand). Thus the comparison is between the effects of a new experience with Carlton and Cambridge or Barclay and Cambridge.

The data illustrated in Figures 2 and 4 indicate that some smokers of Carlton brand cigarettes may have a higher plasma cotinine concentration than they obtain with Cambridge. When the Carlton smokers' cotinine concentrations were compared to their cotinine concentrations while smoking Cambridge brand cigarettes, the regression line slope, which passed through the origin, assured that 90% of the smokers would receive a yield no greater than the slope times the yield from the Cambridge brand. This regression slope is 2.00. However, when the Barclay brand smokers were switched to the Carlton brand this 90% regression line slope was 1.39 times the value for their experience with the Cambridge. Despite the fact that the Barclay brand yield by the standard smoking machine test is 1.8 times greater than the Carlton brand yield, 90% of the Barclay brand smokers, Figure 5, were below a regression line slope of 2.66 times the value obtained while smoking the Cambridge brand. When the Carlton brand smokers were switched to the Barclay brand, Figure 2, the 90% regression line slope was 2.77 times the value obtained from their Cambridge experience.

This difference could be related to differences in the easy-to-draw perception with the brands. Barclay brand is usually considered to be an easy-to-draw cigarette as compared to either the Carlton or Cambridge brands. Figures 2 and 4 contain the same individuals. Figure 4 represents the data from the baseline period when the Carlton smokers remained on their usual brand, while Figure 2 is derived from data obtained during the cross-over period where these Carlton smokers were switched to the Barclay brand. But, regardless of the cause, a few regular smokers of the Carlton brand obtained higher than expected nicotine uptake from their normal brand, Carlton, and also from the Barclay brand.

Additional analysis of the inter-individual variation is shown in Figure 6 and Figure 7. The data are plotted as an accumulative percent of the population sample that provide plasma cotinine at or below a given log of the plasma cotinine value. This plot provides two distinct curves for the smokers of the ultra low tar delivery brands tested. Smokers of the Carlton brand or the Cambridge brand which are equipped with conventional ventilated filters provide curves which overlap for either the 5 weeks or 4 weeks these brands were smoked. In the case of the Carlton smokers the comparisons between Carlton and Cambridge occurred over 4 weeks, two weeks smoking with each brand. In the case of the smokers who usually smoked the Barclay brand the comparisons between Carlton and Cambridge occurred over 5 weeks, three weeks on the Carlton brand and two weeks on the Cambridge brand. The subjects who usually smoked the Barclay brand are shown in Figure 6 while the subjects who usually smoked the Carlton brand are shown in Figure 7. Naturally, the curves providing the lowest log values were obtained with the Carlton and the Cambridge brands since these brands deliver 0.1 mg of nicotine or less. The curves which are shifted to the right, or to higher log values were obtained while the individuals were smoking the Barclay brand cigarettes. The Barclay brand cigarettes deliver 0.2 mg of nicotine.

In each case at population percentile levels one standard deviation above or below the mean value the smokers showed a higher plasma cotinine concentration while smoking the Barclay brand cigarette. This is to be expected since the Barclay brand potential delivery for nicotine is rated between 1.6 and 1.8 times greater by the standard smoking machine test (FTC method). It is interesting to note that over this range the two curves remain parallel. This observation supports the conclusion that the physiological processes by which the body produces and eliminates cotinine is not changed during the period of the study. If there was a change in the physiological processes one would expect the slope of these two curves to be different. This analysis is similar to that usually made of changes in the slope of the population percent response to the log dose plot for the dose response analysis done in pharmacological experiments.

During time periods when the subjects smoked either the Barclay brand or the Cambridge or Carlton brand there was a marked difference from the mean observed for one third of the smokers. This difference from the observed mean value is more than one standard deviation. The smokers with plasma cotinine concentrations more than one standard deviation below the mean plasma cotinine concentration value showed a smoking behavior that limited their intake of nicotine and thus tar. On the other hand the subjects with plasma cotinine concentrations which were more than one standard deviation above the average plasma

cotinine concentration show a smoking behavior that markedly increases their intake of both nicotine and tar. This sample of the population indicate that less than 20% of the population show this latter type of behavior and that the increased uptake of nicotine and thus tar provides overlapping data for all three brands tested.

Figure 8 and Figure 9 compares the shift along th plasma cotinine concentration axis which occurs with a change from either the Cambridge or Carlton brand to the Barclay brand. This change in plasma concentration is compared to the inter-individual difference in plasma concentration which occurs among smokers of any of the three brands. While the shift in the concentration curve occurs with the change to the higher potential nicotine delivery brand, the increase in plasma cotinine concentration among smokers of a particular brand is due to either an increase in nicotine and thus tar uptake related to more aggressive smoking behavior or due to an individual difference in metabolic handling of nicotine and cotinine. The inter-individual differences between the low intake and the high intake while smoking a particular brand was three times the change associated with the increase due to the increased potential nicotine delivery afforded by the Barclay brand.

DISCUSSION

The scattergram and the regression analysis support the conclusion that individual smokers obtain expected nicotine uptake from cigarettes based upon the relative standard smoking machine test yields. The regression analysis, when the slope is forced to pass through the origin, indicates that the individual smokers obtain 1.34 to 1.37 times more nicotine from Barclay brand than they did from the Cambridge brand. Forcing the slope through the origin is necessary since the zero point is the most valid point. Cotinine is only present as a result of nicotine metabolism. A review of Table 1. which provides the standard smoking machine test yields for the three brands indicates an increased nicotine delivery for the Barclay brand of 1.63 to 1.8 times larger than the other two brands. Ninety percent of the Barclay smokers had plasma cotinine concentrations less than 2.77 times their plasma cotinine concentrations while they were smoking Cambridge. Correction for the average number of cigarettes smoked per day did not affect the result because the average number of cigarettes smoked per day usually did not vary substantially with change from one brand to another. There was a significant variation in the average number of cigarettes smoked per day between individuals. However, on the average most individuals consumed 30 cigarettes per day.

Seventy-five per cent of the individuals maintained their relative percentile position regardless of the brand smoked. These individuals are found in either Quandrant II or IV of the scattergrams. The remaining 24% found in Quandrant I or III, are individuals who gave high plasma cotinine values while smoking one of the two brands. In no case was the brand specific high value found in more than 15% of the smokers tested. This value is found in Quandrant III and, since Barclay brand is known to deliver a higher quantity of nicotine, this result is not surprising. Several reasons may be valid to explain the difference seen in the smokers found in Quandrants II and IV. The smokers in Quandrant IV (47.5%) had lower than average plasma cotinine values regardless of the brand smoked while the smokers in Quandrant II (28.2%) had higher than average

concentrations for plasma cotinine with both brands smoked. An increase in the number of cigarettes smoked increases the plasma concentration of cotinine (See data in report of Gori and Lynch). Depth of inhalation and number of puffs are known factors that increase nicotine intake. Naturally, the suggestion of Benowitz, et al, 1982, that individual differences in rate of nicotine metabolism could be responsible for higher or lower than average plasma concentrations of cotinine, must be considered. Individuals who rapidly metabolize nicotine to cotinine, but more slowly metabolize cotinine might be expected to have higher cotinine plasma concentrations. This is especially true if the individual requires more nicotine because of the rapid metabolism. On the other hand, the individual who more slowly metabolizes nicotine to cotinine may be expected to have lower cotinine plasma concentrations. These metabolic differences made it mandatory that a self matching design be used in studies of nicotine and thus tar uptake by smokers.

Figures 2 and 4 show data obtained from smokers who are normally Carlton brand smokers, while Figures 3 and 5 show data obtained from smokers who are normally smokers of Barclay brand cigarettes. The obvious differences in the yields as indicated by the scatter in Figures 2 and 3 where the smokers experienced a new cigarette brand indicate the need for time to adapt to the new brand. The easy-to-draw effect appears to be causing less scatter in Figure 3, whereas, the scatter is quite marked when the Carlton brand smoker encounters the Barclay brand, shown in Figure 2. Nevertheless, when these ultra low yield smokers are compared against the Cambridge brand as a standard experience the individual differences in plasma cotinine concentration, as shown by the regression slope, is minimal.

It has been suggested that up to 40% of the smokers of ultra low tar cigarettes defeat the delivery system by abuse of the filter and air introduction system and thus receive more nicotine and tar than one would expect based upon standard smoking machine test yields of tar and nicotine. The individual with higher than average cotinine plasma concentration may achieve these values by defeating the delivery system. However a large percentage of the individuals studied achieve less than average nicotine intake from the delivery system based upon the plasma cotinine concentrations measured in this sample of ultra low tar cigarettes smokers.

The data presented supports the conclusion that brand differences as a factor which affects nicotine and tar uptake among ultra low tar cigarette smokers is a minimal factor. If some individuals defeat the filter mechanism which limits nicotine and tar delivery their actions are not brand specific and thus the problem is one that exists with the entire class of ventilated cigarettes. These data do not support the conclusion that 40% of the smokers defeat the filter system. The data supports a conclusion that almost fifty percent of the individuals who smoke the ultra low tar brands benefit from low nicotine and thus tar intake.

REFERENCES

BENOWITZ, Neal L.; Jacob, Peyton, III; Jones, Reese T.; and Rosenberg, J. Interindividual Variability in the Metabolism and Cardiovascular Effects of Nicotine in Man. J. Pharm. and Exper. Therap. 221:368-372, 1982.

WALD, Nicholas; Doll, Richard; and Copeland, Graham. Trends in tar, nicotine and carbon monoxide yields of UK cigarettes manufactured since 1934. Br. Med. J. (Clin. Res.), 1981. March 7; 282 (6266): 763-765.

(REFERENCES TO OTHER PERTINENT LITERATURE GIVEN IN PAPERS BY GORI AND LYNCH AND BY VAN ROSSUM AND DARBY)

FIGURE 1.

The points on the scattergram represent the plasma cotinine concentration obtained from the smoker during the period of smoking Barclay brand and Carlton brand cigarettes. Numbers larger than one indicate the number of smokers who gave the same plasma cotinine concentration. The scattergram is divided into four quadrants by drawing a line at the average plasma cotinine concentration obtained from the smokers while they were smoking either Barclay or Carlton brand cigarettes. Thus quadrant I contains those smokers who demonstrated higher than average values while smoking Carlton brand cigarettes and lower than average values while smoking Barclay brand cigarettes. Those smokers who demonstrated higher than average values while smoking either Barclay brand or Carlton brand cigarettes are located in quadrant II. Quadrant III contains those smokers who demonstrated higher than average values while smoking Barclay brand cigarettes while demonstrating lower than average values while smoking the Carlton brand cigarettes. The smokers in quadrant IV demonstrated lower than average plasma concentrations of cotinine while smoking either Barclay or Carlton brand cigarettes. The percent of the individuals contained in a particular quadrant is listed in Table 2.

FIGURE 1

CARLTON AND BARCLAY SMOKERS

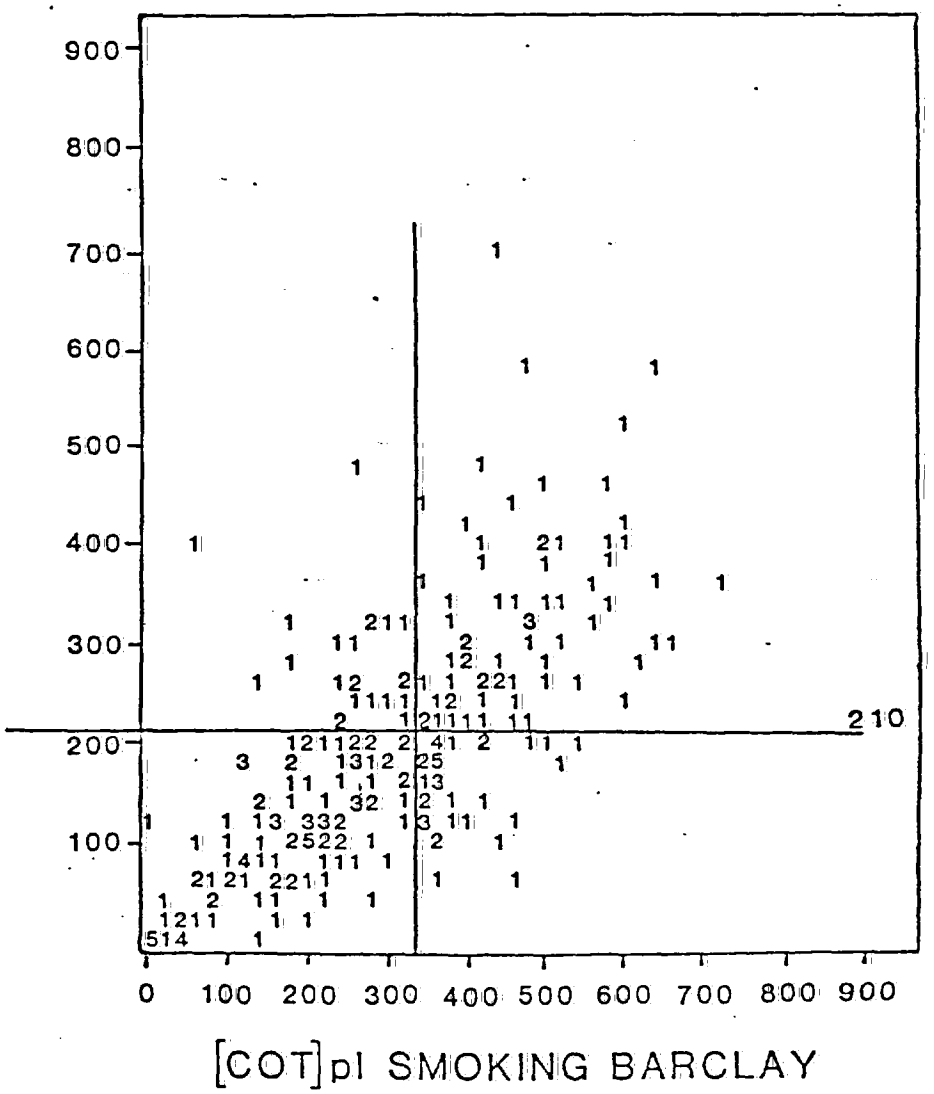

FIGURE 2.

Figure 2 provides a regression analysis comparison of the plasma cotinine concentration obtained while the smokers were smoking Barclay brand cigarettes as compared to their plasma cotinine concentration while they were smoking the Cambridge brand cigarettes. The slope of the line illustrates the difference in the relative uptake of nicotine and thus tar between the brands compared. A slope is also provided which assures that 90% of the individuals studied would have a value less than 2.77 times the plasma concentration obtained while smoking the Cambridge brand. Other pertinent data are given in the legend on the figure.

FIGURE 2

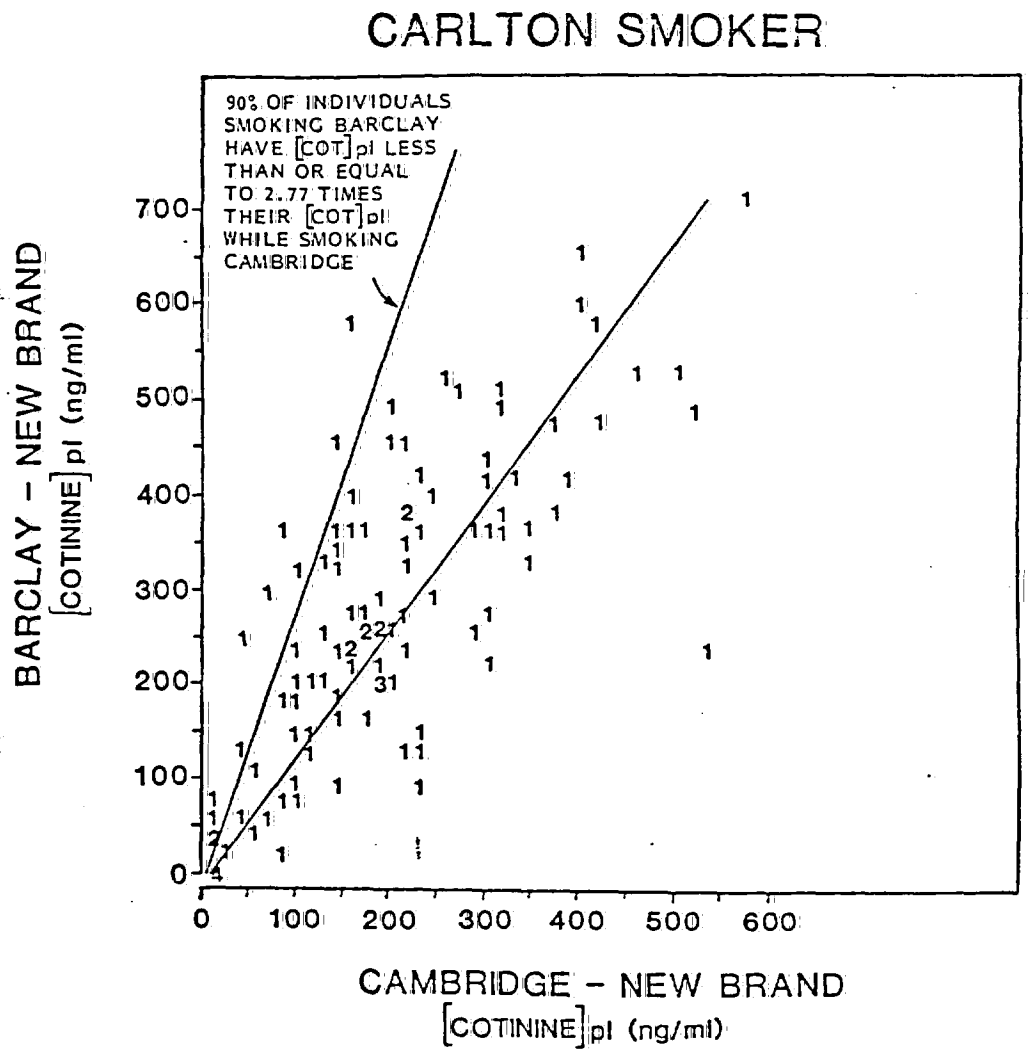

CORRELATION COEFFICIENT (R)	= .74
NO. OF OBSERVATIONS	= 106
STANDARD ERROR OF R	= .06

LINEAR REGRESSION

SLOPE	= .98
Y-AXIS INTERCEPT	= 98

REGRESSION THROUGH ORIGIN

SLOPE (0 INTERCEPT ASSUMED)	= 1.34

FIGURE 3.

See text and the legend for figure 2 for pertinent information.

FIGURE 3

BARCLAY SMOKER

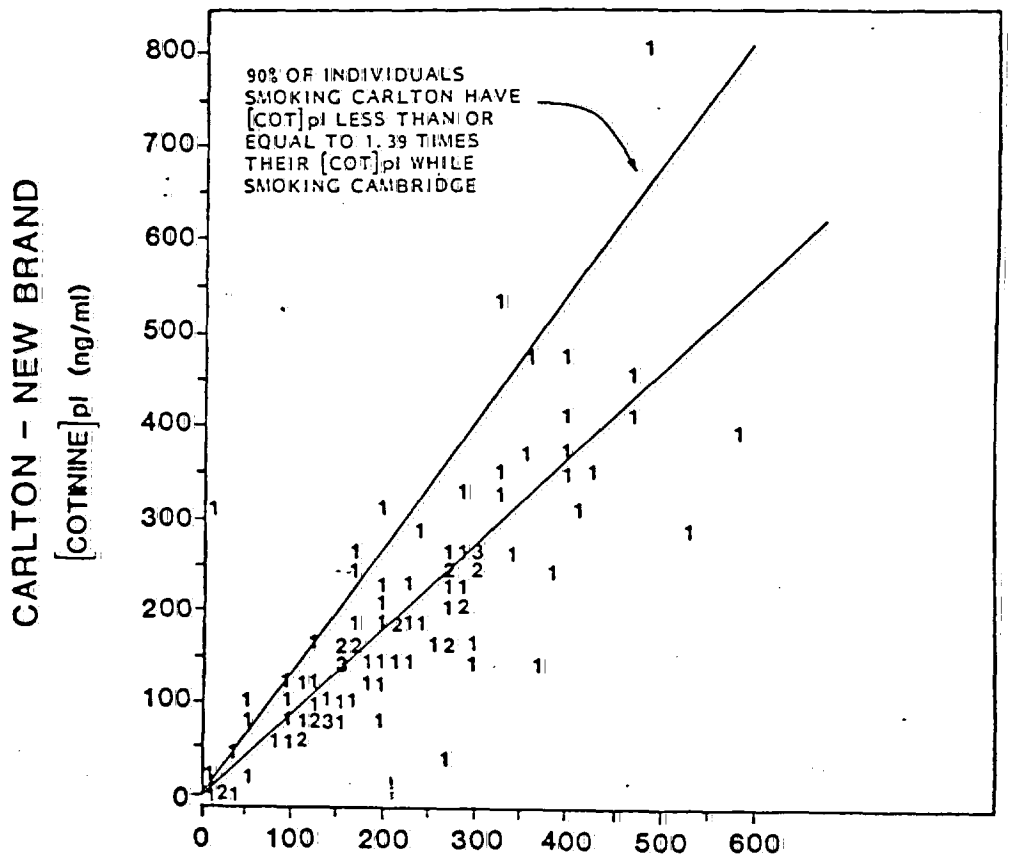

CARLTON - NEW BRAND
[COTININE]pl (ng/ml)

CAMBRIDGE - NEW BRAND
[COTININE]pl (ng/ml)

CORRELATION COEFFICIENT (R)	= 0.79	LINEAR REGRESSION SLOPE	= 0.85
NO. OF OBSERVATIONS	= 98	Y - AXIS INTERCEPT	= 24
STANDARD ERROR OF R	= 0.06	SLOPE 0 INTERCEPT ASSUMED (REGRESSION THROUGH ORIGIN)	= 0.93

10050630 37

Figure 4.

See text and the legend for figure 2 for pertinent information.

FIGURE 4

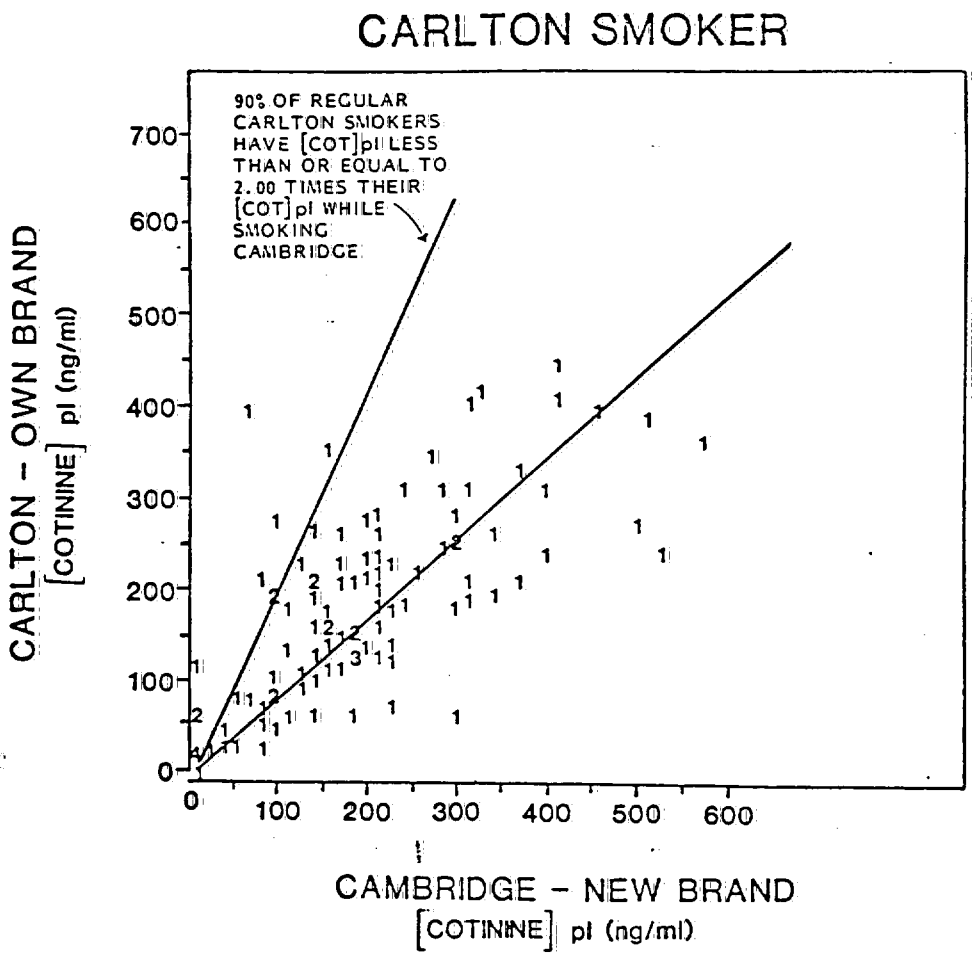

CORRELATION COEFFICIENT (R)	= 0.70	LINEAR REGRESSION SLOPE	= 0.60
NO. OF OBSERVATIONS	= 106	Y - AXIS INTERCEPT	= 69
STANDARD ERROR OF R	= 0.07	SLOPE 0 INTERCEPT ASSUMED (REGRESSION THROUGH ORIGIN)	= .85

10050630 39

Figure 5.

See text and the legend for figure 2 for pertinent information.

FIGURE 5

BARCLAY SMOKER

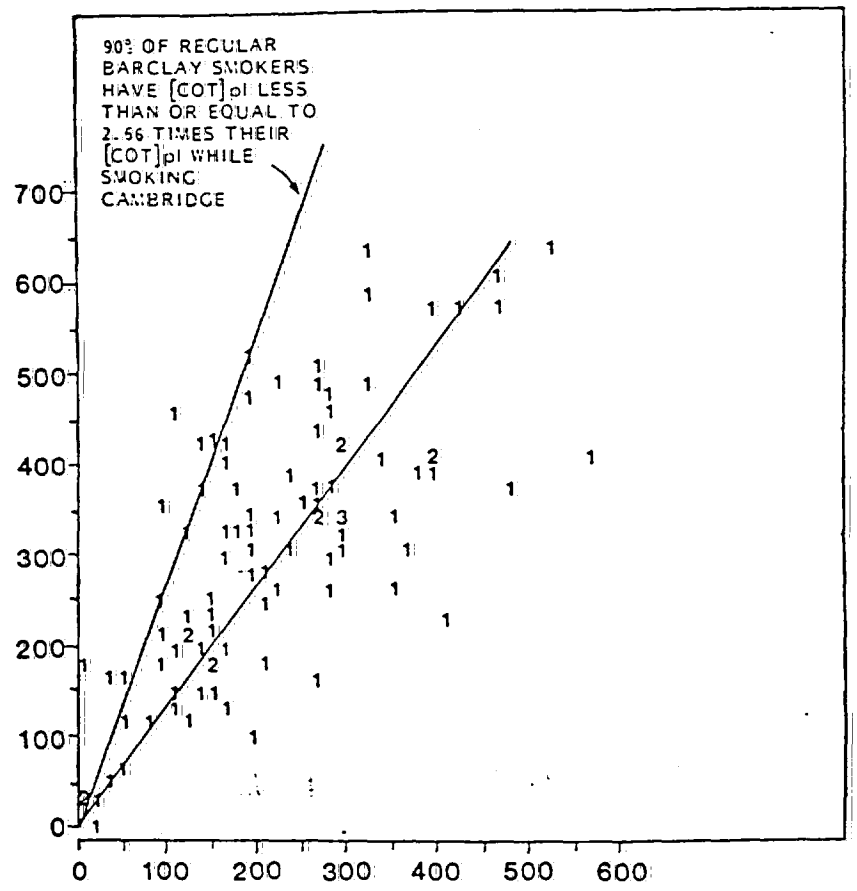

CORRELATION COEFFICIENT (R)	= .69
NO. OF OBSERVATIONS	= 98
STANDARD ERROR OF R	= .07

LINEAR REGRESSION

SLOPE	= .84
Y AXIS INTERCEPT	= 137

REGRESSION THROUGH ORIGIN

SLOPE (0 INTERCEPT ASSUMED) = 1.33

Figure 6.

This figure presents a plot of the cumulative percentile of the population vs. the log of the plasma cotinine concentration. These data illustrate the large inter-individual differences seen in uptake of nicotine and thus tar as measured by analysis of plasma for cotinine concentration. While it is reasonable to assume that the increased uptakes are due to smoking behavior differences, it is not unreasonable to assume that individual differences in rate of metabolism of nicotine to cotinine could account for some to the increased cotinine concentration. However, since the curves obtained with Carlton and Cambridge on the one hand and with Barclay on the other are parallel, there are no individual differences in the matabolic handling of nicotine occurring during the study period. These data support the conclusion that the Actron Filter cigarettes, Barclay, are similar in their delivery of nicotine and thus tar to other conventional air dilution filter cigarette deliveries, i.e., the delivery of Carlton and Cambridge.

FIGURE 6

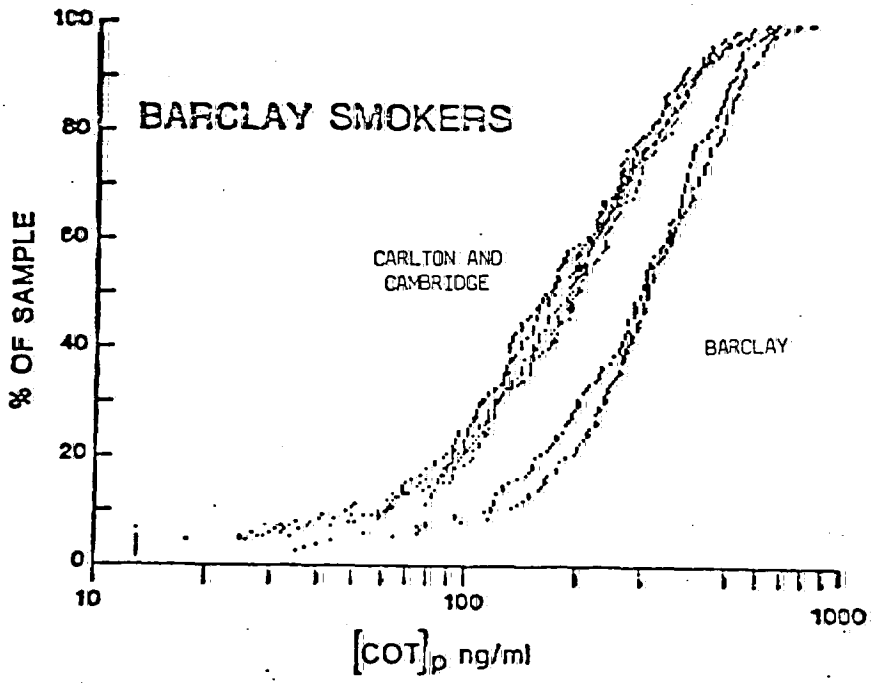

Figure 7.

This figure presents data similar to that provided in Figure 6. however, in this case the smokers represent the individuals who normally smoked the Carlton brand cigarettes. The curves obtained with the Carlton brand smokers are not different from the curves shown for Barclay brand smokers in Figure 6.

FIGURE 7

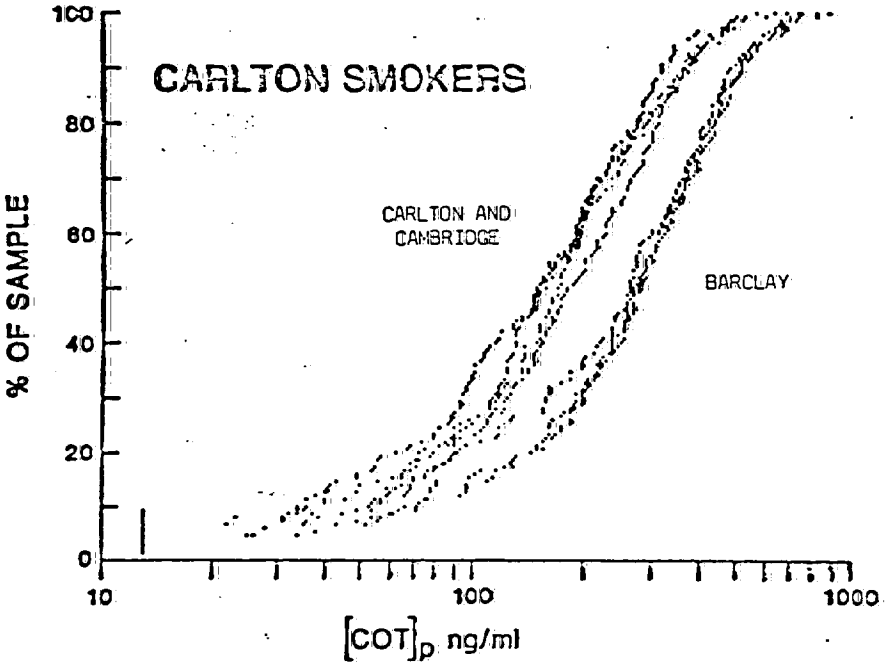

Figure 8.

This figure presents the percentile data plotted vs. the plasma cotinine values. The shift to the right is caused by the higher potential nicotine delivery of Barclay. This shift is only one-third the increase caused by smoking behavior differences. The increase in plasma cotinine concentration based upon inter-individual differences is 320 ng/ml over a two standard deviation range. A switch from Barclay provided an intra-individual difference of 110 ng/ml over this two standard deviation range.

FIGURE 8

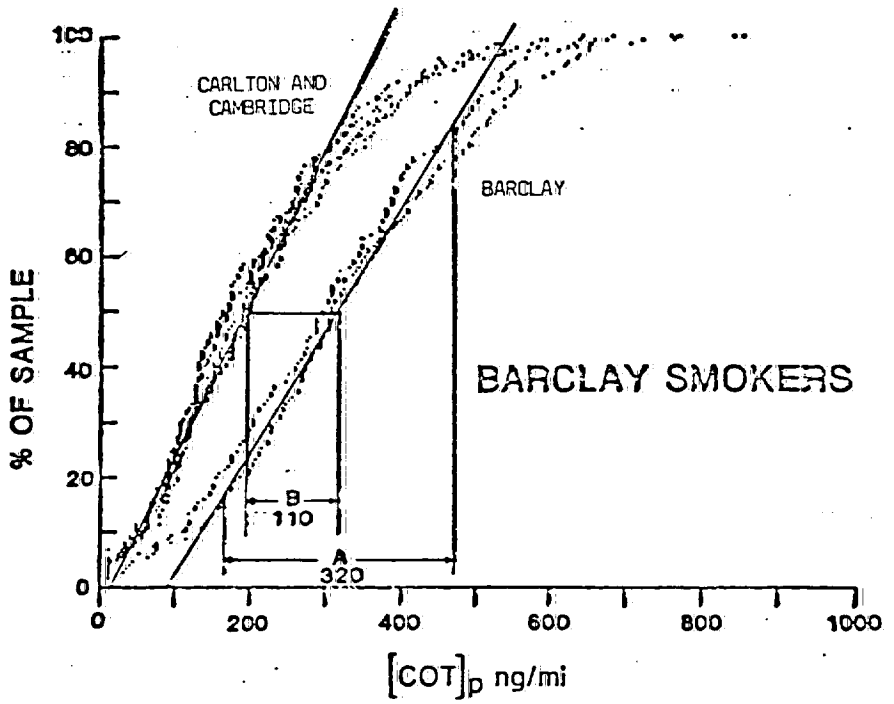

Figure 9

This figure presents data similar to that shown in Figure 8 however in this case the Carlton smokers are shown. Notice the similar smoking behavioral effects and the similar shift due to the increased potential nicotine delivery seen with the Barclay brand cigarette. There is no difference in delivery seen with the population sample of Carlton smokers and the population sample of Barclay smokers.

FIGURE 9

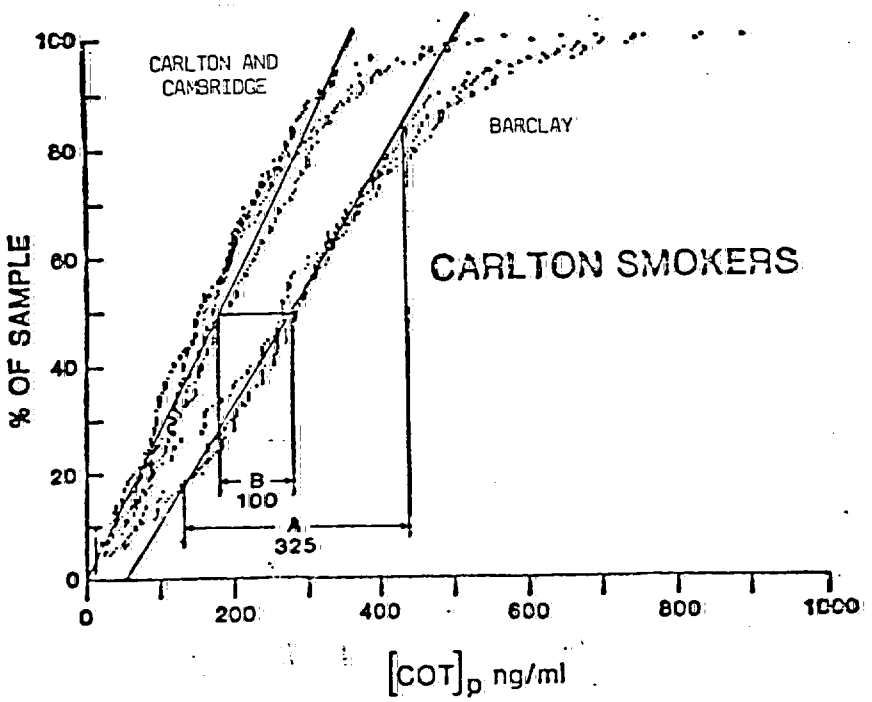

DRAFT
COMMERCIAL IN CONFIDENCE

TABLE 1.

NICOTINE AND TAR YIELD DERIVED BY STANDARD FTC TEST METHOD.

BRAND TESTED	BATCH	MILLIGRAMS/CIGARETTE TAR	NICOTINE
BARCLAY	IXL	0.9	0.18
CARLTON	00025	0.5	0.10
CAMBRIDGE	EB	0.6	0.11

In each case the stardard deviation of the measurement was 0.02

Table 1 provides the analytical data for the batch code of the brand listed. Only cigarettes from one batch of each brand were used in the study. The batch represented 85 mm length, filter, soft pack cigarettes. With the air introduction and the filtration provided, the tar measurements are difficult. However, each of the brands tested provided less than 1 mg. tar.

TABLE 2.

	Number of Individuals	Percent of the Total Number
QUADRANT I	23	9.3
QUADRANT II	70	28.2
QUADRANT III	37	15.0
QUADRANT IV	117	47.5

Table 2. provides the number and the percentage of the total number of individuals studied found in each of the four quadrants delineated in Figure 1. The average plasma cotinine concentration for smokers of Carlton brand cigarettes was 210 ng/ml. The average plasma cotinine concentration for smokers of Barclay brand cigarettes was 340 ng/ml.

TABLE 2.

	Number of Individuals	Percent of the Total Number
QUADRANT I	23	9.3
QUADRANT II	70	28.2
QUADRANT III	37	15.0
QUADRANT IV	117	47.5

Table 2. provides the number and the percentage of the total number of individuals studied found in each of the four quadrants delineated in Figure 1. The average plasma cotinine concentration for smokers of Carlton brand cigarettes was 210 ng/ml. The average plasma cotinine concentration for smokers of Barclay brand cigarettes was 340 ng/ml.

ADDENDUM TO APPENDIX IV

EFFECTS OF FILTRONA AND BORGWALDT LATEX
SLEEVE HOLDERS ON BARCLAY TAR YIELDS

Two smoking machine cigarette holders use stretched latex sleeves. The Filtrona holder was originally designed for joining experimental filters to standard tobacco rods. It is 17 mm long and requires application of vacuum to insert filters. The force applied to the filter by the latex sleeve depends on its diameter, wall thickness and "stretch" when placed in the holder. The Borgwaldt holder, designed for their rotary smoking machine, is based on similar principles but is 12 mm long.

Dr. Roger Kamm of the Massachusetts Institute of Technology has measured the pressures exerted by various cigarette holders and by human lips.

Human lip pressures average about 35 torr and rarely exceed 100 torr. The dental dam used by the FTC and U.S. industry in the Cambridge pad holder exerts a pressure of 50 torr. The Borgwaldt holder with standard 8 mm i.d. tubing exerts a pressure of 120 torr. The Filtrona holder pressure ranges from 200 to 500 torr depending on the type of latex and its insertion.

Tar measurements performed by Brown & Williamson are summarized in the attached graph. The Borgwaldt holder increases tar by 0.3 mg. The Filtrona holder in the extreme case increases tar to 3.3 mg.

Separate measurements on Actron filters by Dr. Kamm show a ventilation reduction of 5% at a pressure of 200 torr. This is in line with the observed tar changes.

Barclay tar deliveries can be increased by exerting extreme pressure on the filter. Within the range of observed human lip pressures, however, tar increases are negligible, 0.5 mg at most. Much greater changes are much more easily achieved by human smokers by varying either puff volume or puffing frequency.

EFFECT OF HOLDER PRESSURE
ON BARCLAY TAR

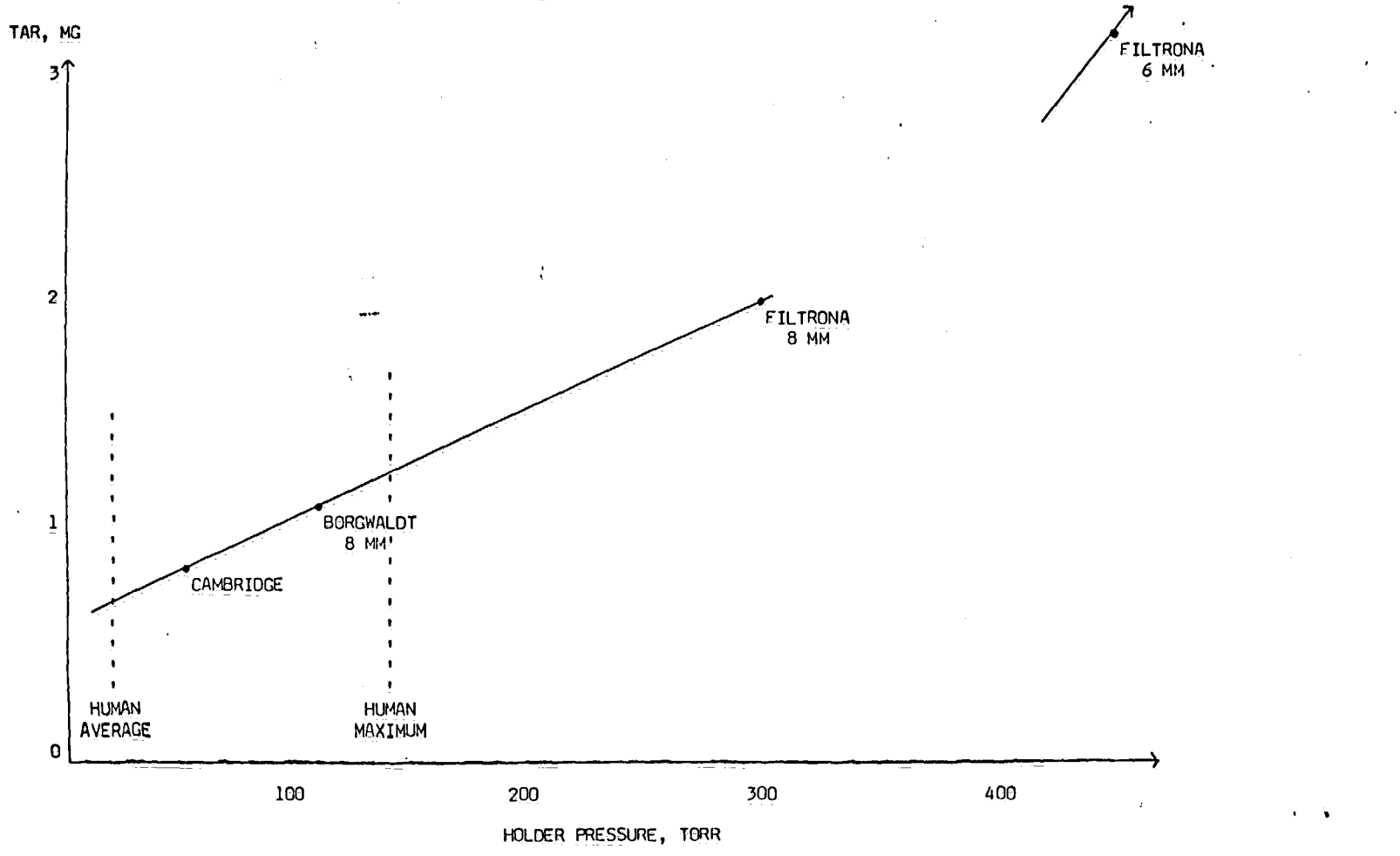

1005063055